IV.1.   <u>**Introduction**</u>

The epoxidation of olefins is still a great challenge due to its importance in industrial and organic synthetic methodologies.[1,2] Epoxides are essential intermediates, particularly for the synthesis of various polymers (polyglicols, polyamides, polyurethanes, etc.)[3] and fine chemicals such as pharmaceuticals, food additives or flavor and fragrance compounds.[4] The biggest market is propylene oxide, which is produced at 8 million TON/year with an expected annual increase of 5%.[5]

Ru complexes are excellent catalyst for redox transformations such as alcohol oxidation,[6] sulfoxidation,[7] water oxidation[8] and epoxidation.[9] In all these cases $Ru^{IV}=O$ species have shown to be the active catalytic unit. Most of the literature related to redox catalysis using Ru complexes is based on mononuclear complexes since they are generally easily accessible from a synthetic point of view. In sharp contrast, a powerful diruthenium epoxidation catalyst in terms of epoxide selectivity, and conversions has been recently reported by our research group.[11a] In addition, this new catalyst displays distinctive reactivity with regards to *cis* and *trans* alkenes. Both features are proposed to be caused by a supramolecular hydrogen bonding interaction between the second $Ru^{IV}=O$ site and the substrate employed, together with steric effects.

Our group has an extensive experience on the synthesis, characterization and oxidative catalytic performance of several dinuclear Ru complexes, most of them inspired on the well-known $\{[Ru^{II}(trpy)]_2(\mu\text{-}bpp)(\mu\text{-}Cl)\}^{2+}$ water oxidation catalyst.[10] Modifications around this paradigmatic compound such as the replacement of the trpy auxiliary ligands by facially coordinating scaffolds such as bpea or tpym (see Chart 1 for a drawing of these ligands), as well as the exchange of the bpp⁻ bridge by other tetradentate bridges such as pyr-dc³⁻ or pbl⁻ (Chart 1) have been prepared, characterized and catalytically evaluated.[11] The use of facial ligands such as bpea and tpym allowed an *"up, down"* dispositon of the metal centers, thing that dramatically affected both the steric and electronic properties of these complexes as well as their final reactivity and water oxidation reaction mechanism.[12,13]

The use of a bis-facial bridging ligand to prepare dinuclear Ru catalysts for water oxidation and/or olefin epoxidation has never been attempted. Therefore, in order to explore the properties of this kind of systems herein we report the synthesis,

spectroscopic and redox propierties of a new dinuclear complex with formula $\{[Ru^{II}(bpy)]_2(\mu\text{-bimp})(\mu\text{-Cl})\}^{2+}$, **$2^{2+}$** and its bis-aquo derivative $\{[Ru^{II}(bpy)(H_2O)]_2(\mu\text{-bimp})\}^{3+}$, **$3^{3+}$** (*bpy* is the 2,2'-bipyridine; *bimp⁻* is the 3,5-bis[bis(1,4,5-trimethyimidazol-2-yl)-methoxymethyl]pyrazolate). The already reported *bimp⁻* ligand will act as bridging and bis-facial coordinating ligand. The reactivity of **3^{3+}** towards the oxidation of water and olefins and the comparative discussion with the already reported family of related dinuclear complexes is reported in this work.
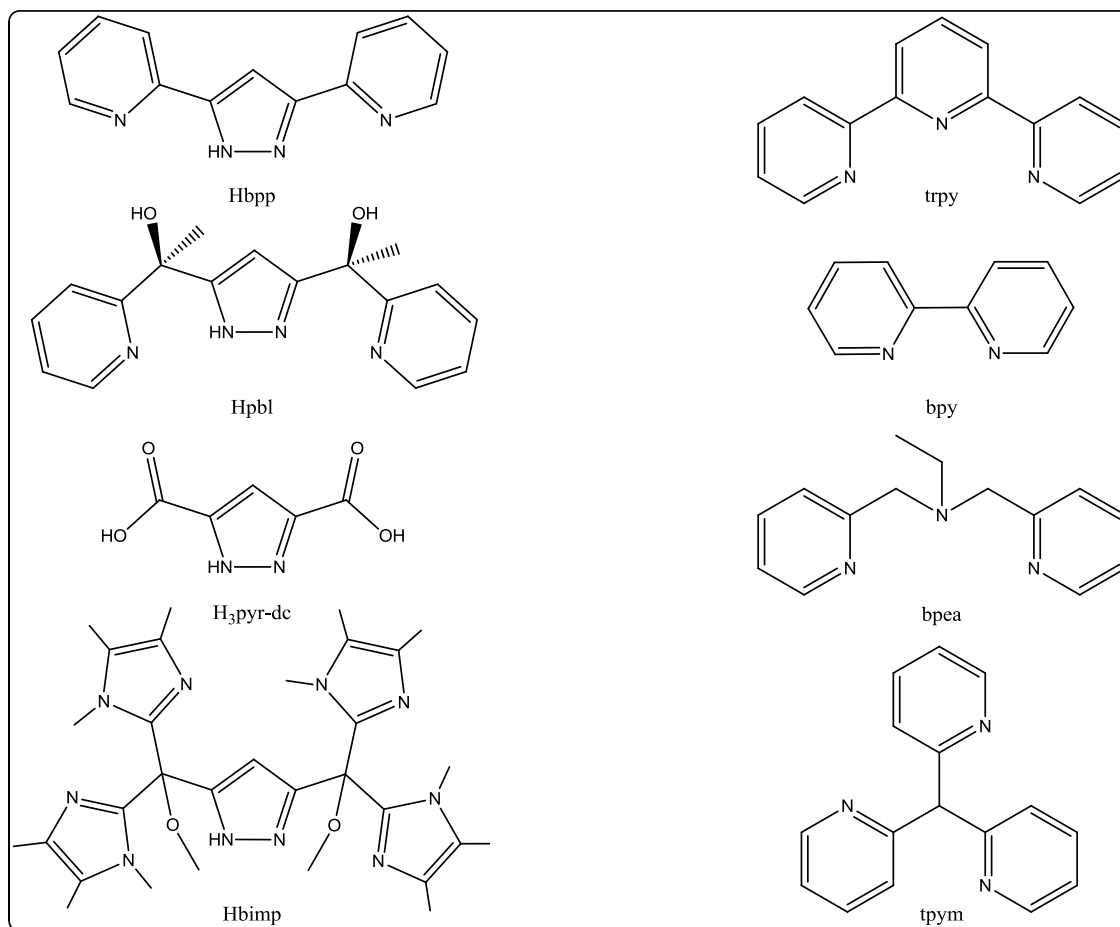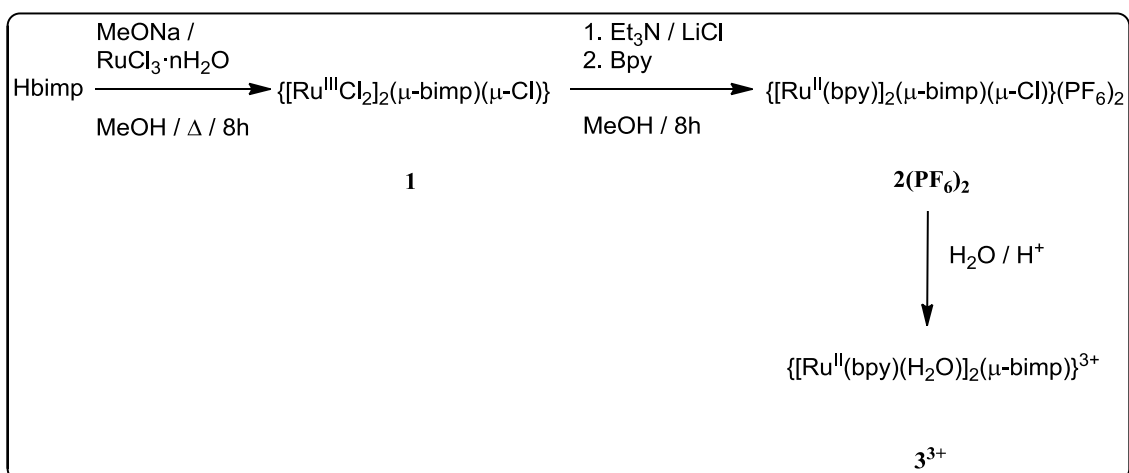

Chart 1. Bridging and auxiliary ligands discussed in this work.

IV.2.   Results & Discussion

IV.2.1.   Synthesis and characterization of 1, 2(PF$_6$)$_2$ and 3^{3+}

The synthetic strategy followed for the preparation of the dinuclear complexes **2(PF$_6$)$_2$** and **3^{3+}** is depicted in Scheme 1.

Hbimp $\xrightarrow[\text{MeOH / } \Delta \text{ / 8h}]{\begin{array}{c}\text{MeONa /}\\\text{RuCl}_3\cdot n\text{H}_2\text{O}\end{array}}$ {[Ru^{III}Cl$_2$]$_2$(μ-bimp)(μ-Cl)} $\xrightarrow[\text{MeOH / 8h}]{\begin{array}{c}\text{1. Et}_3\text{N / LiCl}\\\text{2. Bpy}\end{array}}$ {[Ru^{II}(bpy)]$_2$(μ-bimp)(μ-Cl)}(PF$_6$)$_2$

1   **2(PF$_6$)$_2$**

$\downarrow$ H$_2$O / H$^+$

{[Ru^{II}(bpy)(H$_2$O)]$_2$(μ-bimp)}$^{3+}$

3^{3+}

Scheme 1.   Synthetic pathway for the preparation of and **2(PF$_6$)$_2$** and **3^{3+}**.

IV

Preparation of precursor **1** from RuCl$_3\cdot$nH$_2$O involved the presence of sodium methoxide as a base to deprotonate the pyrazolic nitrogen of the Hbimp ligand.[*] Because of the high solubility of **1** in the reaction media, the addition of diethyl ether was mandatory to precipitate the desired product as a green powder (see ESI-MS spectra of **1** in Figure S7). The reaction of **1** in the presence of LiCl, triethylamine and 2,2'-bypyridine (2 equivalents) ended up generating **2^{2+}** after overnight stirring at room temperature. The addition of water and 1 ml of a saturated aqueous solution of NH$_4$PF$_6$ yielded a violet powder corresponding to the desired complex, **2(PF$_6$)$_2$**. The dissolution of **2(PF$_6$)$_2$** in a pH=1 aqueous solution (triflic acid 0.1 M) resulted in the generation of the bis-aqua complex **3^{3+}**.

Each tridentate unit of the hexadentate Hbimp ligand, given its configuration, can only coordinate in a facial fashion to an octahedral metal centre. In addition, the Hbimp ligand can potentially generate the C_s *(cis)* and C_2 *(trans)* isomers depicted in Figure 2. The terms *cis* and *trans* indicate whether the two bipyridines are located one above and

---

[*] The Hbimp ligand has been gently provided by Pr. Franc Meyer (University of Gottingen).

one below (*trans*) or both on the same side (*cis*) of the distorted plane formed by the pyrazolate ring, the Ru metal centers and the chlorido bridged or the two coordinated aqua ligands. A schematic view of these isomers is shown in Scheme 2.
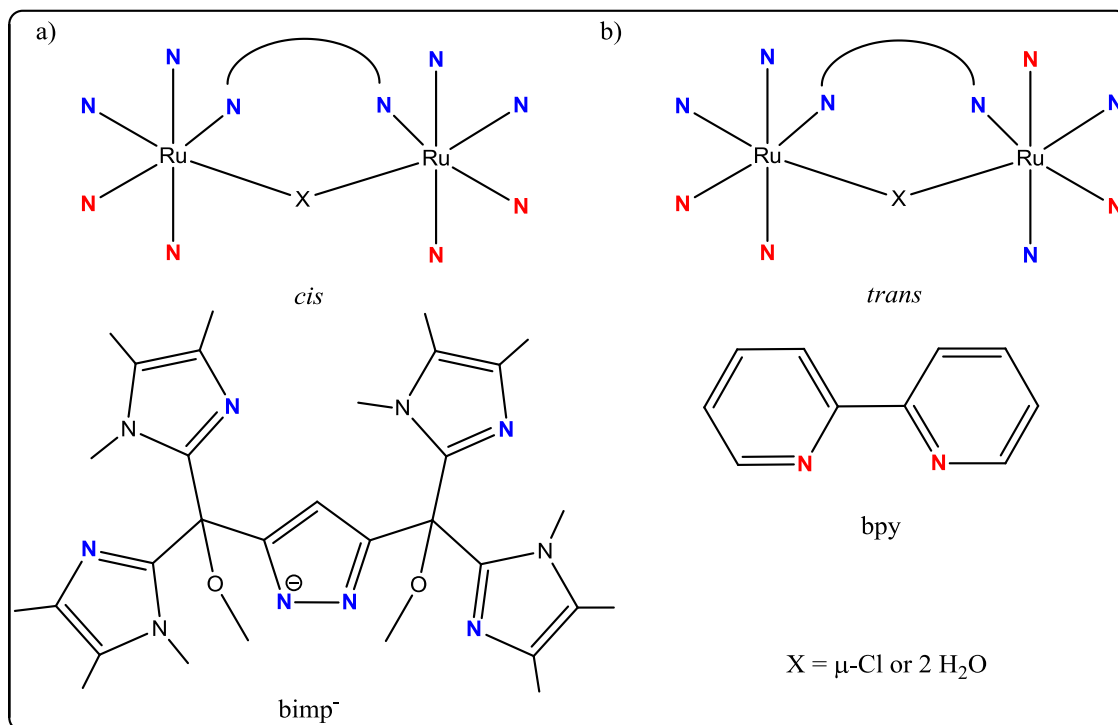
Scheme 2. Schematic plot of the potential isomers of complexes **2(PF$_6$)$_2$** and **3^{3+}**. (a) *cis* and (b) *trans*. Color code: *bimp$^-$* ligand (blue nitrogen atoms). bpy (red nitrogen atoms).

In order to structurally characterize complex **2(PF$_6$)$_2$** in solution a set of NMR experiments have been performed. Figure 1a displays the ^{1}H-NMR in acetone-d$_6$ of **2^{2+}**. The broad kind of signals observed clearly reveals the paramagnetic character of the sample, probably due to the partial oxidation of **2^{2+}**.

On the other hand, Figure 1b displays the ^{1}H-NMR of the same sample when acquired in the presence of a reducing agent (Zn amalgam). The much nicer resonances here observed clearly corroborate the ease of oxidation of **2^{2+}**, as proposed above.
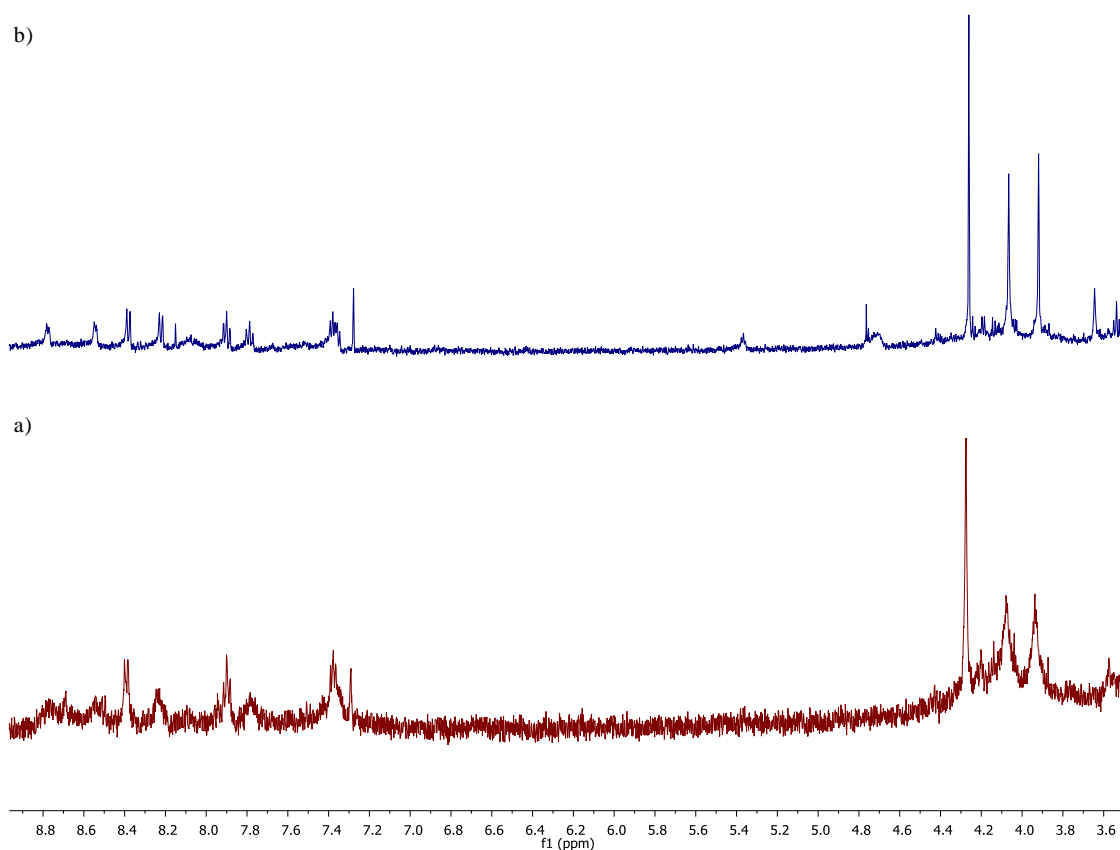
Figure 1. ^{1}H-NMR (400 MHz, acetone-d_6) for 2^{2+} (a) without and (b) with Zn amalgam.

Figure S2 in the Supporting Information displays both 1D (^{1}H and ^{13}C {^{1}H}) and 2D (COSY, HSQC and HMBC) NMR experiments for 2^{2+}. NMR experiments were a mandatory tool in order to confirm the presence signals of a unique isomer of $2(PF_6)_2$, thus excluding the formation of mixture of isomers. Due to the low solubility in the regular deuterated solvents and the ease of oxidation above-mentioned all our attempts to record a Noesy NMR spectrum failed, thus the pyridine rings of each bipyridine and the four methyl groups bonded to the imidazole moieties could not be distinguished. For this reason, only partial assignment of the proton and carbon resonances of complex 2^{2+} could be accomplished (See the Experimental Section).

Due to the unfruitful attempts to obtain good enough crystals for X-ray diffraction analysis and the lack of information extracted from the NMR experiments, DFT calculations have been carried out in order to assess the relative stability of theses isomers.[†] These calculations gave energy values 5.7 Kcal/mol lower for the *trans* isomer

---

[†] DFT calculations have been carried out in collaboration with Dr. Albert Poater (University of Girona).

with regard to the *cis* in the case of the chlorido-bridged complex 2^{2+} (Figure 2). When the same calculation was applied for the corresponding *cis* and *trans*-$\{[Ru^{II}(bpy)(H_2O)]_2(\mu\text{-bimp})\}^{3+}$, 3^{3+} (see Figure S1 in the Supporting Information for the corresponding plots), the cis/trans energy gap increased until 8.1 Kcal/mol, again demonstrating the higher thermodynamic stability of the latter. Despite these values are not high enough to discard the formation of the *cis* isomer under the reaction conditions, they are the unique argument we have to decide that the formed isomer is the *trans* one.

cis   *trans*

cis   *trans*
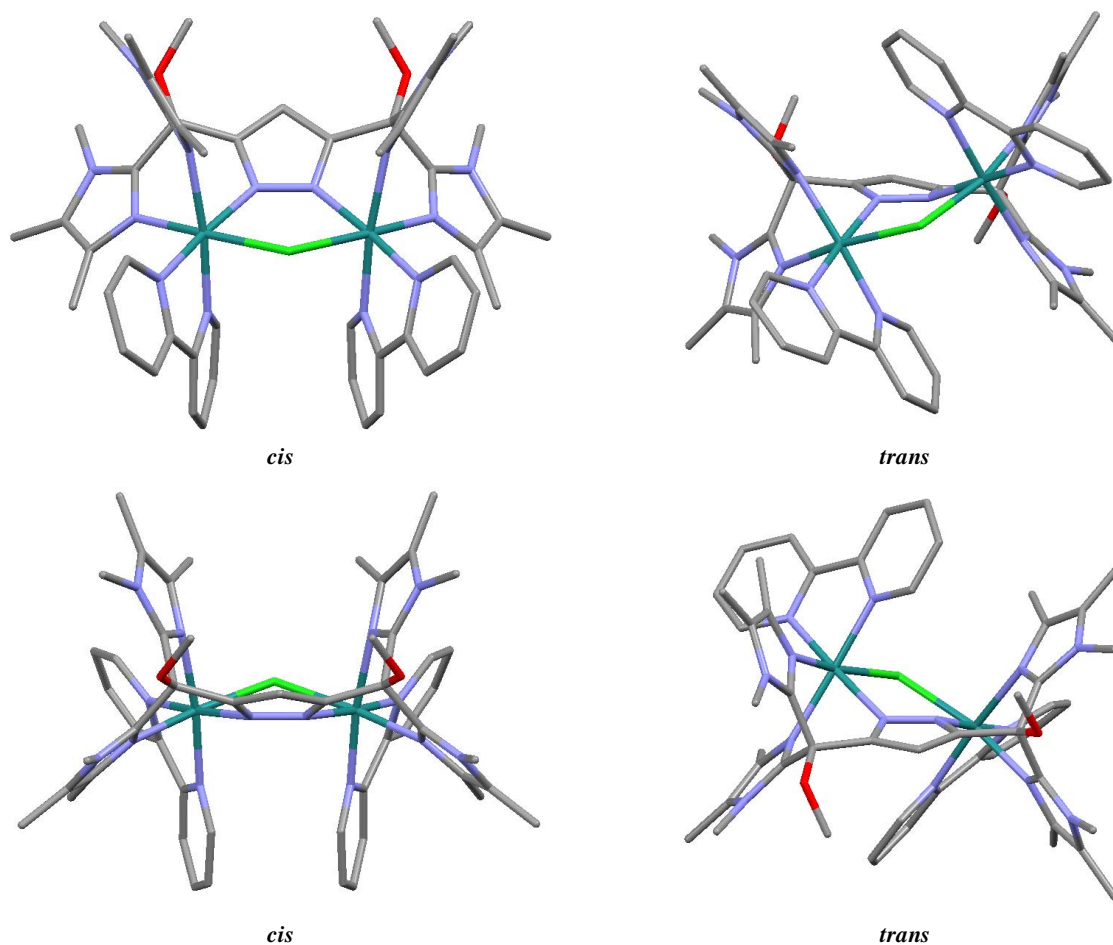
Figure 2. Plot of μ-Cl front view (top) and pyrazole front view (bottom) of the proposed isomeric structures of *cis* (left) and *trans*-$\{[Ru^{II}(bpy)]_2(\mu\text{-bimp})(\mu\text{-Cl})\}^{2+}$ (right), 2^{2+}.

$2(PF_6)_2$ and 3^{3+} have also been characterized in terms of their electronic spectra and electrochemical properties. The most relevant results about these data are reported in the following sections. Further information about their ESI-MS spectra is depicted in the Supporting Information (Figures S8-S9).

IV.2.1.1. Electrochemistry

The redox properties of complexes 2^{2+} and 3^{3+} described in the present work were investigated by means of CV and DPV and are reported in Table 1 together with those corresponding to previously reported related compounds. Figures 3-4 and Figures S3-S6 in the Supporting Information display these experiments. The electrochemistry of 2^{2+} is reported in both DCM (Figures S4 and S5) and acetone (Figures 3 and S3), in which the solubility is higher. An aqueous solution at pH=1 (0.1 M triflic acid) was used for 3^{3+}.

Table 1. Redox potentials in V (vs. SSCE) at a scan rate of 100 mV/s for 2^{2+}, 3^{3+} and related Ru complexes for comparison purposes.

Entry		III/II				$N_{pyridine}$	$N_{pyrz/imidz}$	Cl	*Ref.*
1	$[Ru(bpy)_3]^{+\,d}$	1,28				6	-	-	*14*
2	$[Ru(tpy)(bpy)Cl]^{+\,d}$	0,80				5	-	1	*15*
3	$[Ru(tpy)(bpy)(H_2O)]^{2+\,b}$	0,80				5	-	-	*17b*
		III,II/ II,II	III,III /III,II	IV,III/ III,III	IV,IV/ IV,III				
4	$\{[Ru^{II}(trpy)]_2(\mu\text{-bpp})(\mu\text{-Cl})\}^{2+\,a}$	0.71	1.12	-	-	4	1	0,5	*16*
5	$2^{2+\,a}$	0.55	0.98	-	-	2	3	0,5	*c*
6	*trans*-$\{[Ru^{II}(Cl)(tpym)]_2(\mu\text{-bpp})\}^{+\,a}$	0.54	0.84	-	-	4	1	1	*13*
7	*trans*-$\{[Ru^{II}(Cl)(bpea)]_2(\mu\text{-bpp})\}^{+\,a}$	0.37	0.72	-	-	3	2	1	*12*
8	*cis*-$\{[Ru^{II}(trpy)(H_2O)]_2(\mu\text{-bpp})\}^{3+\,b}$	0.59	0.65	0.88	1.10	4	1	-	*16*
9	*trans*-$\{[Ru^{II}(tpym)(H_2O)]_2(\mu\text{-bpp})\}^{3+\,b}$	0.54	0.75	1.18	1.52	4	1	-	*13*
10	$3^{3+\,b}$	0.27	0.46	0.69	1.06	2	3	-	*c*
11	*trans*-$\{[Ru^{II}(bpea)(H_2O)]_2(\mu\text{-bpp})\}^{3+\,b}$	0.21	0.43	0.61	-	3	2	-	*12*

[a] CH_2Cl_2 using 0.1 M of TABH as electrolyte. [b] Aqueous solution at pH=1 (0.1 M triflic acid). [c] This work. [d] Acetonitrile using 0.1 M of TABH as electrolyte.

The CV of 2^{2+} in DCM (Figure S4) exhibits two reversible waves, which are assigned to

the following electrochemical reactions (the chlorido-bridged ligands are not shown for the sake of clarity):

$$[Ru^{III}(\mu\text{-}\textbf{L1})Ru^{II}]^{3+} + 1e^- \quad \rightarrow \quad [Ru^{II}(\mu\text{-}\textbf{L1})Ru^{II}]^{2+} \quad (0.55\ V) \qquad (2)$$

$$[Ru^{III}(\mu\text{-}\textbf{L1})Ru^{III}]^{4+} + 1e^- \quad \rightarrow \quad [Ru^{III}(\mu\text{-}\textbf{L1})Ru^{II}]^{3+} \quad (0.98\ V) \qquad (3)$$

Table 1 displays the $E_{1/2}$ values for the chlorido-bridged 2^{2+} and the bis-aquo derivate 3^{3+} as well as for a set of related compounds with a high diversity of N-donor ligands. In this manner the compounds are classified depending on how σ-donor is the coordinated N-donor ligand (pyridine < pyrazole ≈ imidazole) as well as according to the number of chlorido anions coordinated per Ru center (0, 0.5 when a chlorido-bridge connects two Ru metal ions or 1). For the set of chlorido compounds (Table 1, entries 2 and 4-7) each Ru center is influenced by the two effects; meanwhile for the set of bis-aqua derivates (entries 3 and 8-11) only the σ-donation of the N-ligand influences the final $E_{1/2}$ values. With all these rationalities on hand, and considering that the higher the electronic donation of the ligands, the lower the redox potential ($E_{1/2}$); the electrochemical behavior of 2^{2+} and 3^{3+} can be explained as follows.

A clear down-shift of the $E_{1/2}$ is observed when comparing the redox potentials of 2^{2+} (Table 1, entry 5) with the ones previously reported for the related $\{[Ru^{II}(trpy)]_2(\mu\text{-}bpp)(\mu\text{-}Cl)\}^{2+}$ complex (entry 4). This is in agreement with the higher σ-donation and lower π-acceptor capacity of the imidazole rings with regards to the pyridines conforming the trpy ligand. On the other hand, the redox potentials of the III,III-III,II and III,II-II,II couples of complex 2^{2+} can also be compared with the ones previously reported for other bis-facial Ru dinuclear complexes (entries 6 and 7). When comparing with the bpea complex (entry 7), both processes are anodically shifted by 240 and 180 mV. This shift is a consequence of both the lower σ-donation and higher π-acceptor capacity of the imidazole rings in 2^{2+} with regards to the central tertiary amine in the bpea ligand and the lower σ-donation of the chlorido-bridged anion in contrast to the two chlorido anions present in the *trans*-$\{[Ru^{II}(Cl)(bpea)]_2(\mu\text{-}bpp)\}^+$ complex. The redox potentials are surprisingly similar to those reported for the tpym chlorido complex (entry 6). While in *trans*-$\{[Ru^{II}(Cl)(tpym)]_2(\mu\text{-}bpp)\}^+$ each Ru is coordinated to 4 pyridines, 1 pyrazole and one chlorido anion, in 2^{2+} (entry 5) each Ru is electronically modulated by 2 pyridines, 3 imidazole/pyrazole rings and only half chlorido ligand. The latest reveals, once again, the influence of both the N-ligands and chlorido anions into the final $E_{1/2}$ and how this value is a perfect combination of both factors.
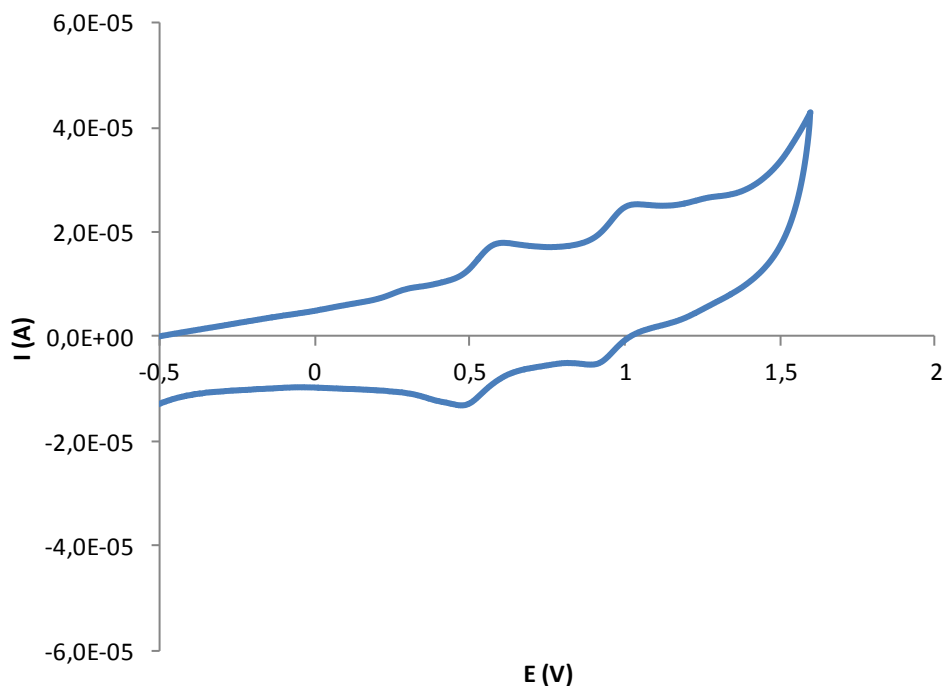
Figure 3. Cyclic voltammogram for the chlorido-bridged complex 2^{2+} in 0.1 M *n*-Bu$_4$NPF$_6$ in acetone at 100 mV/s scan rate. Glassy carbon electrode is used as working electrode and the potential is measured vs. SSCE.

IV

The electrochemistry of 3^{3+} has been investigated after its *"in-situ"* generation in an acetone:pH 1 aqueous solution (0.1 M triflic acid) 10:90 using 2^{2+} as a precursor (see Scheme 1). From the CV (Figure S6) and DPV (Figure 4) of 3^{3+} a total of four waves are observed. These have been tentatively assigned, taking into account previous results on related complexes,[16] to a total of four redox processes:

$$[Ru^{III}\text{-}Ru^{II}] + 1e^- \quad \rightarrow \quad [Ru^{II}\text{-}Ru^{II}] \quad (0.27\ V) \quad (4)$$

$$[Ru^{III}\text{-}Ru^{III}] + 1e^- \quad \rightarrow \quad [Ru^{III}\text{-}Ru^{II}] \quad (0.46\ V) \quad (5)$$

$$[Ru^{IV}\text{-}Ru^{III}] + 1e^- \quad \rightarrow \quad [Ru^{III}\text{-}Ru^{III}] \quad (0.69\ V) \quad (6)$$

$$[Ru^{IV}\text{-}Ru^{IV}] + 1e^- \quad \rightarrow \quad [Ru^{IV}\text{-}Ru^{III}] \quad (1.06\ V) \quad (7)$$

When the potential is increased further up to 1.3 V a large anodic current is observed in the DPV that is associated with a further one electron oxidation of the complex concomitant with the electrocatalytic oxidation of water to dioxygen in agreement with equations (8) and (9).

$$\{O=Ru^V\text{-}Ru^{IV}=O\}^{4+} \; + \; 1e^- \qquad \rightarrow \qquad \{O=Ru^{IV}\text{-}Ru^{IV}=O\}^{3+} \qquad\qquad (8)$$

$$\{O=Ru^V\text{-}Ru^{IV}=O\}^{4+} \; + \; 2H_2O \qquad \rightarrow \qquad \{H_2O\text{-}Ru^{III}\text{-}Ru^{II}\text{-}OH_2\}^{4+} + O_2 \qquad (9)$$

The oxidation process related to the equation 8 is not observed in the DPV (Figure 5) given the concomitant and fast electrocatalytic current corresponding to the oxidation of water (equation 9).

As can be observed in Table 1, relevant changes are observed when comparing the redox potentials of 3^{3+} with regard to those of the related bis-aquo species of the Hbpp family (compare entries 8 and 10 in Table 1). While when comparing the $E_{1/2}$ of the chlorido derivates (Table 1, entries 3-6) the presence of one bridging or two independent chlorido anions and the more or less σ-donor/π-acceptor character of the ligands were the arguments used to discussed the different $E_{1/2}$ values, for the bis-aquo compounds only the latter applies. Therefore, the clear down-shift of the $E_{1/2}$ values of 3^{3+} (entry 10) with regards to the ones reported for the related *cis*-$\{[Ru^{II}(trpy)(H_2O)]_2(\mu\text{-}bpp)\}^{3+}$ complex (entry 8) can be explainded by the more σ-donating and less π-acceptor character of the imidazole rings with respect to pyridine. It is worth to mention how the redox processes of 3^{3+} are cathodically shifted comparing with the ones observed for the related and also bis-facial *trans*-$\{[Ru^{II}(tpym)(H_2O)]_2(\mu\text{-}bpp)\}^{3+}$ (entry 9), meanwhile its chlorido derivates (entries 5 and 6) displayed similar redox values due to the different number of these anions. Thus, here again, the more σ-donating and less π-acceptor character of the imidazole rings with respect to pyridine rationalizes this observation. Finally, similar $E_{1/2}$ values were obtained for the *trans*-$\{[Ru^{II}(bpea)(H_2O)]_2(\mu\text{-}bpp)\}^{3+}$ complex (entry 11) and 3^{3+} (entry 10). The mixture in the bpea ligand of a strong σ-donor such as the tertiary amine and 3 pyridine scaffolds per metal ion seems to average similar donor/acceptor properties than when combining 2 imidazol and 2 pyridine scaffolds per metal ion such as in 3^{3+}.
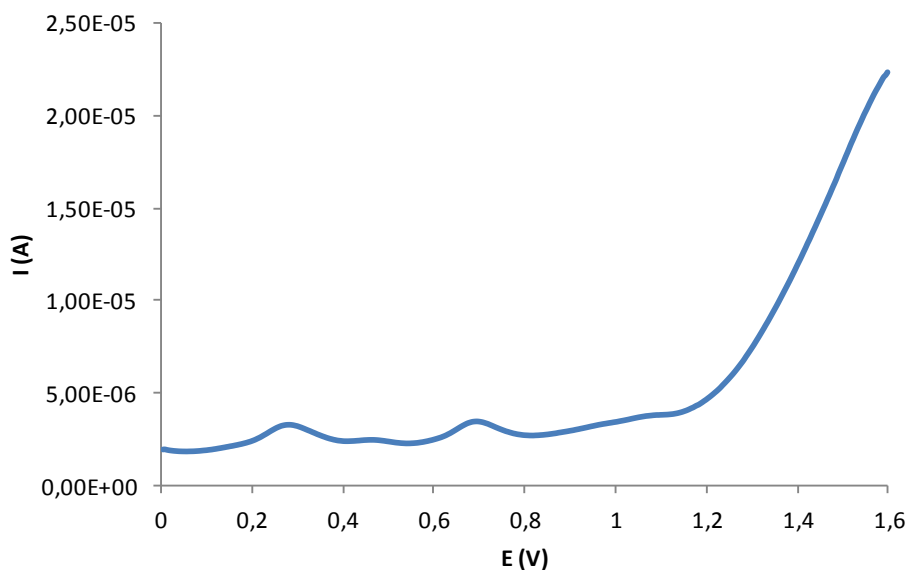
Figure 4. Differential pulse voltammetry for the bis-aquo complex **3³⁺** in a mixture acetone:water (pH = 1.0 in 0.1 M triflic acid aqueous solution) 90:10. Scan rate: 100 mV/s. Glassy carbon electrode is used as working electrode and the potential is measured vs. SSCE.

IV.2.1.2. UV-Vis

The UV-vis spectra of **2²⁺** and **3³⁺** have been recorded in acetone and acetone:water(pH=1) 80:20 respectively and are displayed in Figure 5. The region between 250 nm and 350 nm, usually displaying very intense bands due to the intraligand π→π∗ transitions, could not be registered here as they were out of the solvent range. In the region between 350 nm and 550 nm, unsymmetrical broad metal-to-ligand charge transfer (MLCT) bands appear.[17] For the chlorido-bridged complex **2²⁺** the MLCT bands are shifted to longer wavelength due to the relative destabilization of the dπ(Ru) levels provoked by the chlorido ligand with regard to the related aquo derivate **3³⁺**.

CHAPTER IV
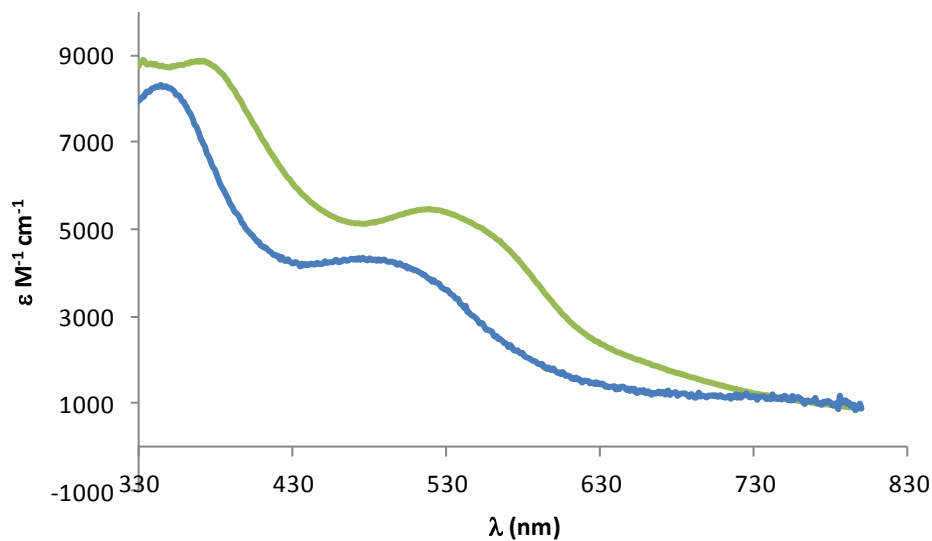
Figure 5. UV-vis spectra for **2²⁺** (green line) in a 59 μM acetone solution and **3³⁺** (blue line) in a 18 μM acetone:water(pH=1) (20:80) solution.

IV.2.2. Water Oxidation Catalysis

Complex **3³⁺** has been tested as potential catalyst towards the oxidation of water to dioxygen in the presence of $(NH_4)_2Ce^{IV}(NO_3)_6$ as sacrificial oxidant. The total gas evolved has been manometrically measured (Figure 6a) and its composition (in terms of $O_2:CO_2$ ratio) analyzed by means of *on-line* Mass Spectrometry (Figure 6b).
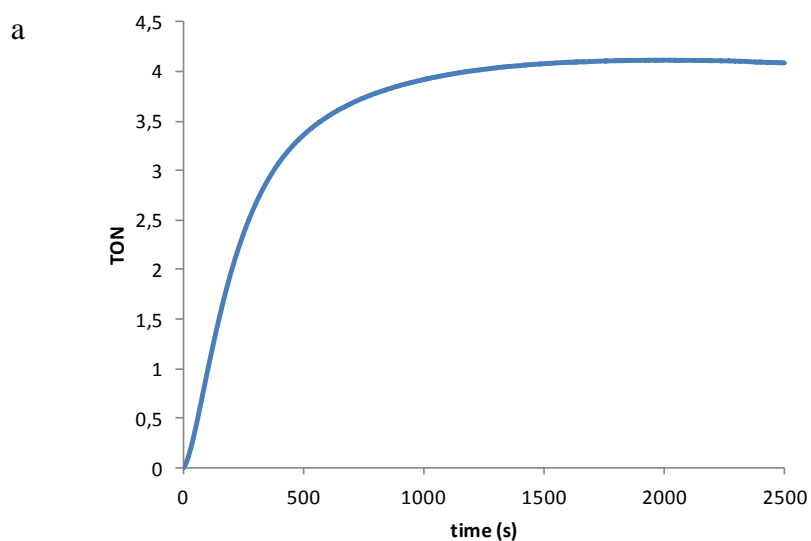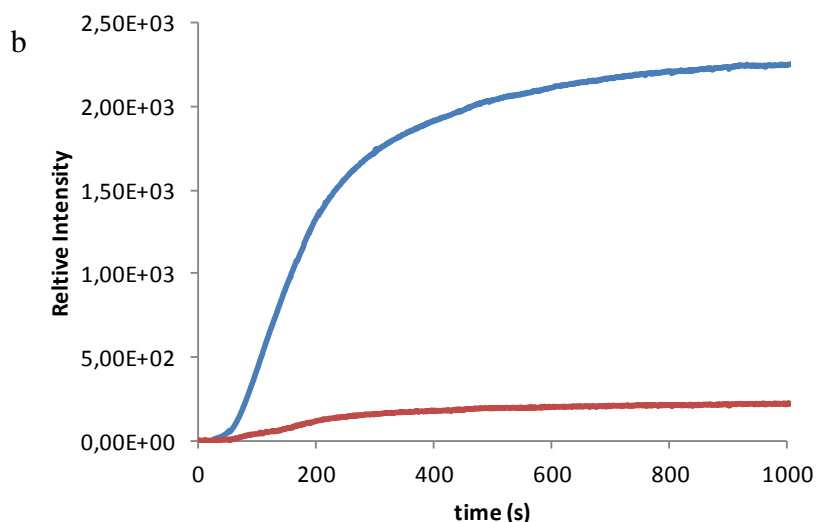
Figure 6. Chemically triggered water oxidation with 3^{3+} (1 mM) at pH =1.0 in 0.1M triflic acid solution in the presence of $(NH_4)_2Ce^{IV}(NO_3)_6$ (100 mM) as sacrificial oxidant. (a) Manometric measurment. (b) *On-line* mass spectroscopy (red line: O_2, blue line: CO_2)

In the presence of 100 equivalents of Ce(IV) at pH 1, only 4 TON of gas were produced after 30 min of reaction, corresponding to a CO_2:O_2 ratio of 90:10 as could be inferred from mass spectrometry (Figure 6b). This low activity and fast CO_2 evolution is attributed to deactivation process that can involve the degradation of 3^{3+} via intermolecular pathways between the highly oxidant Ru(IV)-O species (as previously reported for other dinuclear Ru complexes)[18] or by the direct degradation of 3^{3+} by the Ce(IV) employed as sacrificial oxidant.

IV.2.3. Epoxidation Catalysis

3^{3+} has also been tested with regards to its ability to oxidize alkenes (Scheme 3). The catalytic reactions have been carried out following the conditions exposed in Table 2, whereas the most relevant results are displayed in Table 3. The products of each catalytic reaction have been identified by GC-MS (see Figures S10-S12 in the Supporting Information for further information).
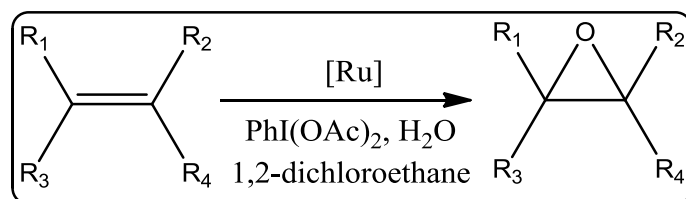
Scheme 3. Catalytic epoxidation of alkenes by Ruthenium catalysts.

Table 2.   Reaction conditions for the epoxidation of alkenes with 3^{3+}. Final volume $\approx$ 1.47 ml.

Specie	mmols	Concentration (M)	Ratio cat:X
3^{3+}	1,25E-03	8,48E-04	-
Alkene	2,5	1,7	2000
Dodecane	1	0,7	800
(diacetoxyiodo)benzene	5	3,4	4000
Water	5	3,4	4000

A vial containing 1 ml of 1,2-dichloroethane (DCE) as solvent, (diacetoxyiodo)benzene as oxidant, dodecane as internal standard, catalyst 2^{2+}, and water, was initially stirred for 120 min. This "incubation" period before substrate addition was observed to be key in order to improve the rate of the catalytic reaction. Finally, the substrate was added to the previous mixture. The excess of water is mandatory to ensure the generation of PhIO from PhI(OAc)$_2$[19] and to transform 2^{2+} into the bis-aqua derivative 3^{3+}. Figure 7 summarizes the set of reactions that take place during the catalytic epoxidation of alkenes for the proposed system.
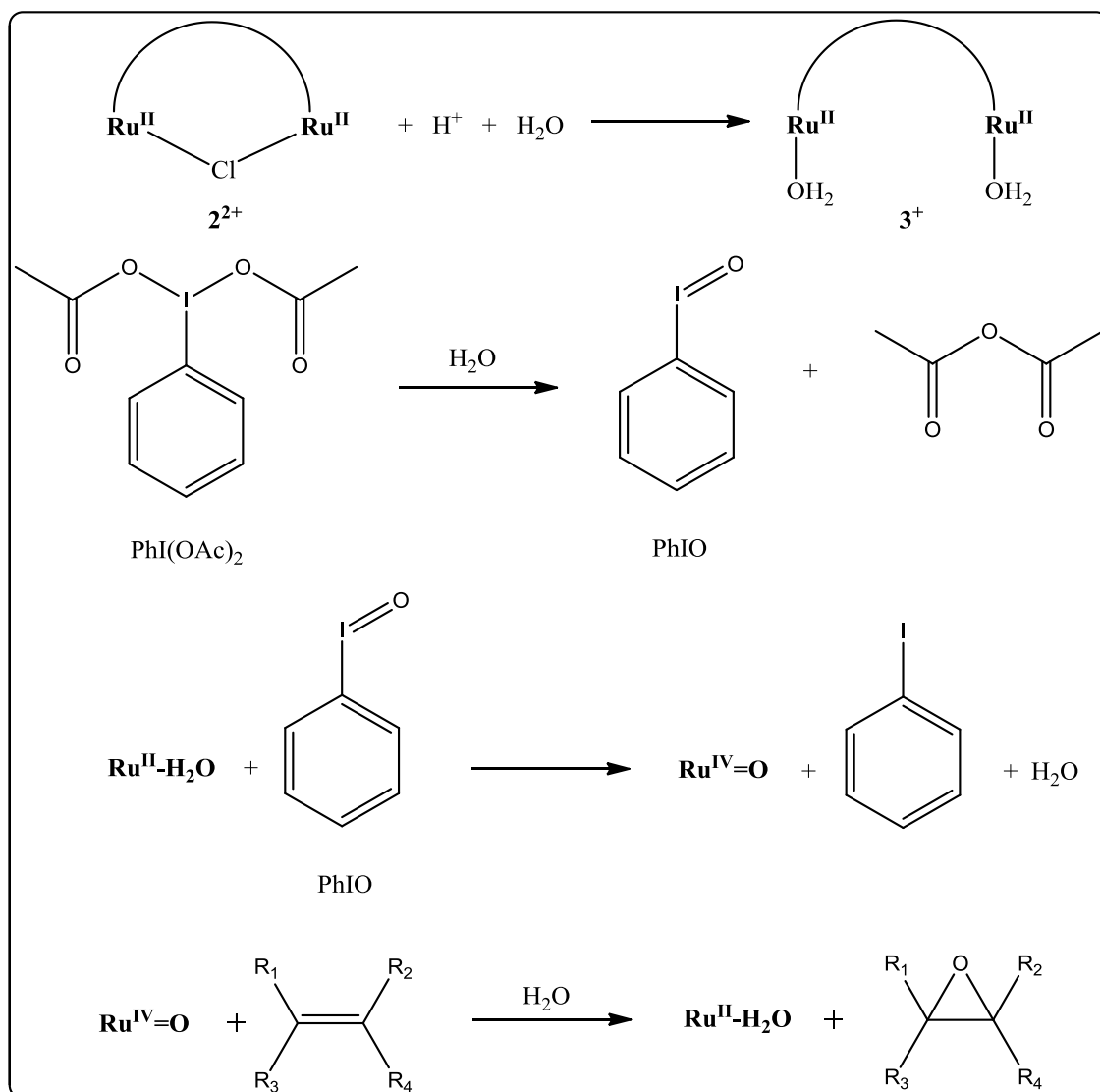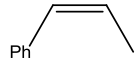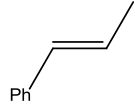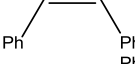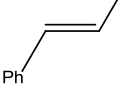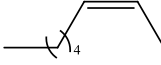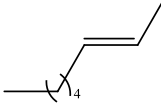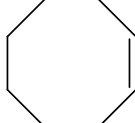
Figure 7.   Summary of the reactions taking place in the catalytic epoxidation of alkenes with 3^{3+}.

The catalytic activity of 3^{3+} towards the epoxidation of alkenes has been initially tested and optimized for the oxidation of *cis*-β-methylstyrene and the reaction evolution monitored by GC and GC-MS. The results obtained for all the alkenes tested are gathered in Table 3. As it can be observed in entry 1, the system: 3^{3+} 0.85 mM/*cis*-β-methylstyrene 1.7 M/PhI(OAc)$_2$ 3.4 M/H$_2$O 3.4 M in DCE gives 1.50 M *cis*-β-methylstyrene epoxide that represents 1760 turnover numbers (TONs) with regard to the initial catalyst in 90 minutes. After this time the conversion of the initial substrate is 100% and thus represents an epoxide selectivity of 88%. The activity of 3^{3+} for the epoxidation of a variety of alkenes is remarkable and the results are reported in entries 2-7 of Table 3. For instance, the system 3^{3+}/*cis*-2-octene generates an impressive 1.62 M

cis-2-octene oxide that represents a TON of 1900 with regard to the epoxide with an initial turnover frequency (TOFi) of 34.0 cycles per minute (see entry 5 in Table 3). Althought the results herein reported are difficult to compare with those of related complexes from the literature, due to the catalysts and oxidants used are substantially different, some conclusions can be extracted. Thus, as a general trend, the reported mononuclear species gave lower yield of epoxide and conversion of the substrate.[20] Additionally $\mathbf{3^{2+}}$ is more than 30 times faster than the best mononuclear reference; this fact suggests a potential cooperation effect between the two metal centers for the dinuclear $\mathbf{3^{3+}}$ catalyst. Potentially one of the Ru^{IV}=O groups generate a hydrogen bonding with the alkene, fixing the substrate, while the other Ru^{IV}=O group can be responsible for the oxygen atom transfer. An additional glance at Table 3 shows that with electron-donor groups $\mathbf{3^{3+}}$ performs much better than with electron-withdrawers. Thus *cis*-2-octene (entry 5) is the best whereas *trans*-stilbene (entry 4) is the worst. The latter also suffers from potential steric effects due to the bulkiness of its two phenyl rings. The electronic effects are in agreement with the electrophilic character of the Ru^{IV}=O active group proposed in related works.[11b] As can be observed in Figure 8, it is worth to mention the lower activity and selectivity towards the *trans* substrates with regard to the related *cis* counterparts, which is in agreement with the high steric constrictions imposed by the cavity of the catalyst around the active sites. Another interesting feature of the systems studied here is the stereospecific nature of the catalysis performed in the sense that no *cis*/*trans* isomerization takes place for neither the *cis*-alkenes (entries 1,3,5,7) nor the *trans*-alkenes (entries 2,4,6). This points out towards a mechanism of either (A) a concerted oxygen atom transfer from the Ru^{IV}=O active site to the double bond of the alkene or (B1) a radical path were the C-C rotation of the generated radical is much slower than the ring closing that generates the final epoxide, as shown in Figure 10.[21]

Table 3. Catalytic performance of **3³⁺** for the epoxidation of alkenes using PhI(OAc)$_2$ as oxidant in DCE (Cat:Sub:Ox. 1:2000:4000).[a]

Entry	Substrate	Substrate conversion (%)[b]	[Epoxide], M; (Selectivity, %)[c]	TON/TOF$_i$[d]
1	*cis*-β-methylstyrene	100	1.50; (88)[e]	1760/73
2	*trans*-β-methylstyrene	50	0.68; (80)[f]	800/21
3	*cis*-stilbene	100	0.41; (24)[e]	480/11
4	*trans*-stilbene	100	0.24; (14)[f]	280/4
5	*cis*-2-octene	95	1.62; (100)[e]	1900/34
6	*trans*-2-octene	42	0.71; (100)[f]	840/24
7	*cis*-cyclooctene	95	1.05; (65)[e]	1235/17

[a] Reaction conditions: **2(PF₆)₂** (1.8 mg, 1.25 E⁻³ mmols, final concentration 0.85 mM) in DCE (1 ml), substrate (2.5 mmols, 1.7 M), PhI(OAc)$_2$ (5 mmols, 3.4 M), H$_2$O (5 mmols, 3.4 M), dodecane (1 mmol, 0.68 M); final volume ≈ 1.47 ml. [b] Substrate conversion = {([substrate]$_i$ − [substrate]$_f$)/[substrate]$_i$}·100. [c] Epoxide selectivity = {[epoxide]$_f$/([substrate]$_i$ − [substrate]$_f$)}·100. [d] TON with regard to epoxide; TOFi = TON/min. [e] 100% *cis* epoxide. [f] 100% *trans* epoxide.

IV

a)
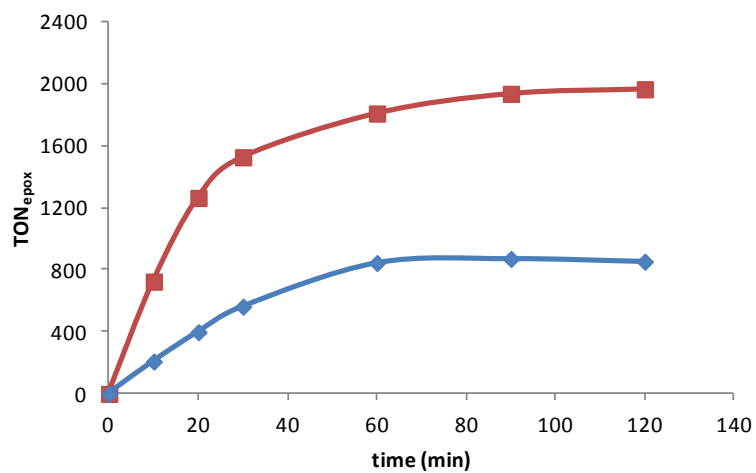
b)
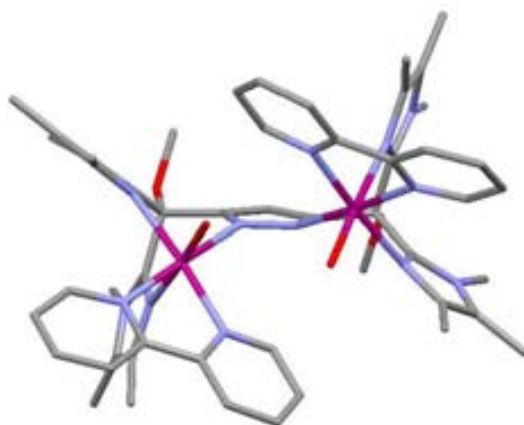
Figure 8. (a) Evolution of *cis*-β-methylstyrene oxide (red line) and *trans*-β-methylstyrene oxide (blue line) when employing $\mathbf{3^{3+}}$ as catalyst. (b) Plot of the O=Ru(IV)-Ru(IV)=O proposed structure.
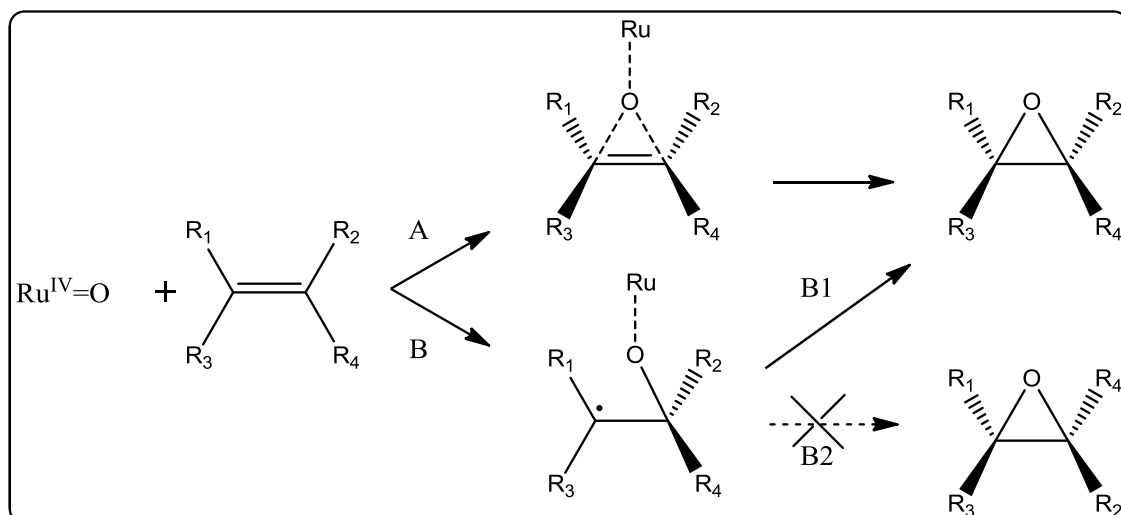
Figure 9. Proposed stereoselective (A and B1) and non-stereoselective (B2) mechanisms for the epoxidation of alkenes by $Ru^{IV}=O$ species.

IV.3. <u>Conclusions</u>

A new Ruthenium bis-facial dinuclear complex, $\mathbf{2^{2+}}$, containing the hexadentate pyrazolate-bridging ligand Hbimp and bpy as auxiliary ligands has been synthesized and fully characterized in solution by means of spectrometric, spectroscopic and electrochemical techniques. The new compound has been tested with regard to its capacity to oxidize water and alkenes. The in situ generated bis-aqua complex $\mathbf{3^{3+}}$ resulted in low effiencies and selectivities when performing as WOC, which was attributed to the intramolecular catalyst-catalyst degradation of the surrounding ligands in the harsh and highly oxidative reaction conditions. On the other hand, $\mathbf{3^{3+}}$ has shown to be an excellent catalyst for the epoxidation of a wide range of alkenes. From the scope of substrates analyzed, the following conclusions can be pointed out: (a) *cis* alkenes were epoxided faster and in higher yields than their corresponding *trans* counterparts, thus reveling the important effect of the steric hindrance around the catalytically active sites in the final catalytic output. (b) Substrates containing electron-donor groups yielded better results than those bearing electron-withdrawers, which points out the high electrophilic behavior of the $Ru^{IV}=O$ active site; (c) The catalytic systems described here are stereospecific in nature, in the sense that no *cis/trans* isomerization takes place for the c*is*-alkenes. Therefore, either a concerted oxygen atom transfer from the $Ru^{IV}=O$ active site to the alkene double bond or a radical path were the

C-C rotation of the generated radical is much slower than the ring closing that generates the final epoxide can be plausible mechanisms for this transformation. Further mechanistic work is in progress in our laboratories to unfold the elemental steps that take place in the epoxidation catalytic cycle and to fully understand the potential cooperative effects in the dinuclear catalysts.

IV.4. <u>Experimental Section</u>

Materials: All reagents used in the present work were obtained from Aldrich Chemical Co. and were used without further purification. Reagent-grade organic solvents were obtained from Scharlab. $RuCl_3 \cdot 3H_2O$ was supplied by Alfa Aesar and was used as received. Synthesis and characterization of Hbimp ligand are reported in the literature.[22] All synthetic manipulations were routinely performed under nitrogen atmosphere using Schlenk tubes and vacuum-line techniques.

Instrumentation and Measurements: UV-Vis spectroscopy was performed by a HP8453 spectrometer using 1 cm quartz cells. NMR spectroscopy was performed on a Bruker DPX 250 MHz, DPX 360 MHz or a DPX 400 MHz spectrometer or in a Varian NMR System 500MHz or 300MHz. Samples were run in $CDCl_3$, CD_3CN or acetone-d_6 with internal references. Electrospray ionization mass spectrometry (ESI-MS) experiments were carried out on an HP298s gas chromatography (GC-MS) system from the CAS-UAB. Cyclic voltammetry and Differential pulse voltammetry experiments were performed on an Ij-Cambria HI-660 potentiostat using a three-electrode cell. A glassy carbon electrode (2 mm diameter) was used as working electrode, platinum wire as auxiliary electrode and a SSCE as a reference electrode. Working electrodes were polished with 0.05 micron Alumina paste washed with distillated water and acetone before each measurement. The complex was dissolved in acetone containing the necessary amount of n-Bu_4NPF_6 (TABH) as supporting electrolyte to yield 0.1 M ionic strength solution. $E_{1/2}$ values reported in this work were estimated from CV experiments as the average of the oxidative and reductive peak potentials $(E_{p,a} + E_{p,c})/2$.

Computational Details: The density functional theory (DFT) calculations have been carried out with the hybrid B3PW91 density functional,[23] as implemented in the Gaussian 09 package.[24] The Ru atoms have been represented with the quasi-relativistic effective core pseudo-potentials (RECP) of the Stuttgart group and the associated basis sets augmented with a f polarization function ($\alpha = 1.235$).[25] The remaining atoms (H, C,

N, O, and Cl) have been represented with 6-31G(d,p) basis sets.[26] The B3PW91 geometry optimizations were performed without any symmetry constraints, and the nature of minima was checked by analytical frequency calculations.

The reported energies have been obtained including solvent effects with the polarizable continuum solvation model (PCM) using dichloromethane as a solvent,[27] via single point calculations on the B3PW91 geometries with a triple-ζ valence plus polarization basis set (TZVP keyword in Gaussian) of Ahlrichs and co-workers for H, C, N, O, and Cl,[28] and for Ru we used the small-core, quasi-relativistic Stuttgart/Dresden effective core potential, with an associated valence basis set contracted (standard SDD keywords in gaussian09),[29] using the M06 functional.[30]

Overall, the relative Gibbs energies reported in this work include energies computed using the M06/TZVP//B3PW91/6-31G(d,p) method together with solvent effects obtained at the M06/TZVP level and zero-point energies, thermal corrections, and entropy effects calculated at 298 K with the B3PW91/6-31G(d,p) method.

Synthetic preparations

{[Ru^{III}(Cl)$_2$]$_2$(μ-bimp)(μ-Cl)} (**1**): A sample of 0.382 mmols of Hbimp was solved in 40 mL of dry methanol, then 1.8 mL of MeONa 0.2108 M (0.382 mmols) were added. The mixture was stirred at RT during 10 minutes, and 200 mg (0.765 mmols) of RuCl$_3$·3H$_2$O were added. The resulting solution was heated at reflux overnight while vigorous magnetic stirring was maintained. After this time the volume was reduced in the rotary evaporator and diethyl ether was added. The resulting solid was filtered and washed with diethyl ether. Yield: 336 mg (91%). ESI-MS (MeOH): *m/z*= 926.1 ([M-2Cl+MeO$^-$]$^+$)

trans-{[Ru^{II}(bpy)]$_2$(μ-bimp)(μ-Cl)}$^{2+}$ (**2(PF$_6$)$_2$**). A mixture of 300 mg (0.311 mmols) of complex **1**, 39 mg (0.933) of LiCl and 172.5 μl (1.244 mmols) of NEt$_3$ were solved in 90 ml of dry methanol. The mixture was stirred during 30 min and then 96 mg (0.622 mmols) of bpy were added. The resulting solution was overnight stirred at r.t.. After this time the crude was filtered and 3ml of NH$_4$PF$_6$ saturated aqua solution and 30 ml of water were added to the filtrate. The volume was reduced until a violet precipitate appeared, which was filtered and washed with cold diethyl ether. Yield: 200 mg (45%).^{1}H NMR (400MHz, [D$_6$]acetone): δ = 8.76 (d, 2H, J = 5.20 Hz, H20 or H23),

8.53 (d, 2H, J = 5.20 Hz, H20 or H23), 8.36 (d, 2H, J = 7.30 Hz, H17 or H26), 8.20 (d, 2H, J = 7.30 Hz, H17 or H26), 7.88 (t, 2H, J = 8.90 Hz, J = 7.75 Hz, H18 or H25) 7.77 (t, 2H, J = 8.90 Hz, J = 7.75 Hz, H18 or H25), 7.36 (t, 2H, H19 or H24), 7.34 (t, 2H, H19 or H24), 7.26 (s, 1H, H1), 4.25 (s, 3H, H16), 4.05 (s, 3H, H9 or H15), 3.90 (s, 3H, H9 or H15), 2.02, 1.96, 1.93, 0.16.). $^{13}C\{^1H\}$ NMR (400MHz, [D_6]acetone): δ = 161,57 (C21/22), 161,07 (C21/22), 157,32 (C20/23), 156,51 (C20/23), 154,86 (C2), 145,41 (C4/10), 143,32 (C4/10), 137,37 (C7/13), 136,06 (C7/13), 135,60, (C18/25), 134,53 (C18/25), 128,47 (C5/11), 126,66 (C19/24), 125.80 (C5/11), 124,30 (C17/24), 124,07 (C19/24), 122,88 (C17/24), 106,28 (C1), 85,35 (C3), 57,03 (C16), 33,05 (C9/15), 32,83 (C9/15), 13,62, 9,13, 8,67, 8,51. ESI-MS (MeOH): *m/z*= 1283.2 ([M-PF_6]$^+$)

Acknowledgements

IV.5.   <u>References</u>

[1] Sheldon, R.A. *J. Mol. Catal.* **1980**, *7*, 107-126.

[2] Joergensen, K.A. *Chem. Rev*. **1989**, *89*, 431-458

[3] Cavani, F.; Teles, J.H., *ChemSusChem*, **2009**, *2*, 508.

[4] Roberts, S.M.; Whittall, J., Eds., *Catalysts for fine chemical synthesis: Regio- and stereo-controlled oxidations and reductions*, Vol. 5; John Wiley Sons, Ltd: England, **2007**.

[5] Nijhuis, T.A.; Makkee, M.; Moulijn, J.A.; Weckhuysen, B.M., Ind. Eng. Chem. Res., 2006, 45, 3447.

[6] (a) Keene, F. R. *Coord. Chem. Rev.* **1999**, *187*, 121. (b) Wang G. Z., A. U., Bäckvall J. E. *J. Chem. Soc. Chem. Commun.* **1994**. (c) Csjernyik, G.; Ell, A. H.; Fadini, L.; Pugin, B.; Baeckvall, J.-E. *J. Org. Chem.* **2002**, *67*, 1657. (d) Bäckvall J. E., C. R. L., Karlsson U. *J. Chem. Soc. Chem. Commun.* **1991**, 47. (e) Murahashi, S.-I.; Komiya, N.; Wiley-VCH Verlag GmbH & Co. KGaA: 2004, p 165. (f) Murahashi, S.; Naota, T. *Adv. Met.-Org. Chem.* **1994**, *3*, 225. (g) Friedrich, H. B. *Platinum Met. Rev.* **1999**, *43*, 94. (h) Murahashi, S.; Naota, T. *Sekiyu Gakkaishi* **1991**, *34*, 1. (i)   Murahashi, S. I.; Naota, T. *Zh. Org. Khim.* **1996**, *32*, 223.

[7] (a) Mlodnicka, T.; James, B. R. *Catal. Met. Complexes* **1994**, *17*, 121. (b) Benet-Buchholz, J.; Comba, P.; Llobet, A.; Roeser, S.; Vadivelu, P.; Wiesner, S. *Dalton Trans.* **2010**, *39*, 3315. (c) Hamelin, O.; Ménage, S. p.; Charnay, F.; Chavarot, M.; Pierre, J.-L.; Pécaut, J.; Fontecave, M. *Inorg. Chem.* **2008**, *47*, 6413. (d) Huynh, M. H. V.; Witham, L. M.; Lasker, J. M.; Wetzler, M.; Mort, B.; Jameson, D. L.; White, P. S.; Takeuchi, K. J. *J. Am. Chem. Soc.* **2003**, *125*, 308.

[8] (a) Gersten, S. W.; Samuels, G. J.; Meyer, T. J. *J. Am. Chem. Soc.* **1982**, *104*, 4029. (b) Gilbert, J. A.; Eggleston, D. S.; Murphy, W. R., Jr.; Geselowitz, D. A.; Gersten, S. W.; Hodgson, D. J.; Meyer, T. J. *J. Am. Chem. Soc.* **1985**, *107*, 3855. (c) Sala, X.; Romero, I.; Rodriguez, M.; Escriche, L.; Llobet, A. *Angew. Chem., Int. Ed.* **2009**, *48*, 2842. (d) Xu, Y.; Fischer, A.; Duan, L.; Tong, L.; Gabrielsson, E.; Aakermark, B.; Sun, L. *Angew. Chem., Int. Ed.* **2010**, *49*, 8934. (e) Sens, C.; Romero, I.; Rodríguez, M.; Llobet, A.; Parella, T.; Benet-Buchholz, J. *J. Am. Chem. Soc.* **2004**, *126*, 7798. (f) Tseng, H.-W.; Zong, R.; Muckerman, J. T.; Thummel, R. *Inorg. Chem.* **2008**, *47*, 11763. (g) Xu, Y.; Aakermark, T.; Gyollai, V.; Zou, D.; Eriksson, L.; Duan, L.; Zhang, R.; Aakermark, B.; Sun, L. *Inorg. Chem.* **2009**, *48*, 2717. (h) Zong, R.; Thummel, R. P. *J. Am. Chem. Soc.* **2005**, *127*, 12802. (i) Concepcion, J. J.; Jurss, J. W.; Templeton, J. L.; Meyer, T. J. *J. Am. Chem. Soc.* **2008**, *130*, 16462. (j) Duan, L.; Bozoglian, F.; Mandal, S.; Stewart, B.; Privalov, T.; Llobet, A.; Sun, L. *Nat Chem* **2012**, *4*, 418.

[9] (a) Bäckvall, J.-E.; Editor *Modern Oxidation Methods, 2nd Completely Revised*; Wiley-VCH Verlag GmbH & Co. KGaA, 2010. (b) Murahashi, S.-I.; Komiya, N. *Ruthenium in Organic Synthesis*; Wiley-VCH, Weinheim, 2004. (c) Bhor, S.; Tse, M. K.; Klawonn, M.; Doebler, C.; Maegerlein, W.; Beller, M. *Adv. Synth. Catal.* **2004**, *346*, 263. (d) Porter, M. J.; Skidmore, J. *Chem. Commun.* **2000**, 1215. (e) Serrano, I.; López, M. I.; Ferrer, I. n.; Poater, A.; Parella, T.; Fontrodona, X.; Solà, M.; Llobet, A.; Rodríguez, M.; Romero, I. *Inorg. Chem.* **2011**, *50*, 6044. (f) Groves, J. T.; Quinn, R. *J. Am. Chem. Soc.* **1985**, *107*, 5790. (g) Bailey, C. L.; Drago, R. S. *J. Chem. Soc., Chem. Commun.* **1987**, 179. (h) Barf, G. A.; Sheldon, R. A. *J. Mol. Catal. A: Chem.* **1995**, *102*, 23. (i) Arends, I. W. C. E.; Kodama, T.; Sheldon, R. A. *Top. Organomet. Chem.* **2004**, *11*, 277. (j) Stultz, L. K.; Binstead, R. A.; Reynolds, M. S.; Meyer, T. J. *J. Am. Chem. Soc.* **1995**, *117*, 2520.

[10] García-Antón, J.; Bofill, R.; Escriche, L.; Llobet, A.; Sala, X *Eur. J. Inorg. Chem.***2012**, *30*,4775–4789

[11] (a) Francàs, L., Universitat Autònoma deBarcelona, **2011**. (b) Di Giovanni, C., Universitat Rovira i Virgili, **2012**.

[12] Mola, J.; Dinoi, C.; Sala, X.; Rodriguez, M.; Romero, I.; Parella, T.; Fontrodona, X.; Llobet, A. *Dalton Trans*., **2011**, *40*, 3640.

[13] Maji, S.; Vigara, L.; Cottone, F.; Bozoglian, F.; Benet-Buchholz, J.; Llobet, A. *Angew. Chem.* **2012**, *124*, 6069-6072.

[14] Kaveevivitchai, N.; Ruifa Zong, R.C.; El Ojaimi, M.; Thummel, R.P. *J. Am. Chem. Soc.* **2012**, *134*, 10721−10724

[15] Wasylenko, D.J.; Ganesamoorthy, C.; Koivisto, B.D.; Berlinguette, C.P. *Eur. J. Inorg. Chem.* **2010**, 3135–3142.

[16] Sens, C.; Romero, I.; Rodríguez M.; Llobet A.; Parella, T.; Benet-Buchholz, J. *J. Am. Chem. Soc.* **2004**, *126*, 7798-7799.

[17] (a) Rodríguez, M.; Romero, I.; Llobet, A. *Inorg. Chem.* **2001**, 40, 4150-4156. (b) Takeuchi, K.J.; Thompson, M.S.; Pipes, D.W.; Meyer, T.J. *Inorg. Chem.* **1984**, 23, 1845-1851.

[18] Francas, L.; Sala, X.; Escudero-Adan, E.; Benet-Buchholz, J.; Escriche, L.; Llobet, A. *Inorg. Chem.* **2011**, 50(7), 2771-2781.

[19] In, J.-H.; Park, S.-E.; Song, R.; Nam, W. *Inorg. Chim. Acta* **2003**, *343*, 373.

[20] (a) Vaquer, L., Universitat Autònoma de Barcelona, **2011**. (b) Sala, X.; Santana, N.; Serrano, I.; Plantalech, E.; Romero, I.; Rodríguez, M.; Llobet, A.; Jansat, S.; Gómez, M.; Fontrodona, X. *Eur. J. Inorg. Chem.* **2007**, 5207–5214. (c) Serrano, I.; Sala, X.; Plantalech, E.; Rodríguez, M.; Romero, I.;

Jansat, S.; Gómez,M.; Parella, T.; Stoeckli-Evans, H.; Solans, X.; Font-Bardia, M.; Vidjayacoumar, B.; Llobet, A. *Inorg. Chem.,* **2007**, *46*, 5381-5389.

[21] (a) Muray, E.; Illa, O.; Castillo, J. A.; Alvarez-Larena, A.; Bourdelande, J. L.; Branchadell, V.; Ortuno, R. M. *J. Org. Chem.* **2003**, *68*, 4906. (b) Kumar, D.; de, V. S. P.; Shaik, S. *Chem.--Eur. J.* **2005**, *11*, 2825. (c) Baciocchi, E.; Boschi, T.; Cassioli, L.; Galli, C.; Jaquinod, L.; Lapi, A.; Paolesse, R.; Smith, K. M.; Tagliatesta, P. *Eur. J. Org. Chem.* **1999**, 3281. (d) Zona, T. A.; Goodman, J. L. *J. Am. Chem. Soc.* **1995**, *117*, 5879. (e) Srinivasan, K.; Michaud, P.; Kochi, J. K. *J. Am. Chem. Soc.* **1986**, *108*, 2309.

[22] Müller, H.; Bauer-Siebenlist, B.; Csapo, E.; Dechert, S.; Farkas, E.; Meyer, F. *Inorg. Chem.* **2008**, *47*, 5278-5292.

[23] (a) Becke, A. D. *J. Chem. Phys.* **1993**, *98*, 5648-5652. (b) Perdew, J. P.; Wang, Y. *Phys. Rev. B* **1992**, *45*, 13244-13249.

[24] Gaussian 09, Revision A.1, Frisch, M. J.; Trucks, G. W.; Schlegel, H. B.; Scuseria, G. E.; Robb, M. A.; Cheeseman, J. R.; Scalmani, G.; Barone, V.; Mennucci, B.; Petersson, G. A.; Nakatsuji, H.; Caricato, M.; Li, X.; Hratchian, H. P.; Izmaylov, A. F.; Bloino, J.; Zheng, G.; Sonnenberg, J. L.; Hada, M.; Ehara, M.; Toyota, K.; Fukuda, R.; Hasegawa, J.; Ishida, M.; Nakajima, T.; Honda, Y.; Kitao, O.; Nakai, H.; Vreven, T.; Montgomery, Jr., J. A.; Peralta, J. E.; Ogliaro, F.; Bearpark, M.; Heyd, J. J.; Brothers, E.; Kudin, K. N.; Staroverov, V. N.; Kobayashi, R.; Normand, J.; Raghavachari, K.; Rendell, A.; Burant, J. C.; Iyengar, S. S.; Tomasi, J.; Cossi, M.; Rega, N.; Millam, J. M.; Klene, M.; Knox, J. E.; Cross, J. B.; Bakken, V.; Adamo, C.; Jaramillo, J.; Gomperts, R.; Stratmann, R. E.; Yazyev, O.; Austin, A. J.; Cammi, R.; Pomelli, C.; Ochterski, J. W.; Martin, R. L.; Morokuma, K.; Zakrzewski, V. G.; Voth, G. A.; Salvador, P.; Dannenberg, J. J.; Dapprich, S.; Daniels, A. D.; Farkas, Ö.; Foresman, J. B.; Ortiz, J. V.; Cioslowski, J.; Fox, D. J. Gaussian, Inc., Wallingford CT, 2009.

[25] (a) Andrae, D.; Haussermann, U.; Dolg, M.; Stoll, H.; Preuss, H. *Theor. Chim. Acta* **1990**, *77*, 123-141. (b) Bergner, A.; Dolg, M.; Kuchle, W.; Stoll, H.; Preuss, H. *Mol. Phys.* **1993**, *80*, 1431-1444.

[26] (a) Hehre, W. J.; Ditchfield, R.; Pople, J. A. *J. Chem. Phys.* **1972**, *56*, 2257-2261. (b) Hariharan, P. C.; Pople, J. A. *Theor. Chim. Acta* **1973**, *28*, 213-222.

[27] (a) Barone, V.; Cossi, M. *J. Phys. Chem. A* **1998**, *102*, 1995-2001. (b) Tomasi, J.; Persico, M. *Chem. Rev.* **1994**, *94*, 2027-2094.

[28] Schaefer, A.; Horn, H.; Ahlrichs, R. *J. Chem. Phys.* **1992**, *97*, 2571-2577.

[29] (a) Haeusermann, U.; Dolg, M.; Stoll, H.: Preuss, H. *Mol. Phys.* **1993**, *78*, 1211-1224. (b) Kuechle, W.; Dolg, M.; Stoll, H.; Preuss, H. *J. Chem. Phys.* **1994**, *100*, 7535-7542. (c) Leininger, T.; Nicklass, A.; Stoll, H.; Dolg, M.; Schwerdtfeger, P. *J. Chem. Phys.* **1996**, *105*, 1052-1059.

[30] Zhao, Y.; Truhlar, D. *Theo. Chem. Acc.* **2008**, *120*, 215-241.

IV.6.   <u>**Supporting Information**</u>

- DFT calculations

- NMR

- Electrochemistry

- ESI-MS

- GC-MS chromatograms

IV

Figure S1 Plot of *bis*-H_2O front view (top) and pyrazole front view (bottom) of the proposed isomeric structures of *cis* (left) and *trans,fac*-$\{[Ru^{II}(bpy)(H_2O)]_2(\mu\text{-bimp})\}^{3+}$ (right), **3^{3+}**.
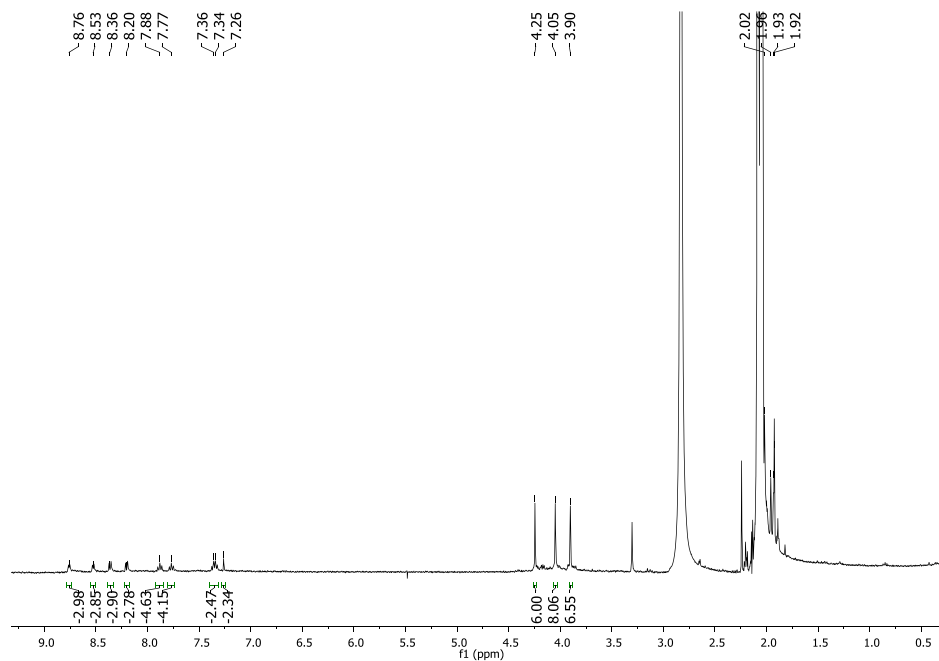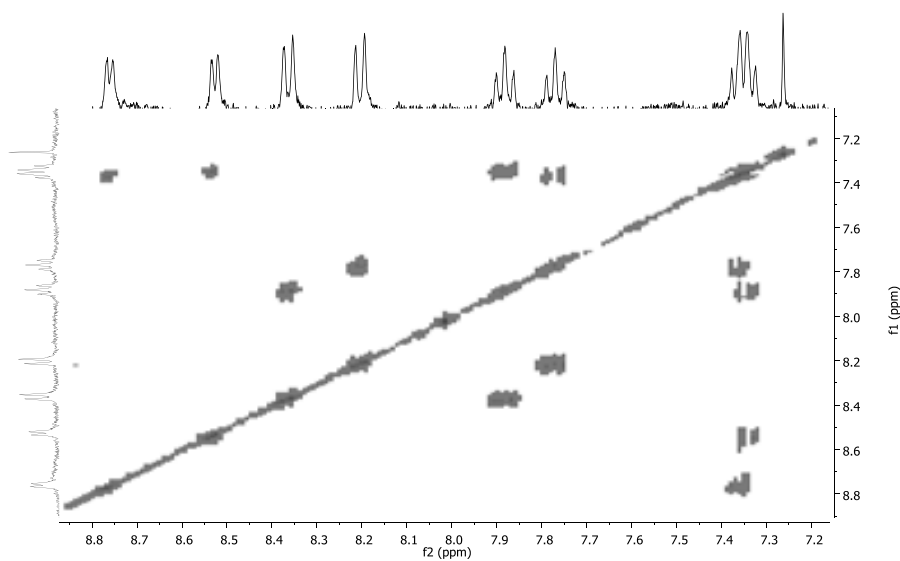

cis   *trans*

cis   *trans*
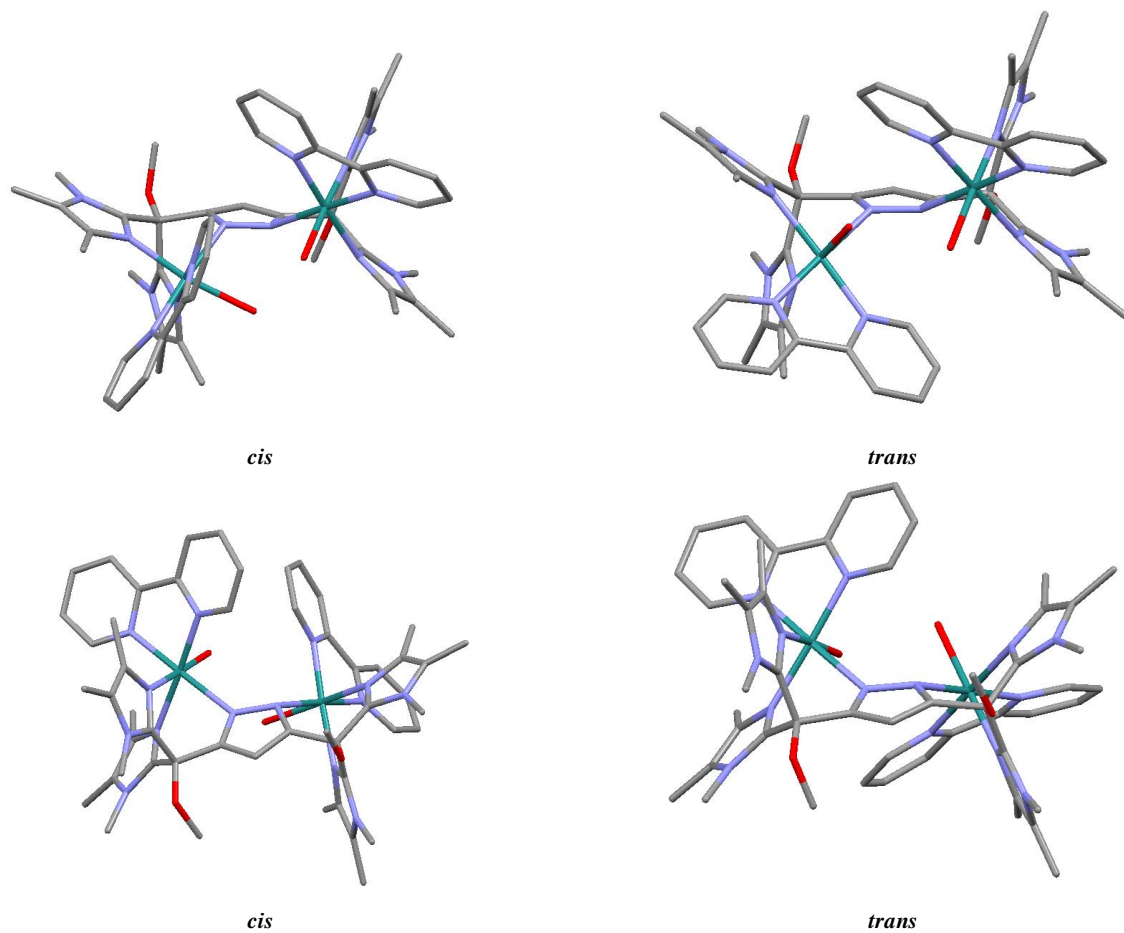
Figure S2 1D and 2D NMR spectra (400 MHz, 298 K, Acetone-d6) for **2^{2+}**: (a) ^{1}H-NMR, (b) COSY, (c) ^{13}C-{^{1}H}-NMR, (d) HSQC-NMR (aromatic region), (e) HMBC-NMR (aromatic region).

(a)

(b)

IV

(c)
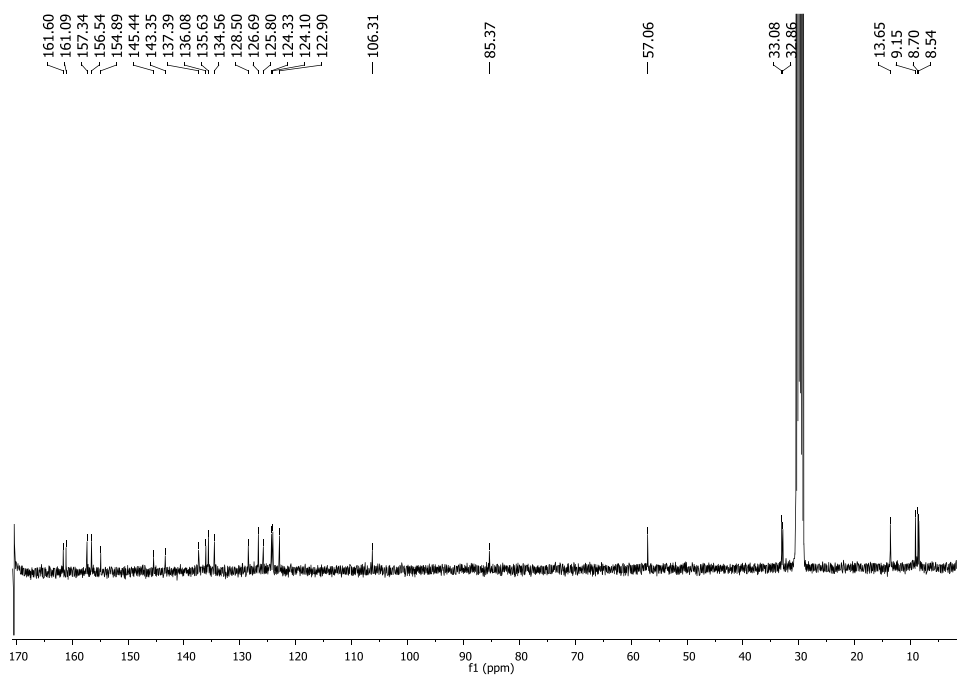
(d)
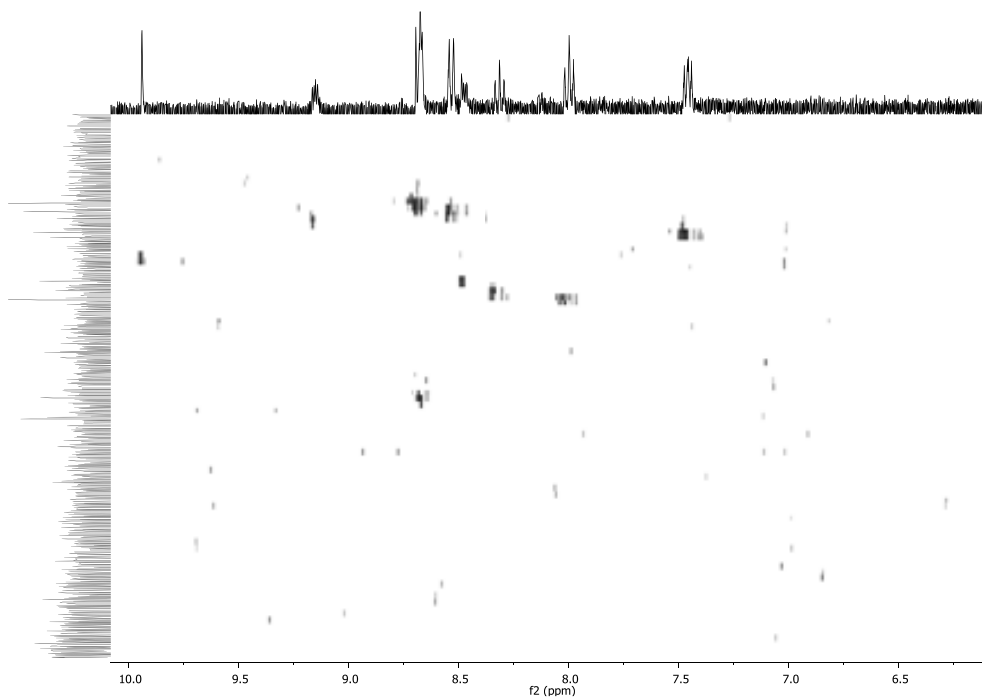
(e)
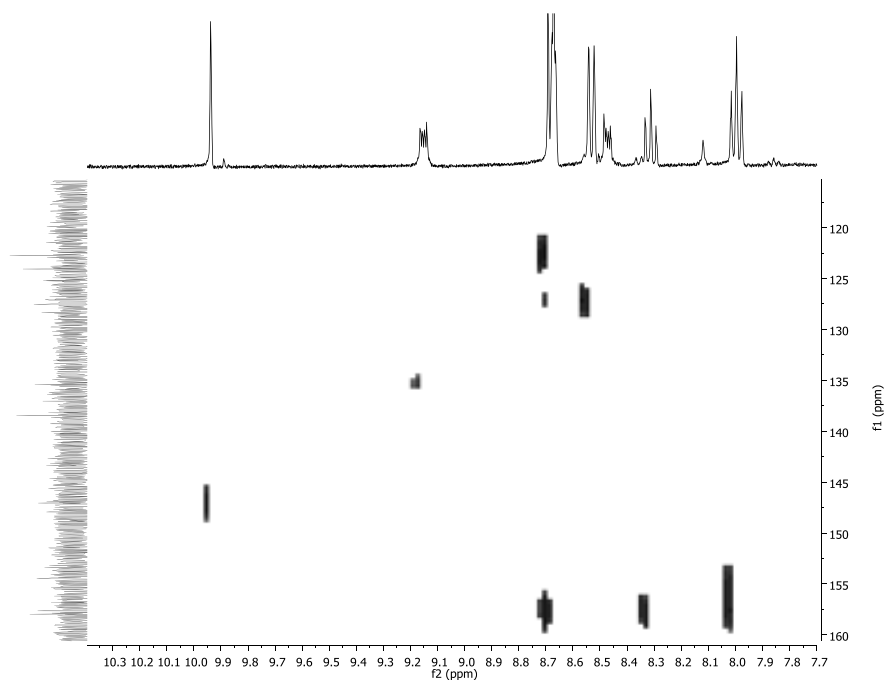
Figure S3 DPV for 2^{2+} in 0.1 M *n*-Bu$_4$NPF$_6$ in acetone at 100 mV/s scan rate. Glassy carbon electrode is used as working electrode and the potential is measured s. SSCE.

IV
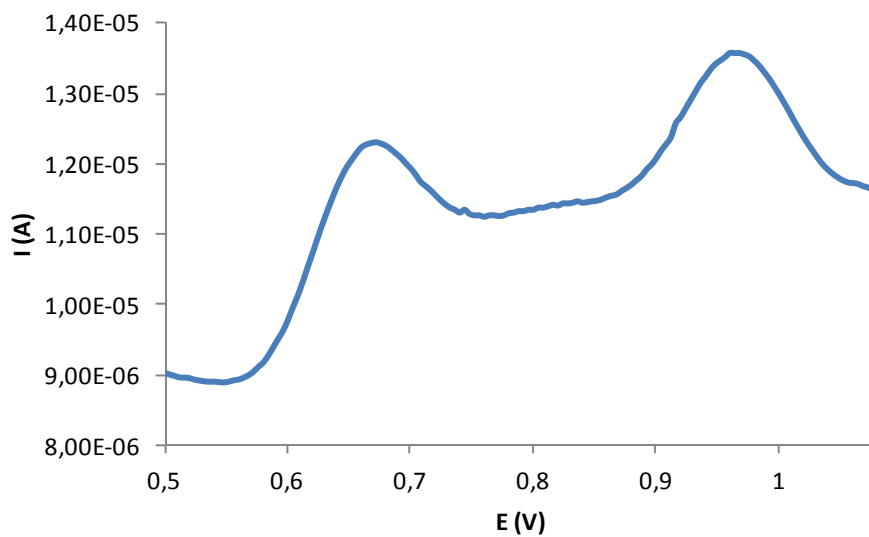
Figure S4 CV for **2^{2+}** in 0.1 M *n*-Bu$_4$NPF$_6$ in DCM at 100 mV/s scan rate. Glassy carbon electrode is used as working electrode and the potential is measured vs. SSCE.
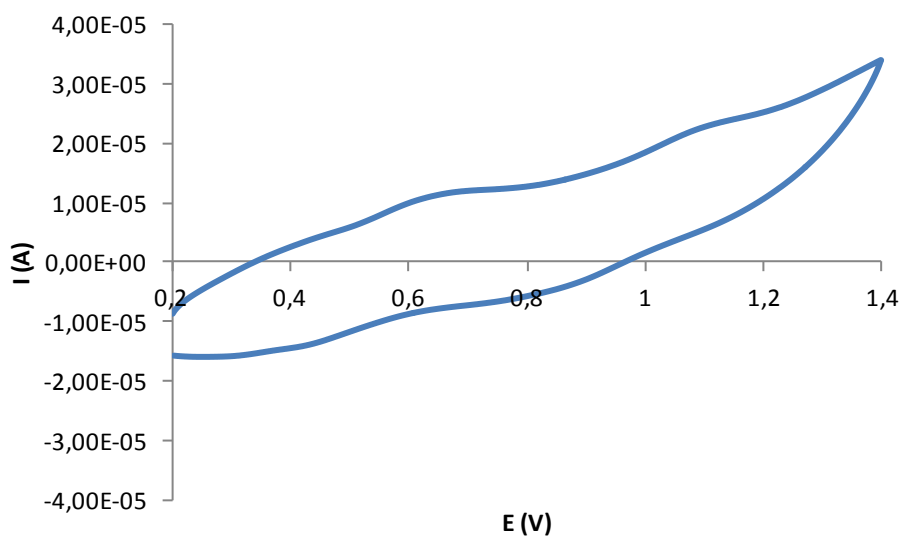
Figure S5 DPV for **2^{2+}** in 0.1 M *n*-Bu$_4$NPF$_6$ in DCM at 100 mV/s scan rate. Glassy carbon electrode is used as working electrode and the potential is measured vs. SSCE.
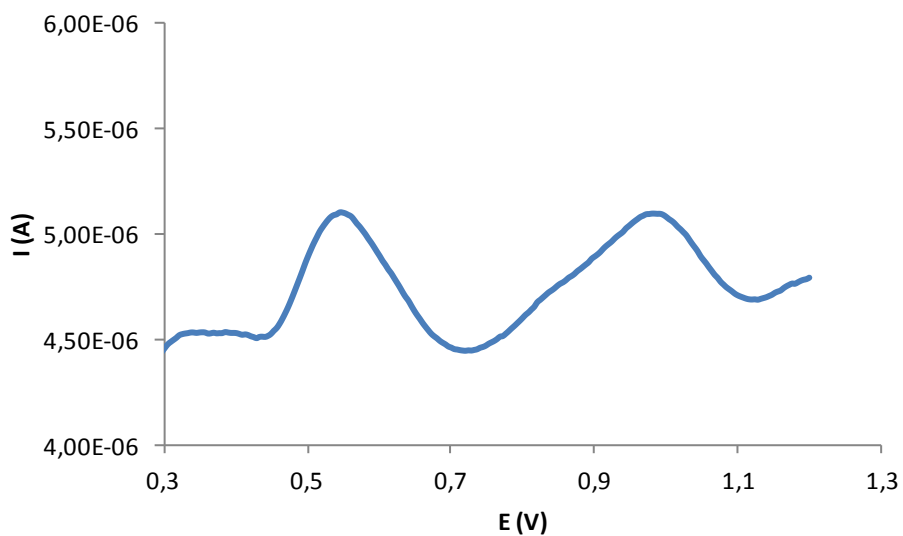
Figure S6 CV for 3^{3+} in a mixture acetone:water (pH = 1.0 in 0.1 M triflic acid aqueous solution) 90:10. Scan rate: 100 mV/s. Glassy carbon electrode is used as working electrode and the potential is measured vs. SSCE.

IV
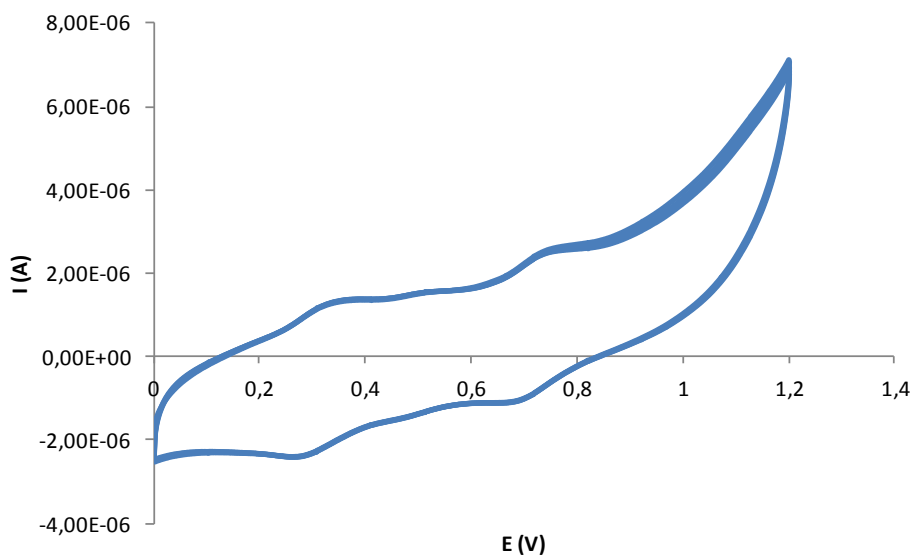
Figure S7 Mass Spectra for complex **1**.
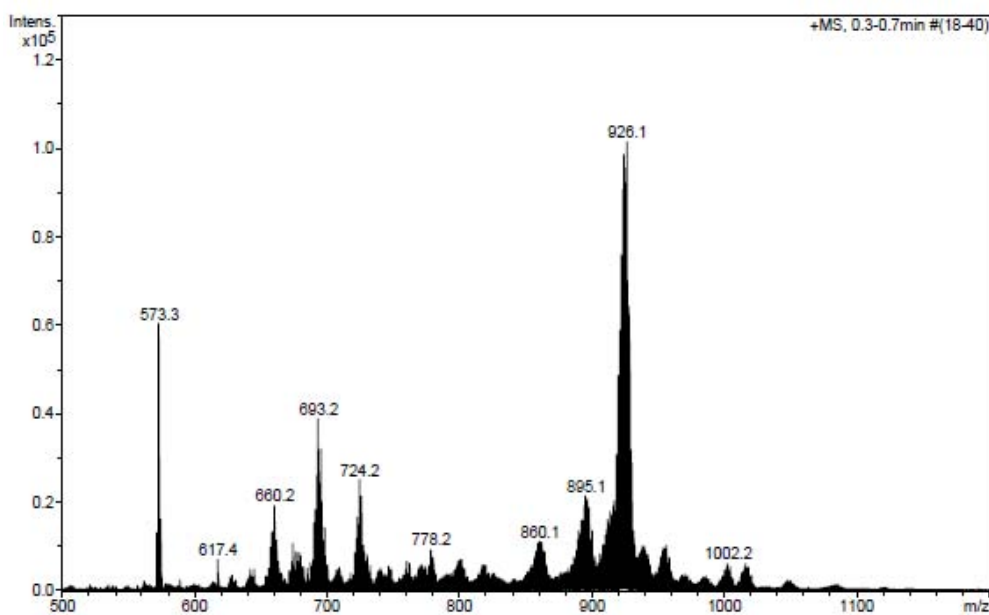
Figure S8 Mass Spectra for complex **2²⁺**.
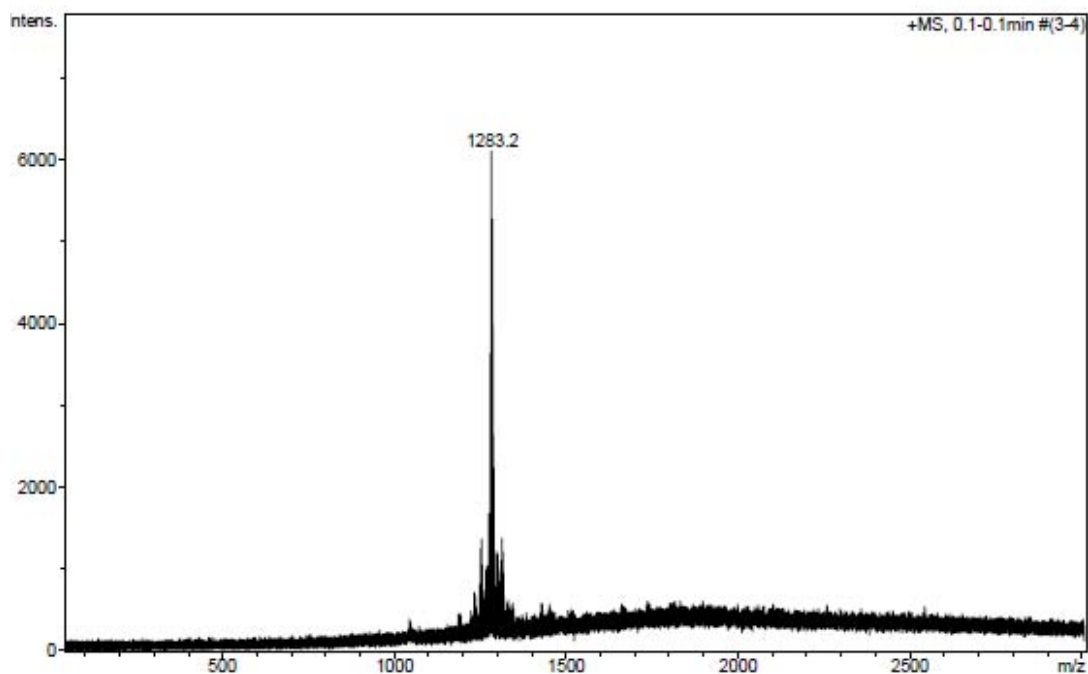
Figure S9 Experimental (right side) and theoretical zoom (left side) Mass Spectra for complex **2²⁺**.
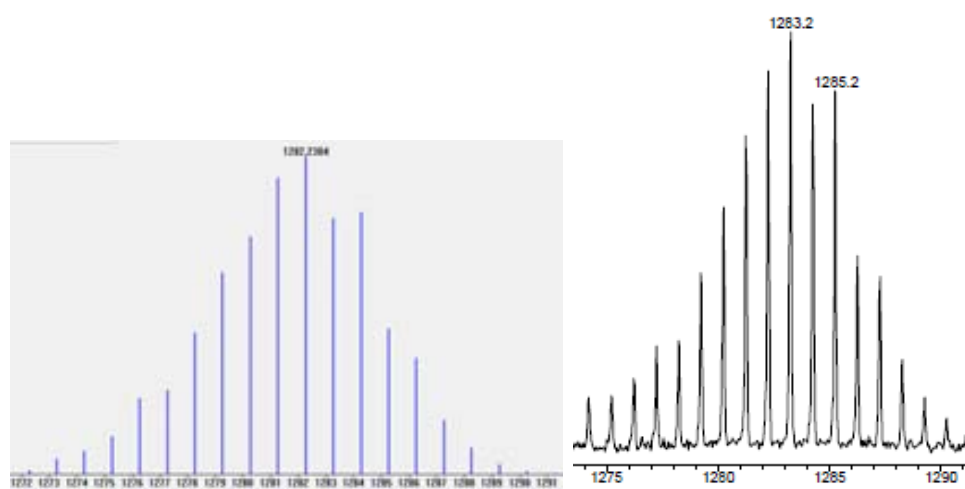
Figure S10 GC-MS chromatogram for the catalytic performance of *cis-* and *trans-*β-methylstyrene with **3³⁺**.
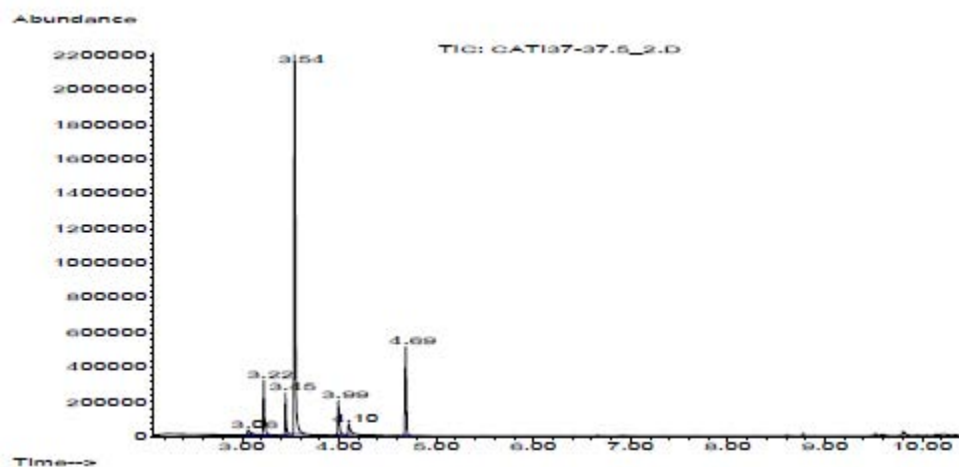
Figure S11 GC-MS chromatogram for the catalytic performance of *trans-*2-octene with **3³⁺**.

IV
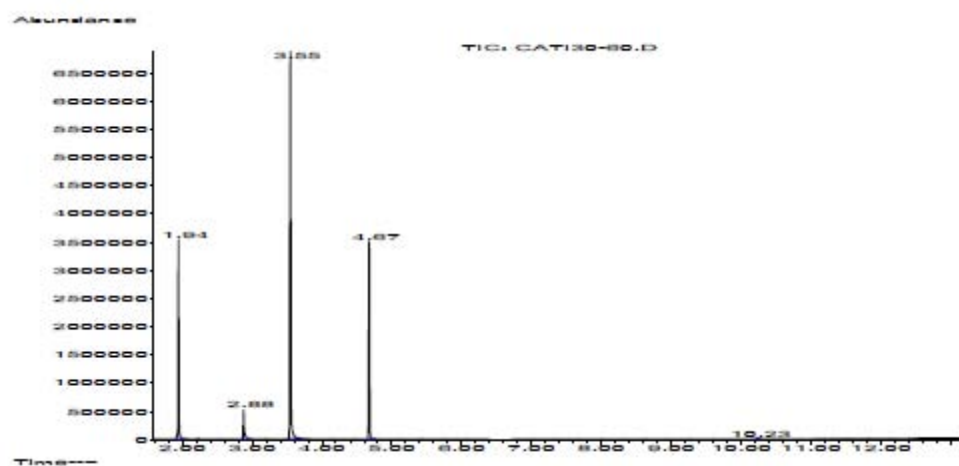
Figure S12 GC-MS chromatogram for the catalytic performance of *cis*-stilbene with **3**[3+].
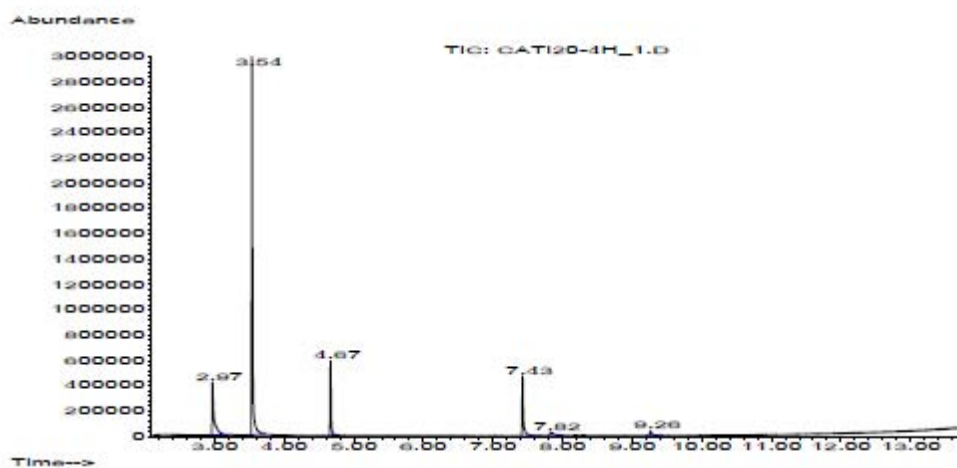
CHAPTER V

Towards new Phthalazine-Triazole N/C-hybrid Ligands:
Synthesis, Coordination Chemistry and Future Prospects
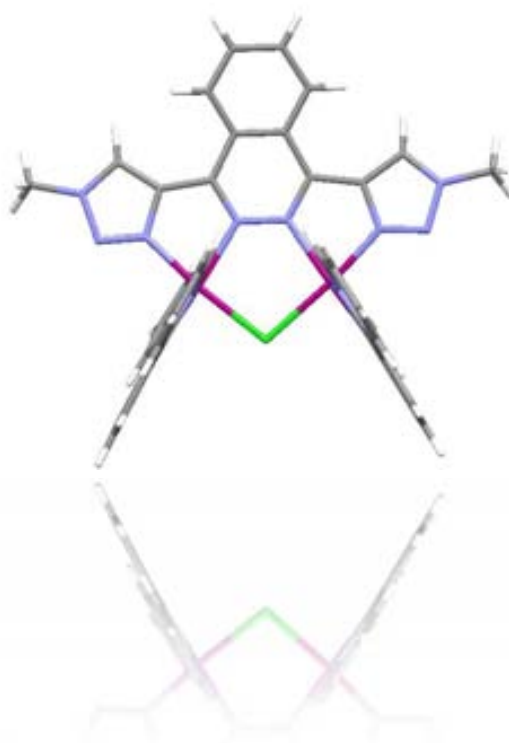
The synthesis of a new family of tetradentate bridging phthalazine-triazole ligands capable to coordinate a metal centre *via* both N and C atoms has been planned and attempted. The synthesis and characterization of a new dinuclear Ru complex containing one of these ligands is here reported and further discussed in this chapter. The work herein described was initially designed and performed in Prof. Martin Albrecht's laboratory at UCD (University College Dublin) during a four months stage of the candidate.

TABLE OF CONTENTS

CHAPTER V. Towards new Phthalazine-Triazole N/C-hybrid Ligands: Synthesis, Coordination Chemistry and Future Prospects

V

V.1.   __Introduction__

A new family of mononuclear iridium complexes containing carbene ligands and capable of oxidize water to dioxygen, likewise the one shown in Chart 1 (**A**), has been recently developed.[1] Because of the multistep redox processes involved in water oxidation, abnormally bound N-heterocyclic carbenes (NHCs) are considered to be advantageous spectator ligands. Abnormal carbenes, while being formally neutral donors, have large contribution from zwitterionic resonance forms,[2] which may assist in stabilizing different metal oxidation states when coordinated to an appropriate transition metal. In addition, those ligands may serve as a transient reservoir of both positive and negative charge, thus providing synergistic effects similar to those observed in bi- and multimetallic complexes.[3]

On the other hand, Sun & co-workers reported complex **B** (Chart 1) in 2010 with a performance in water oxidation catalysis of about 10000 TON.[4] In this case a bis-pyridyl-carboxylate phthalazine ligand behaves as a bridge between both ruthenium metals and contributes with an important sigma donor effect through the anionic carboxylate groups. Both the phthalazine moiety and the carboxylic groups play a significant role in the modification of the electronic properties of the ruthenium metals, thus enhancing the catalytic activity of the complex with regards to other structurally related compounds.[5,6]
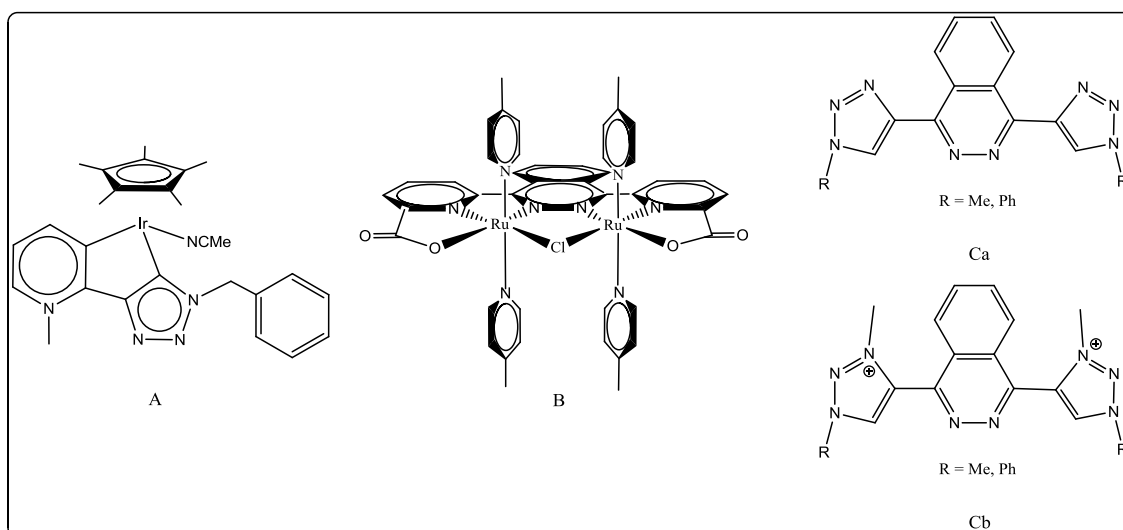

Chart 1.   (A, B) Previously reported Ir and Ru catalysts relevant for this chapter. (Ca and Cb) New bridging ligands proposed for this work.

Based on these previous examples, herein we present the synthesis and characterization of a new family of bridging ligands with combined N/C-donor moieties and the subsequent preparation of the corresponding ruthenium dinuclear complexes. Therefore, the new bridging ligands proposed (**Ca** and **Cb,** Chart 1) preserve the phthalazine scaffold of the Sun's system (**B**, Chart 1) as central unit and replace its donor pyridyl-carboxylate grups by triazole scaffolds (**Ca**), potentially able to function as abnormal-NHCs after N-alkylation (**Cb**). These new bridging ligands merge our knowledge in N-donor ligands and Ru dinuclear complexes with Prof. Albrecht's know-how in NHCs.[7] *

The alkylation (**Cb**) or not (**Ca**) of the free nitrogen atoms of the triazole rings should allow us preparing ruthenium complexes with N-N/N-N or C-N/N-C coordination patterns that could then be evaluated and compared as water oxidation catalysts.

---

* The work herein presented is the fruit of a four months stay of the candidate in Prof. Martin Albrecht's laboratory at UCD (University College Dublin).

V.2.   **Results & Discussion**

V.2.1.   **Ligand Synthesis**

The synthesis of ligands **2a/2b** and **3a/3b** was initially proposed by means of the retrosynthetic route shown in Scheme 1.
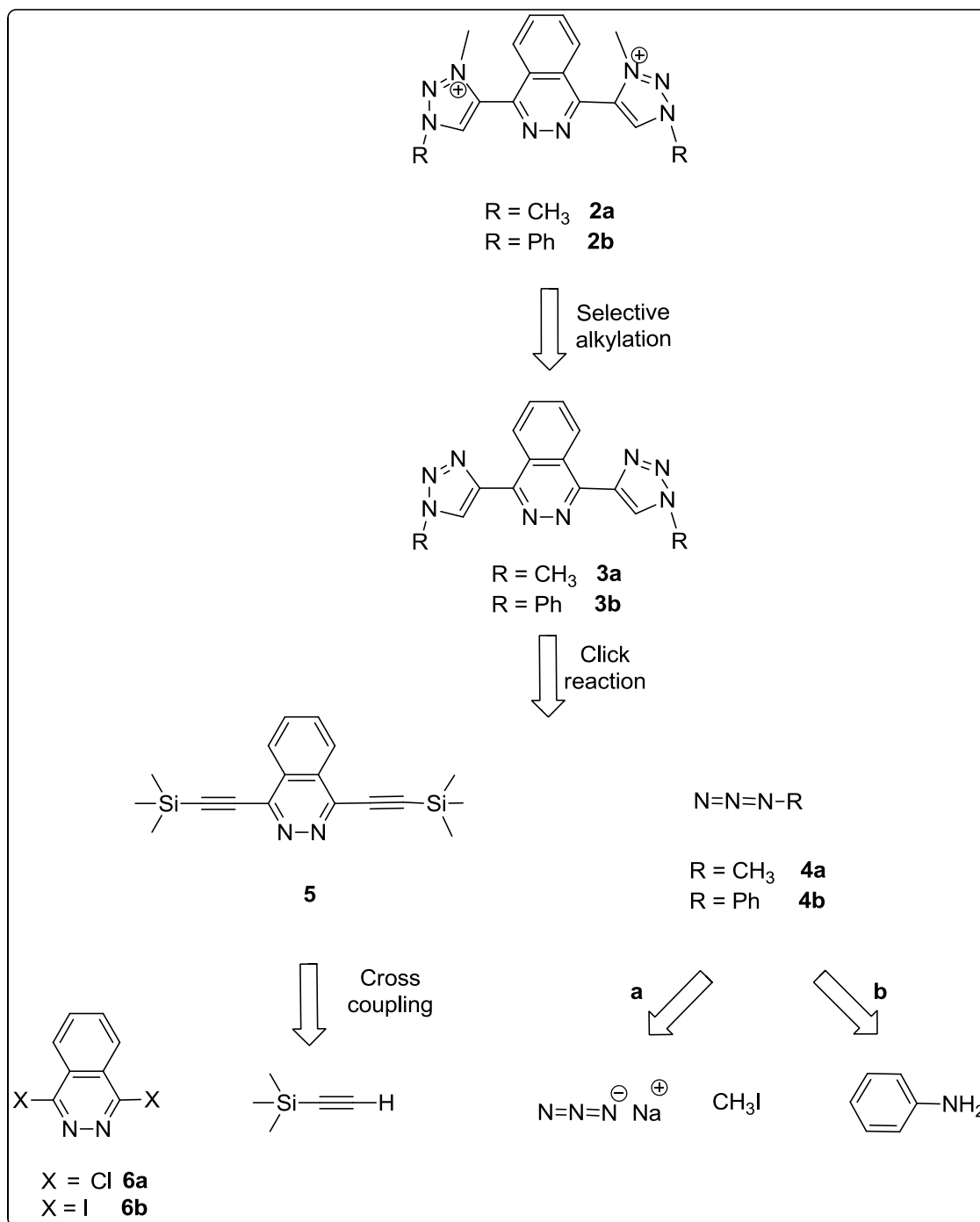
Scheme 1.   Proposed retrosynthesis for **2a/2b** and **3a/3b**

The key steps of this scheme are: (a) the cross-coupling between the di-halo phthalazine ring (**6a**, **6b**) and the acetylene derivate, (b) the click reaction involving the alkyne (**5**) and the azido products (**4a/4b**) and (c) the selective alkylation of the triazole nitrogen atoms of **3a** and **3b**.

As a general trend, the formation of a new C—C bond between aryl halides and terminal acetylenes (such as the reaction of **6a**/**6b** with trimethylsilylacetylene , Scheme 1) concerns a mechanism based on two independent catalytic cycles (cycles A and B in Scheme 2).[8] The so called "Palladium-cycle" (cycle A) starts with the catalytically active Pd(0)L$_2$ species (**1**), which can be formed from both Pd(0) complexes such as Pd(PPh$_3$)$_4$ or Pd(II) complexes such as PdCl$_2$(PPh$_3$)$_2$. Once with the active species formed next is the oxidative addition of the aryl halide (R^1-X) (**2**), which is supposed to be the rate-determining step of the reaction. The energy barriers for the oxidative addition of ArX (X= Cl, Br, I) increase in the order ArI < ArBr < ArCl.[9] Cycle B, which is poorly known, can be triggered by zinc or copper. On one hand, Negishi cross-coupling reactions are based on the use of ZnCl$_2$ and their mechanism is depicted in the left part of Scheme 2. In this case the presence of a strong base seems to be necessary to deprotonate the terminal alkyne and subsequently generate the organozincato adduct (**10**). On the other hand, copper salts such as CuI (**7**) are used in Sonogashira cross-coupling reactions (Figure 1, right). Transmetalation of these metallic adducts (either zinc (**10**) or copper (**8**)) with the palladate derivative (**3**) (Cycle A) and subsequent reductive elimination ends up liberating the Pd catalyst and one molecule of the desired coupled product (**6**).
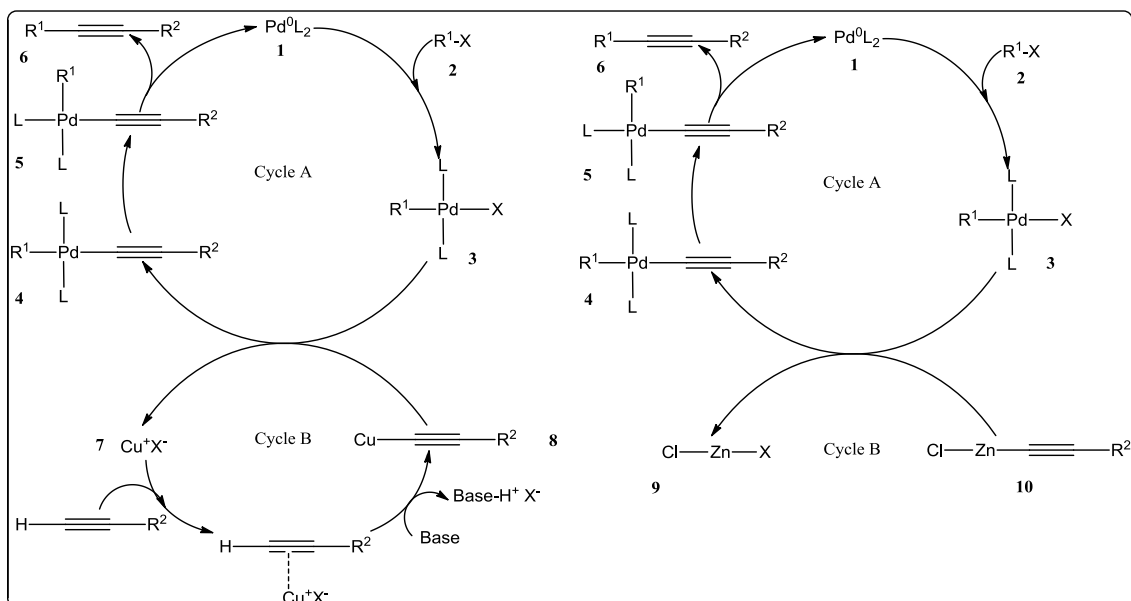
Scheme 2. Mechanistic cycles proposed for Sonogashira (left) and Negishi (right) cross-coupling reactions.

In this project, the cross-coupling of **6a**/**6b** with trimethylsilylacetylene has been attempted by means of several reaction conditions pertaining to both Negishi and Sonogashira settings. The most relevant results are summarized in Table 1.

Table 1. Most relevant reaction conditions used to attempt the cross-coupling step of **6a**/**6b** with trimethylsilylacetylene (Scheme 1) and mechanistically analyzed in Scheme 2.

Entry	Substrate	Cycle A Pd source	Cycle B Metal	Base	T (°C)	Solvent	Time	Yield
1	**6a**	$Pd^0(PPh_3)_4$	$ZnCl_2$	nBuLi	-78	THF	3days/ 4 h	15 %
2	**6b**	$Pd^{II}Cl_2(PPh_3)_2$	CuI	Cs_2CO_3	-15	THF	18 h/ 4 h	20 %

The preparation of **5** was initially attempted by means of an already reported methodology[10] where, instead of the central phthalazine here employed, a pyridazine scaffold was cross-coupled (entry 1). These are typical Negishi conditions. Working in extremely dry conditions and under argon atmosphere, trimethylsilylacetylene was allowed to react with a strong base, n-BuLi in THF at -78°C for one hour, to accomplish the initial deprotonation of the acetylene residue. Then, a solution of $ZnCl_2$ in THF was added and stirred at the same temperature for extra 45 min., thus generating the

corresponding organozincate. Next was the warm up of the reaction to 25ºC and the addition of a mixture containing **6a** and the palladium source, in this case Pd(PPh$_3$)$_4$. The mixture was then reacted for three days at 35ºC. After working up the reaction crude, column chromatography on silica gel (hexanes:ethyl acetate, 98:2) was mandatory to obtain the pure product. However, the low yields and bad reproducibility obtained forced us to optimize the reaction conditions. Several attempts were carried out reducing the reaction time (3 days, 2 days, 24, 12, 5 and 4 h) and the reaction temperature (45, 30 and 25 ºC). However, yields higher than 15% were never obtained. In addition, decomposition/polymerization of **5** was observed at temperatures higher than 35ºC and while stored for long time (also when maintained at very low temperatures).

With these results on hand a new strategy to afford **5**, now based on typical Sonogashira cross-coupling conditions,[11] was attempted (Table 1, entry 2). 1,4-diiodophthalazine, **6b**, was obtained following an already reported methodology.[12] Cs$_2$CO$_3$ (as above mentioned, a softer base than the one used for Negishi conditions) was first mixed with the diido substrate **6b** at -15ºC. Subsequently, a mixture of the palladium catalyst and the copper co-catalyst in THF at -15ºC was added to the former reaction crude. Finally, the acetylsilyl substrate was introduced and the crude was stirred for 30 min at -15ºC and 18 h at room temperature. Similar results to the ones gathered using the Negishi cross-coupling were here obtained. After optimization, best results were obtained when the reaction was performed at low scale, with the product purified by column chromatography on silica gel (hexanes:ethyl acetate, 98:2) and immediately employed for the next step.

The next step was a Click reaction between **5** and the corresponding azide **4a** or **4b**. Methylazide (**4a**) was obtained following a procedure established in Prof. Albrecht's laboratory mixing sodium azide and methyliodide in water:THF (50:50) in the dark and stirring overnight. Phenylazide (**4b**) was obtained following a reported procedure.[13] In both cases the desired products were obtained in quantitative yields and used for the next step without further purification. Click reactions concerning alkynes and azido derivates are catalyzed by copper and need the presence of a base as sodium ascorbate to deprotonate the alkyne, thus enhancing its negative charge density and subsequently the yield of the reaction. The trimethylsylil-protected nature of **5** makes its desilylation unavoidable. This is usually reported by reaction of the protected alkyne with K$_2$CO$_3$ in

MeOH.[10] In our case, modifying the standard conditions, both the deprotection and the click steps were simultaneously performed, thus reducing one reaction step. For this reason, K_2CO_3 has been added to *in situ* deprotect the alkynes.[14] A microwave reactor was employed for all the click reactions increasing the rate and also the yields of these steps. Therefore, after ammonia, water and brine washings to extract all copper residues and remove undesired inorganic salts, ligand **3a** was obtained pure. However, **3b** was purified by means of column chromatography on silica gel (DCM:EtAcO, 90:10).

The selective alkylation of **3a** and **3b** towards **2a** and **2b** (Scheme 1) has been attempted by several strategies, which where unfruitful in all cases. The most relevant results of these alkylation approaches are displayed in Table 2.

Table 2.   Experimental conditions used for the alkylation of **3a** and **3b**.

Entry	Alkylating Agent	Solvent	T (ºC)
1	MeI	CH_3CN	80
2	MeOTf	DCM	45

Despite of failing on the attainment of the bridging ligand **2a**, the methylation of **3a** ended up with two unexpected molecules, **7$^+$** and **8^{2+}** (Scheme 3) which have been characterized in terms of NMR and X-ray.
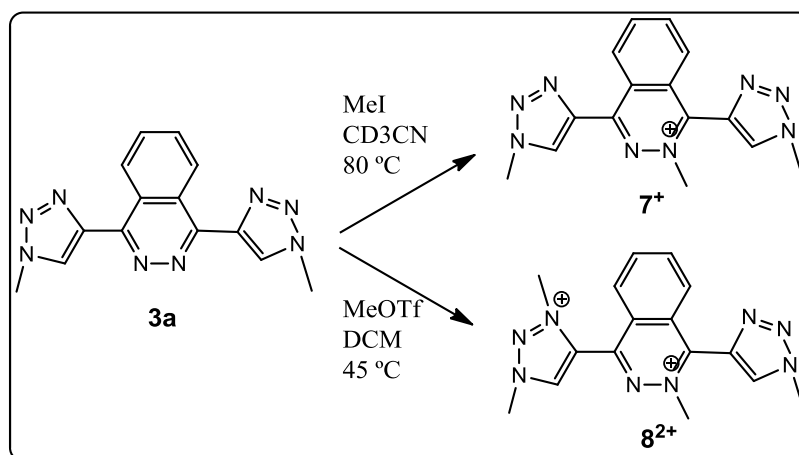
Scheme 3.   Alkylation of **3a** by MeI and MeOTf.

When **3a** was allowed to react with methyl iodide as alkylating agent, in acetonitrile at 80 ºC (Table 2, entry 1), the methylation of one of the phthalazine nitrogen atoms was observed from the third hour of reaction, thus generating **7$^+$** (Scheme 3). The same

result was attained at longer reaction times. However, when **3a** was reacted with methyl triflate as alkylating agent in DCM (Table 2, entry 2) a double methylation (phthalazine and triazole) was observed, now generating 8^{2+} (Scheme 3) as reaction product. In this latter case the final product precipitated as a white powder; therefore it was filtered, washed with cold DCM and dried with diethyl ether. These results were confirmed by ^{1}H-NMR and X-ray and will be discussed in following section. Of course, the alkylation of the phthalazine ring prevents the use of 7^+ and 8^{2+} as bridging ligands. However, they can both be considered as potentially useful bidentate ligands for the preparation of mononuclear transition-metal complexes bearing abnormally bonded NHCs.

The preference of the alkylating agents for the phthalazine nitrogen atoms, demonstrated in the obtention of 7^+ and 8^{2+}, pointed out the higher basicity of those nitrogens with regards to the triazolic ones.

V.2.2. Characterization of 5, 3a-b, 7^+ and 8^{2+}

The new ligands **3a-b**, 7^+ and 8^{2+} and the intermediate **5** have been fully characterized by the usual structural and spectroscopic techniques. In the present section the most important results about this characterization in terms of NMR and X-Ray will be discussed.

V.2.2.1. NMR spectroscopy

Nuclear Magnetic Resonance experiments have been carried out for ligands **3a-b**, 7^+ and 8^{2+} and the intermediate **5** (Figures 1-3 and Figures S1-S4 in the Supporting Information). Both 1D (^{1}H and ^{13}C {^{1}H}) and 2D (COSY, HSQC and HMBC) experiments have proven to be mandatory tools in order to structurally characterize them in solution. The full assignment of the observed resonances can be made based on their integrals, symmetry and multiplicity. When assigning the ^{1}H-NMR of these molecules, their symmetry becomes a very useful tool. **5** and **3a-b** display C$_{2v}$ symmetry in solution, with a symmetry plane containing the whole molecule and a second plane (perpendicular to the former) that bisects both the N-N and the C8-C9 bonds of the same phthalazine ring. The latter interconverts the two alkynes of **5** and the two triazole rings of the **3a-b** ligands. However, both 7^+ and 8^{2+} do not display any symmetry because of the asymmetric alkylation of their nitrogen atoms (see Scheme 3).

As shown in the inset of Figure 1, for the precursor **5**, both H7 and H8 display a doublet of doublets with a mirror effect, which is in agreement with the typical AA'BB' (77'88' in our case) pattern of this kind of systems.[15] These systems are typically characterized by their higher J_{AB} value (J_{78} = 6.3 Hz) than $J_{AB'}$ value ($J_{78'}$ = 3.3 Hz). The coupling of H7 and H8 with C6 and C4 in the 2D HMBC-NMR (Figure S1f) has been a very useful tool to unambiguously assign the structure of **5**. Furthermore, it is worth mentioning that the 18 equivalent protons corresponding to H1 appear at 0.38 ppm, which is a coherent chemical shift for a product so similar to TMS.
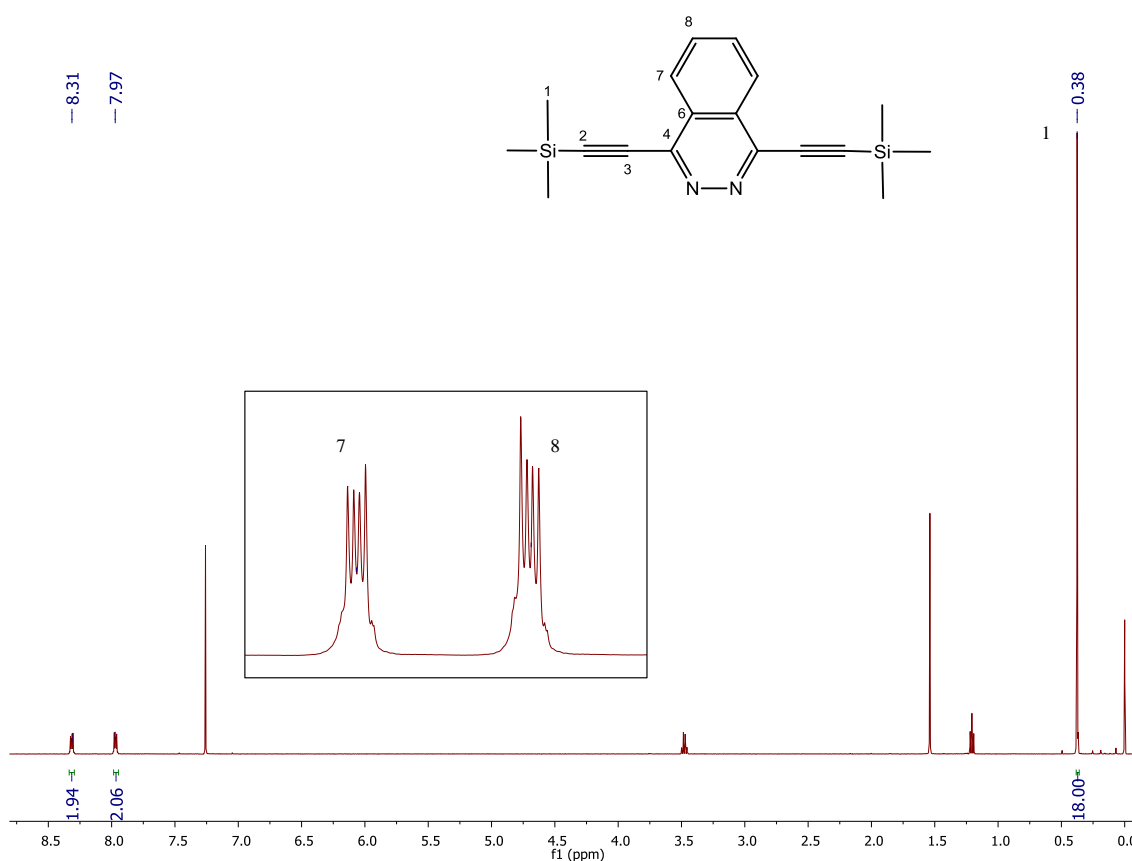
Figure 1. ^{1}H-NMR (500 MHz, CDCl$_3$) for **5**. (Inset) zoom of the aromatic region.

Ligand **3b** displays the NMR shown in Figure 2. As can be observed, the doublet of doublets corresponding to H7 is shifted to lower fields due to the presence of the triazole ring. Furthermore, H1 appears at 8.95 ppm as a lone singlet, thus demonstrating the successful formation of the new ring and the purity of the product. The same arguments apply for the full NMR characterization of **3a** depicted in Figure S2.
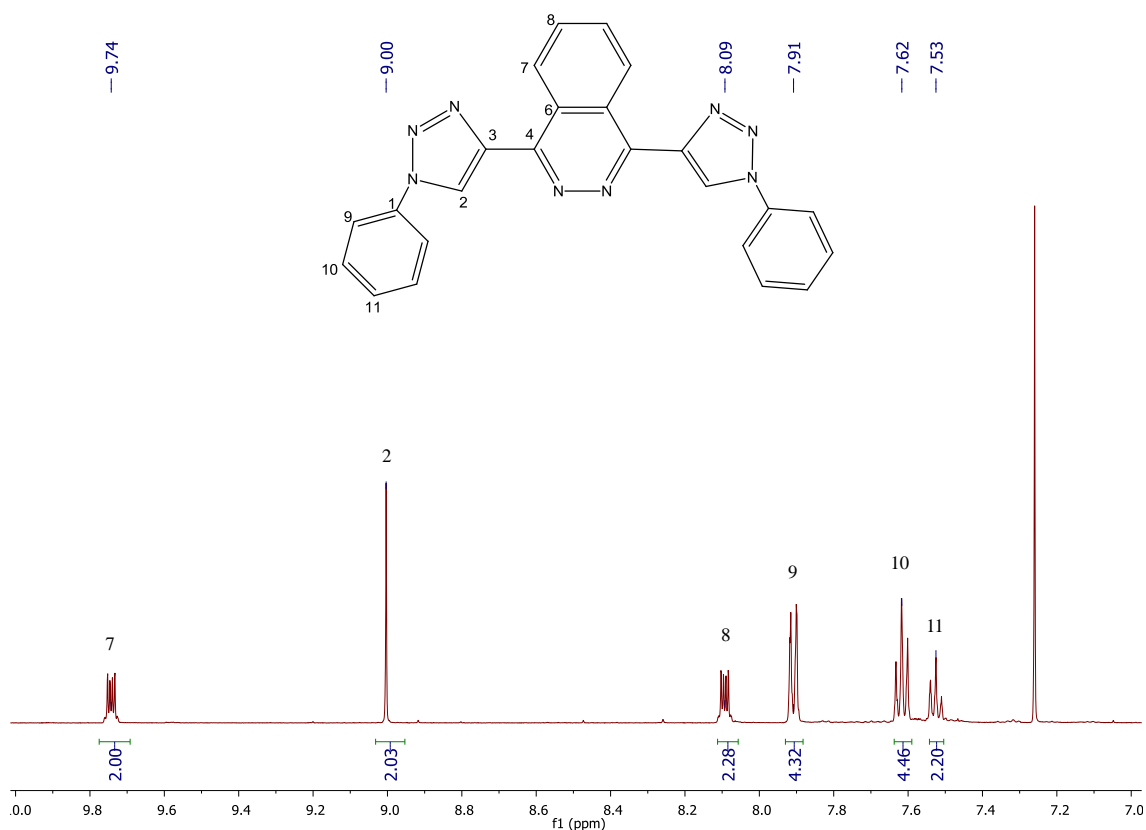
Figure 2. ^{1}H-NMR (500 MHz, CDCl$_3$) for **3b**.

Finally, the ^{1}H-NMR of **8^{2+}** is shown in Figure 3. The lack of symmetry induces here the increase of signals in the spectrums of both **7$^+$** (Figure S4) and **8^{2+}** (Figure S5). In this manner H7 and H8 do not display the singular AA'BB' system and become a doublet and a triplet, respectively. It is interesting to mention that H14 is shifted 0.5 ppm to lower fields with regards to the equivalent H2, due to the positive charge on the triazolium nitrogen.
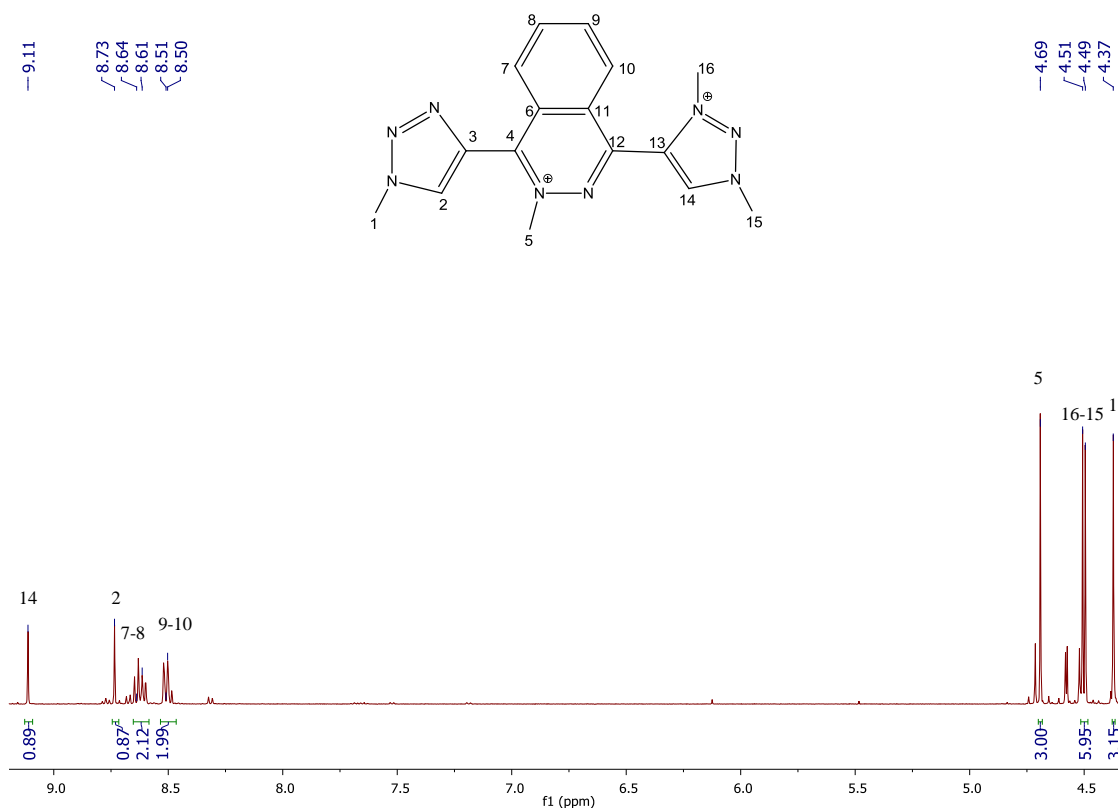
Figure 3. ^{1}H-NMR (500 MHz, CD$_3$CN) for **8^{2+}**.

V.2.2.2. X-ray Crystal Structures

Suitable crystals for X-Ray diffraction analysis have been obtained for **7$^+$** and **8^{2+}**. Figures 4 and 5 display an Ortep plot for the cationic moiety of these two ligands together with their corresponding atom labeling scheme. Acquisition, crystallographic data and stereoscopic views of the crystal packing are reported as Supporting Information.

Monocrystals of **7$^+$** were obtained from the NMR tube upon allowing the CDCl$_3$ solution to stand overnight at room temperature. As shown in Figure 4, each molecule is contained in two planes, one holding the phthalazine moiety and one of the triazole rings and a second one described by the other triazole ring. Their torsion angle is of 75º (C2-C3-C4-N4) (see Figure S11 for further information), which is due to the repulsion between H2 and H5. **7$^+$** crystallized in a cell containing four molecules of the ligand, four chloroform molecules and four iodo anions as shown in Figure S10.

V
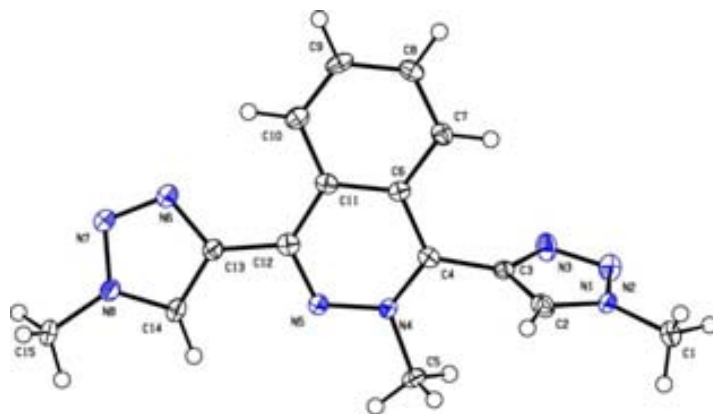
Figure 4.   Ortep plot (ellipsoid at 50 % probability) of the X-ray crystal structure of the cationic moiety of **7⁺** with its corresponding labeling scheme.

Monocrystals of $\mathbf{8}^{2+}$ were obtained from the NMR tube in CD_3CN, upon allowing the solution to stand overnight at room temperature. The X-ray structure of $\mathbf{8}^{2+}$ allowed to better understand where the alkylation took place. As shown in Figure 5, each molecule contains three planes, one for each triazole ring and a third one described by the alkylated phthalazine moiety. The torsion angles between both triazole rings and the central phthalazine scaffold (C2-C3-C4-N4=51° and N6-C13-C12-N5=42°) are here caused by the H2-H5 and H14-H10 interactions, respectivley (See Figure S13 for a draw of these measurements). $\mathbf{8}^{2+}$ crystallized in a cell containing eight molecules of the ligand and sixteen triflate anions as shown in Figure S12.
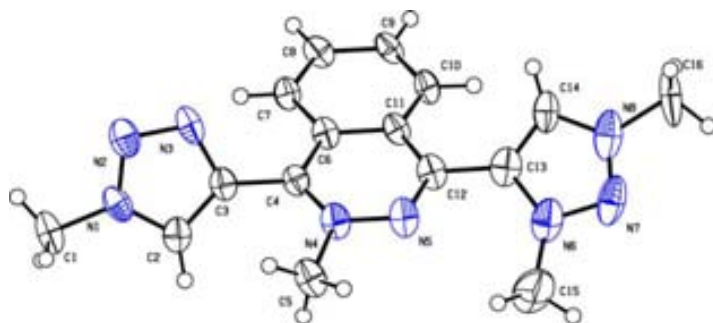
Figure 5.   Ortep plot (ellipsoid at 50 % probability) of the X-ray crystal structure of the cationic moiety of $\mathbf{8}^{2+}$ with its corresponding labeling scheme.

V.2.3. Synthesis and Characterization of 9(PF$_6$)$_3$ and 10(PF$_6$)

The synthesis of complex **9(PF$_6$)$_3$** was carried out by following the usual procedures of our research group for this kind of complexes (Scheme 4).[6] [RuCl$_3$trpy] and the ligand **3a**, were refluxed in methanol for four hours affording the mixture of complexes shown in Scheme 4 (assigned by analyzing the proton NMR spectrum shown in Figure 6a).
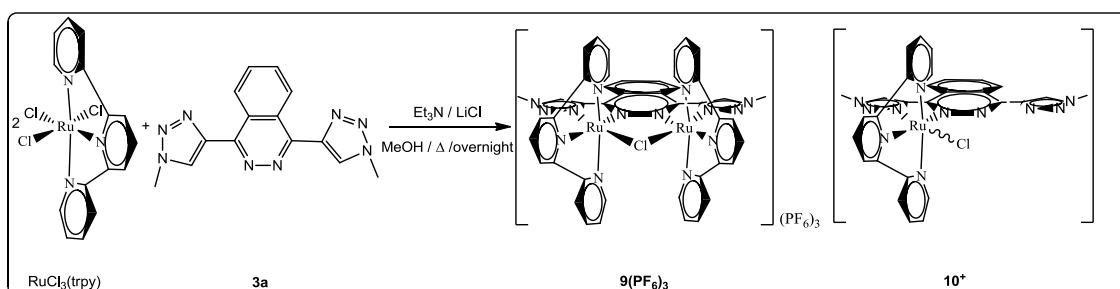
Scheme 4. Synthetic route for complex **9(PF$_6$)$_3$**.

The reaction mixture was then allowed to react for twelve extra hours and a new ^{1}H-NMR spectrum was recorded (Figure 6b). As can be appreciated, no evolution of the crude was observed during this extra reaction time. Column chromatography in alumina was mandatory to separate both products, which were assigned to the desired dinuclear complex **9(PF$_6$)$_3$** and the mononuclear complex **10(PF$_6$)** with the connectivity shown in the Scheme 4.

V

171
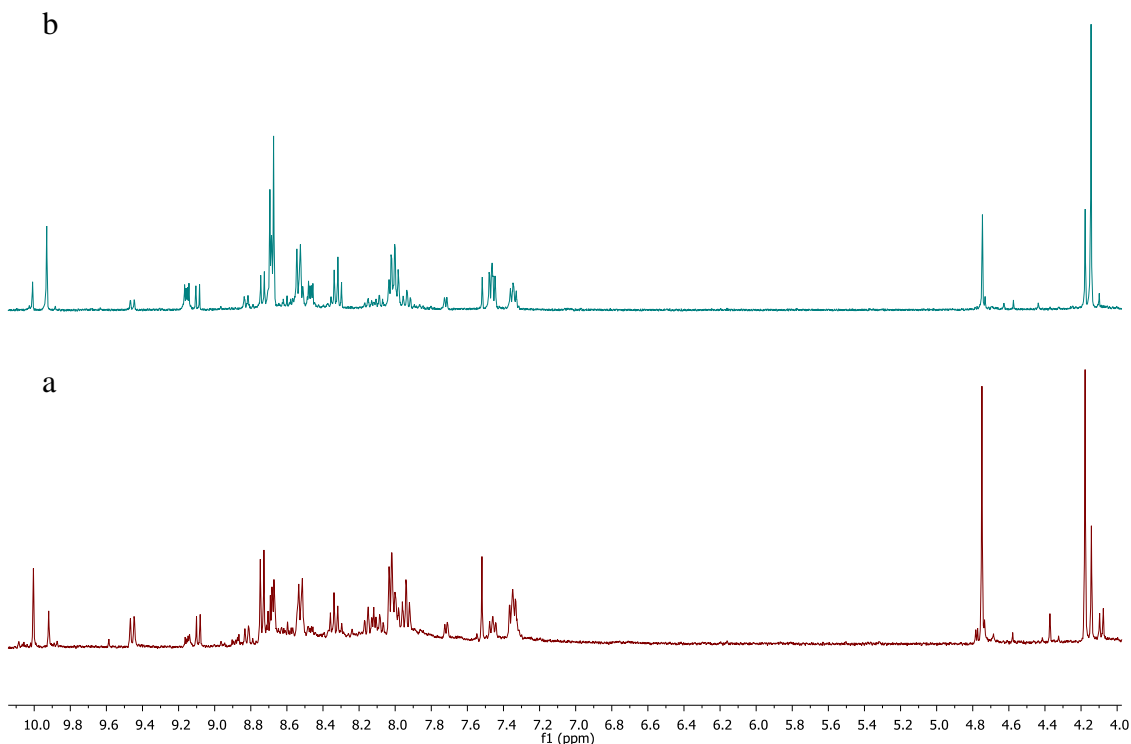
Figure 6. ^{1}H-NMR (400 MHz, acetone-d$_6$) spectra recorded during the synthesis of **9^{3+}**: (a) 4 h of reaction (b) 12 h of reaction.

The new dinuclear complex **9(PF$_6$)$_3$** has been characterized by usual structural, spectroscopic and electrochemical techniques. In the present section the most important results about this characterization, in terms of NMR, X-Ray, and Electrochemistry will be discussed. Due to the trace amounts obtained (less than 5 % yield, see the Experimental Section) **10$^+$** has only been characterized by ^{1}H-NMR and Electrochemistry.

V.2.3.1. NMR spectroscopy

Nuclear Magnetic Resonance experiments have been carried out for the diamagnetic compounds **9(PF$_6$)$_3$** and **10(PF$_6$)** (Figures 7-8 and Figure S6 in the Supporting Information). Both 1D (^{1}H and ^{13}C {^{1}H}) and 2D (COSY, HSQC and HMBC) experiments have proven to be mandatory tools in order to structurally characterize **9^{3+}** in solution. **9^{3+}** displays in solution a C$_{2v}$ symmetry with one symmetry plane containing the **3a** ligand, the two Ru atoms, both central terpyridine nitrogen atoms and the chlorido bridge. A second plane (perpendicularly bisecting the former) passes through the chlorido bridge and bisects the N(4)-N(4a), C(7)-C(7a) and C(5)-C(5a) bonds of the same phthalazine scaffold, thus interconverting the two terpyridine ligands.
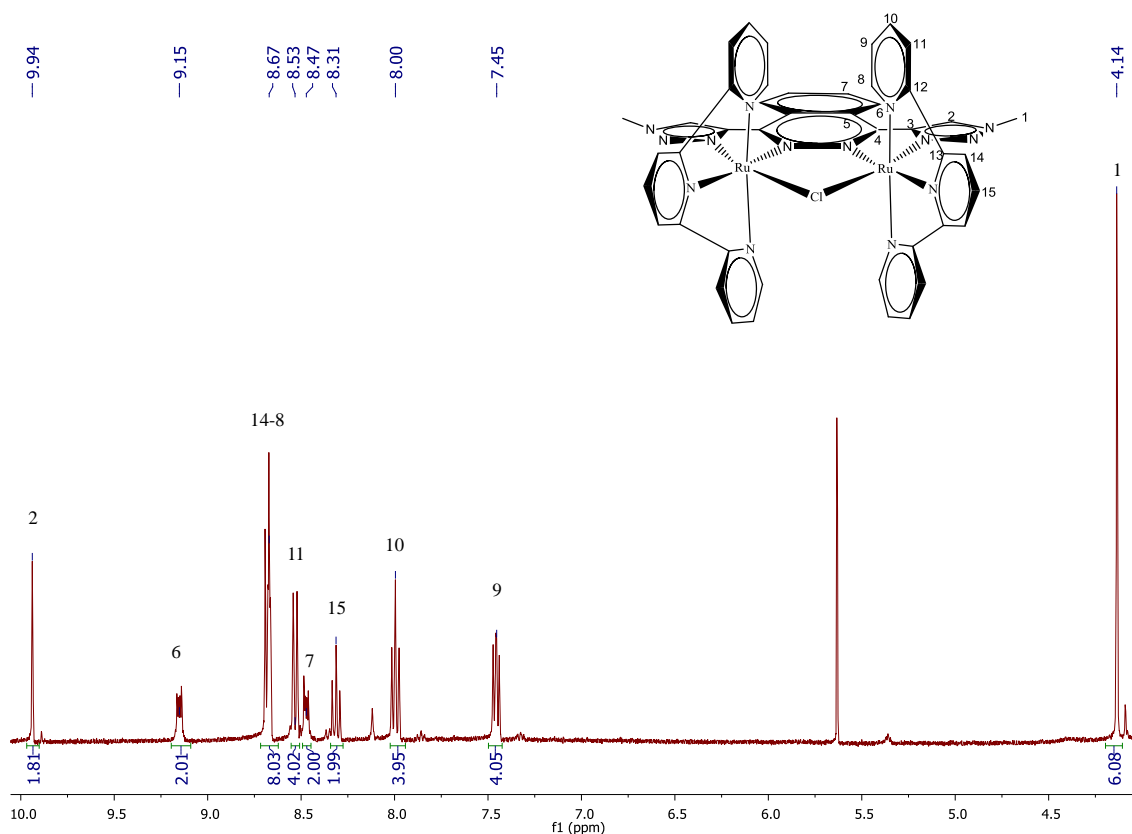
Figure 7. ^{1}H-NMR (400 MHz, acetone-d$_6$) for **9^{3+}**

When comparing this spectrum (Figure 7) with the one corresponding to the free **3a** ligand (Figure S2), a shift from 8.71 to 9.94 ppm is observed for the H2 singlet, an experimental evidence of the coordination effect onto the triazole ring.

Contrary to this, the ^{1}H-NMR of **10$^+$** shows a total absence of symmetry, thus appearing doublets and triplets for the four protons (a, b, c and d) of the central phthalazine scaffold (Figure 8). In addition to this the singlets HA, HB, HC and HD are no longer equivalents, thus four different signals can be observed at 4.2, 4.7, 7.5 and 10.1 ppm (Figure 8). The presence of the trpy signals and the shift to lower fields of HB with regards to its counterpart HC are evidences of the coordination to the ruthenium metal ion.

V
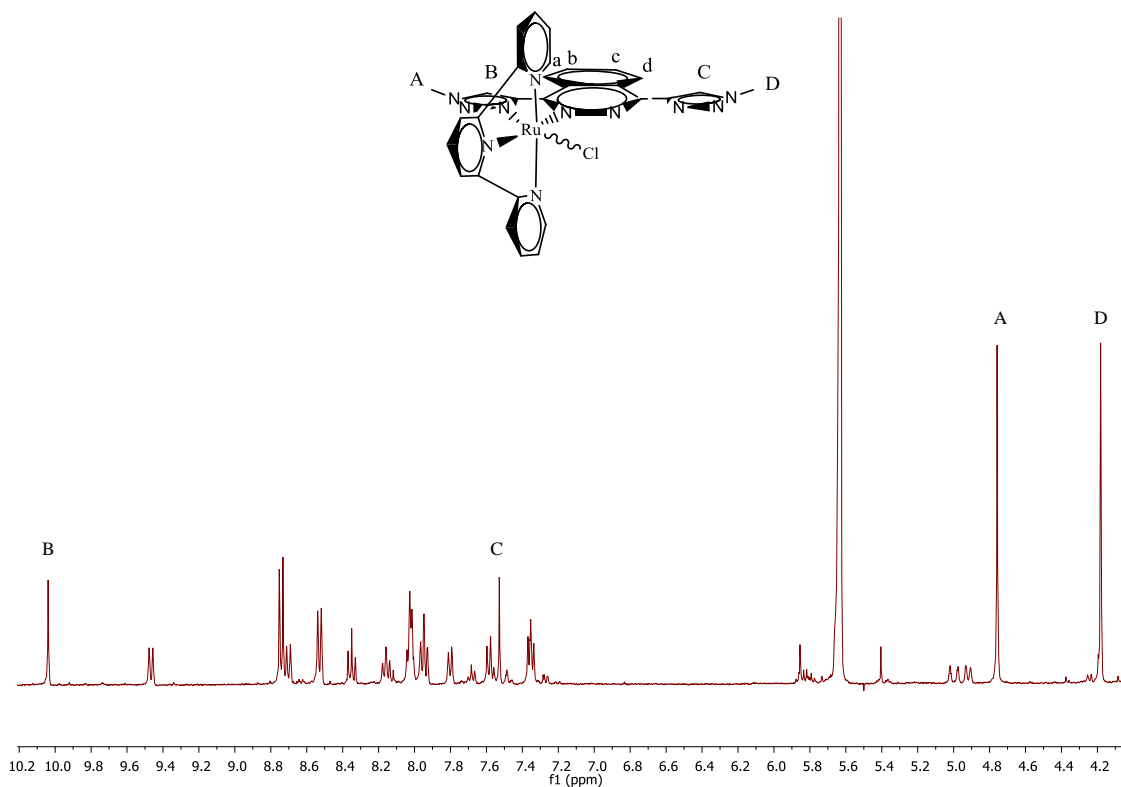
Figure 8. ¹H-NMR (400 MHz, acetone-d_6) for **10⁺**.

V.2.3.2. *X-Ray Crystal Structures*

Suitable crystals for X-Ray diffraction analysis have been obtained for **9(PF₆)₃**. Figure 9 displays an Ortep plot (ellipsoid at 40 % probability) of the cationic moiety of **9³⁺** with the corresponding labeling scheme (see the acquisition data in Table S3 and an stereoscopic view of the crystall packing in Figure S14 of the Supporting Information).
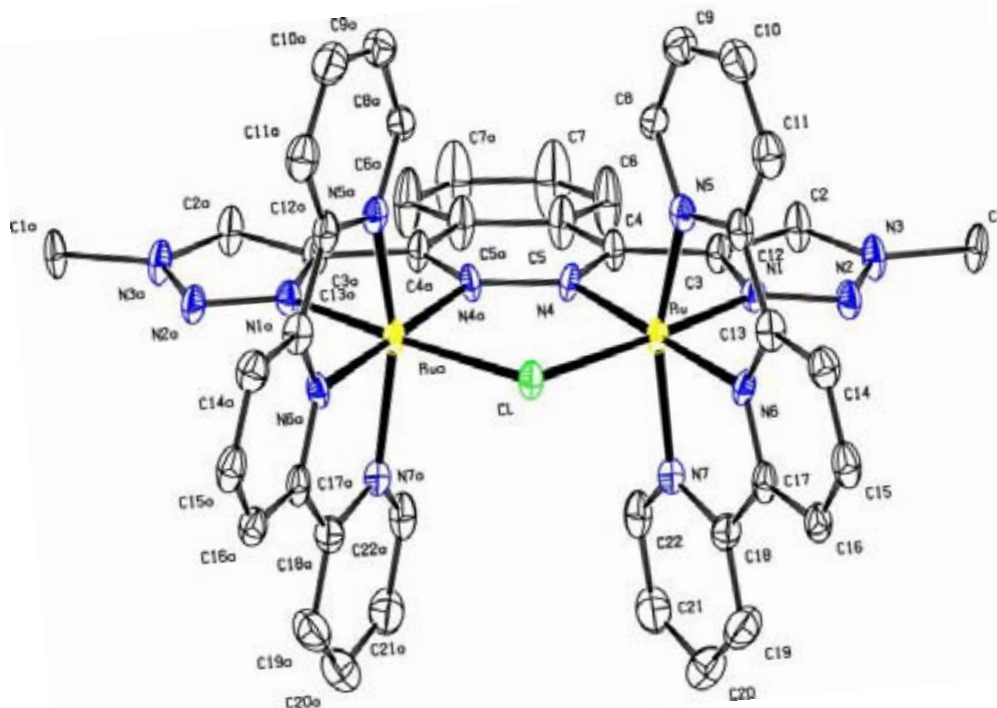
Figure 9.   Ortep plot (ellipsoid at 40 % probability) of the cationic moiety of **9^{3+}** with its corresponding labeling scheme.

$9(PF_6)_3$ crystallizes in a small cell (Figure S14) with two complex molecules, two acetone molecules and twenty PF_6 anions distributed as follows: two in the cell, two on the faces, eight on the vertexs and eight on the edges. The sumatory of all the contributions gives the needed six anions in total. Each ruthenium metal adopts pseudo-octahedral coordination geometry with two positions occupied by the **3a** ligand, three by the meridional terpyridine ligand and the latest by a Cl-bridged ligand. A comparison of the more relevant bond distances and angles of **9^{3+}** with the ones reported for the related Ru-Hbpp complex $[Ru^{II}_2(\mu\text{-Cl})(bpp)(trpy)_2]^{2+}$, is displayed in Table 3. Figure 10 displays the X-ray structure and the corresponding labeling scheme for $[Ru^{II}_2(\mu\text{-Cl})(bpp)(trpy)_2]^{2+}$. The central phthalazine scaffold that coordinates both Ru metal ions is a six membered ring in **9^{3+}**, while the central pyrazol of the bpp ligand in $[Ru^{II}_2(\mu\text{-Cl})(bpp)(trpy)_2]^{2+}$ is five membered. Therefore, higher Ru-N4 distances (Table 3, entry 2) and shorter Ru-Cl and Ru-Ru(a) distances together with an also shorter Ru-Cl-Ru(a) angle are observed in **9^{3+}** with regards to its Ru-Hbpp homologue. All these differences are in agreement with a better accomodation of the Ru metal ions in **9^{3+}** due to the six membered nature of the phthalazine scaffold. This less constrained situation ends up

with an undistorted Ru-N4-N4(a)-Ru(a) angle (0º, Table 3, entry 11) with regards to the slightly distorted one observed for $[Ru^{II}_2(\mu\text{-Cl})(bpp)(trpy)_2]^{2+}$ (18º, Table 3, entry 11).
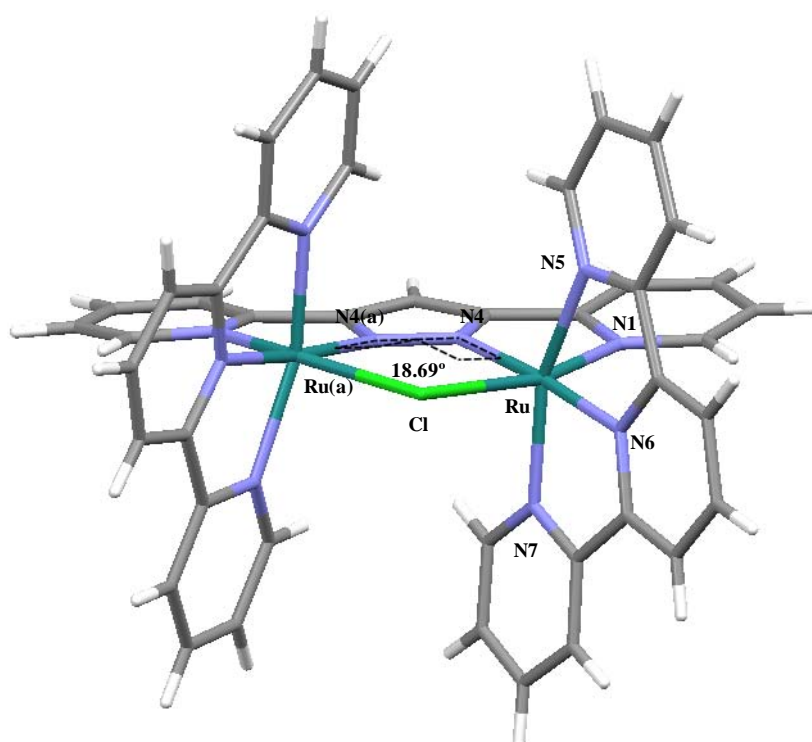
Figure 10.   X-ray structure of the hbpp homologue complex $[Ru^{II}_2(\mu\text{-Cl})(bpp)(trpy)_2]^{2+}$ for comparison purposes.

Table 3.   Selected interatomic distances (Å) and angles (º) for **9^{3+}** and the previously reported $[Ru^{II}_2(\mu\text{-Cl})(bpp)(trpy)_2]^{2+}$.

ENTRY	BOND DISTANCES	9^{3+}	$[Ru^{II}_2(\mu\text{-Cl})(bpp)(trpy)_2]^{2+}$ [6]¡Error! Marcador no definido.
1	Ru-N(1)	1.993(4)	2.054(3)
2	Ru-N(4)	2.089(4)	1.999(3)
3	Ru-N(5)	2.069(4)	2.079(3)
4	Ru-N(6)	1.966(4)	1.967(3)
5	Ru-N(7)	2.068(5)	2.060(3)
6	Ru-Cl	2.396(12)	2.4466(7)
7	Ru(a)-Cl	2.396(12)	2.4466(7)
8	Ru-Ru(a)	3.657	3.876
	ANGLES		
9	Ru-Cl-Ru(a)	99.84(6)	104.77(4)
10	N(5)-Ru-N(7)	158.77(15)	158.15(14)
11	Ru-N(4)-N(4a)-Ru(a)	0.00	18.69

V.2.3.3. *Electrochemistry*

The redox properties of complexes 9^{3+} and 10^+ were investigated by means of CV in acetone, and are displayed in Figure 11.
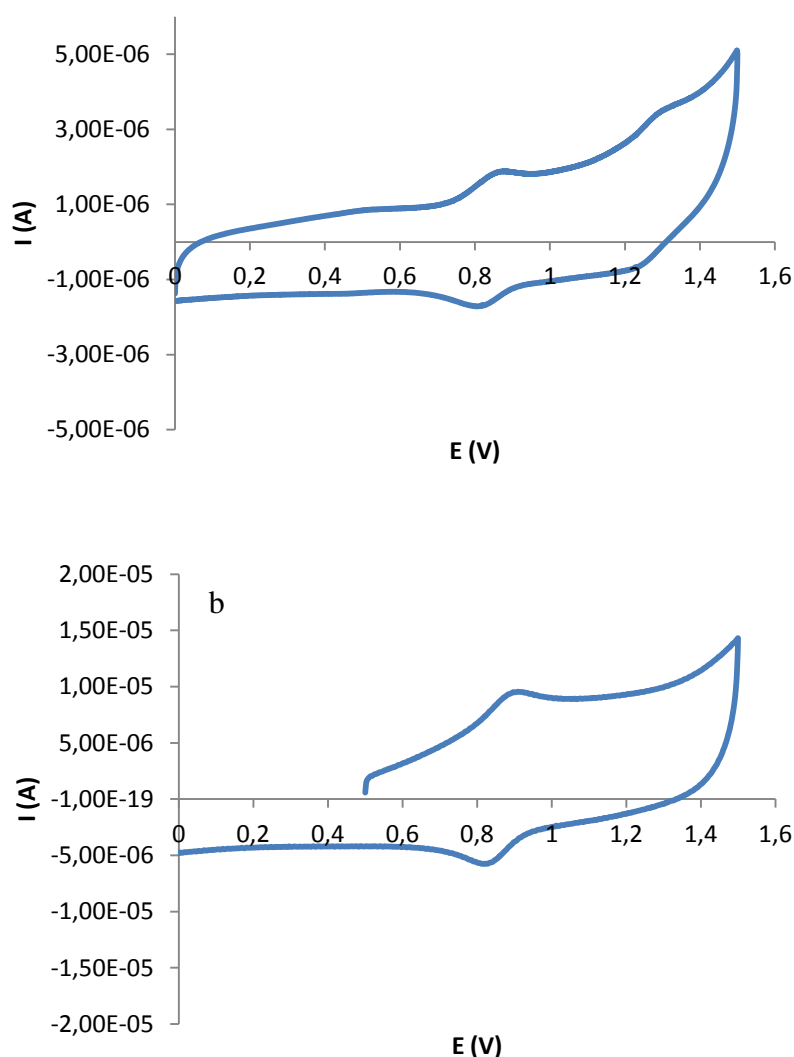
Figure 11. Cyclic voltammogram for the chlorido-bridged complex 9^{3+} (a) and the mononuclear complex 10^+ (b) in 0.1 M n-Bu$_4$NPF$_6$ in acetone at 100 mV/s scan rate. Glassy carbon electrode is used as working electrode and the potential is measured *vs.* SSCE.

The CV of 9^{3+} exhibits two reversible waves that are assigned to the following electrochemical processes (the **3a** and trpy ligands are not shown for the sake of clarity):

$$[Ru^{III}(\mu\text{-Cl})Ru^{II}]^{4+} + 1e^- \quad \rightarrow \quad [Ru^{II}(\mu\text{-Cl})Ru^{II}]^{3+} \quad (0.83 \text{ V}) \quad (1)$$

$$[\text{Ru}^{III}(\mu\text{-Cl})\text{Ru}^{III}]^{5+} + 1e^- \quad \rightarrow \quad [\text{Ru}^{III}(\mu\text{-Cl})\text{Ru}^{II}]^{4+} \quad (1.27 \text{ V}) \quad (2)$$

These two $E_{1/2}$ values are similar to those reported for the structurally related $[\text{Ru}^{II}_2(\mu\text{-Cl})(\text{bpp})(\text{trpy})_2]^{2+}$ complex (0.79V and 1.20V, respectively) containing an anionic bpp⁻ bridge. This behavior can be explained as a consequence of two factors: (a) the less σ-donor effect of the neutral phthalazine scaffold instead of the negatively charged pyrazolic ring and (b) the increase in σ-donor effect when exchange one pyridine ring for a triazole one. The combination of both effects ends up with almost no shift for the redox potentials with regard to the related $[\text{Ru}^{II}_2(\mu\text{-Cl})(\text{bpp})(\text{trpy})_2]^{2+}$ complex.

10⁺ exhibits a unique reversible wave which is assigned to the RuIII/RuII process shown in Eq. 3.

$$[\text{Ru}^{III}(\text{Cl})(\text{3a})(\text{trpy})]^{2+} + 1e^- \quad \rightarrow \quad [\text{Ru}^{II}(\text{Cl})(\text{3a})(\text{trpy})]^+ \quad (0.86 \text{ V}) \quad (3)$$

V.3.   <u>**Conclusions and Future Prospects**</u>

In this chapter we have first prepared intermediate **5** by means of cross-coupling reactions between a di-halo phthalazine and acetylene derivatives. Despite of the intense optimization efforts carried out for this cross-coupling step, neither good yields nor acceptable reproducibility were obtained. Subsequently, the de-protection and Click reaction of **5** with **4a** and **4b** was performed in a single step, thus preparing ligands **3a** and **3b** in low yields. Those two new ligands were fully characterized. **3a** has been employed for the preparation of the dinuclear Cl-bridged Ru complex **9³⁺** that has been structurally (X-ray), spectroscopically and electrochemically characterized. Comparison of **9³⁺** solid state structure with the one of the related and previously reported $[\text{Ru}^{II}_2(\mu\text{-Cl})(\text{bpp})(\text{trpy})_2]^{2+}$ complex pointed out relevant differences about the disposition and constrains of the metal centers. That together with the electrochemical values obtained are promising results towards a potentially interesting (and different from Ru-Hbpp family) catalytic activity of the here-prepared complex.

Finally, and due to the unfruitful attempts of preparing the N/C-donor ligands **2a** and **2b** two new bidentate N/C-donor ligands, **7⁺** and **8⁺**, were prepared and structurally characterized. These new ligands were the result of the always favored alkylation of a N

atom of the the central phthalazine scaffold with regards to the peripheral nitrogens of the triazole rings.

Future prospects should be focused on the optimization of the cross-coupling process to obtain **5** in higher yields and reproducibility. On the other hand, the selective alkylation of **3a** and **3b** should be attempted under acidic media, preventing in this manner the non-desired nucleophilic attack of the phthalazine nitrogen atoms.

V.4.   **Experimental Section**

Materials: All reagents used in the present work were obtained from Aldrich Chemical Co. and were used without further purification. Reagent-grade organic solvents were obtained from Scharlab. $RuCl_3 \cdot 3H_2O$ was supplied by Alfa Aesar and was used as received. The starting ligand 1,4-diiodophthalazine,[9] the complex $PdCl_2(PPh_3)_2$[16] and $[RuCl_3(trpy)]$[17] were prepared as described in the literature. Phenylazide (**4b**) was obtained following a reported procedure.[13] All synthetic manipulations were routinely performed under nitrogen atmosphere using Schlenk tubes and vacuum-line techniques.

Instrumentation and Measurements: NMR spectroscopy was performed on a Bruker DPX 250 MHz, DPX 360 MHz or a DPX 400 MHz spectrometer or in a Varian NMR System 500MHz or 300MHz. Samples were run in $CDCl_3$, CD_3CN or acetone-d_6 with internal references. Electrospray ionization mass spectrometry (ESI-MS) experiments were carried out on an HP298s gas chromatography (GC-MS) system from the CAS-UAB. Cyclic voltammetry experiments were performed on an Ij-Cambria HI-660 potentiostat using a three-electrode cell. A glassy carbon electrode (2 mm diameter) was used as working electrode, platinum wire as auxiliary electrode and a SSCE as a reference electrode. Working electrodes were polished with 0.05 micron Alumina paste washed with distillated water and acetone before each measurement. The complex was dissolved in acetone containing the necessary amount of n-Bu_4NPF_6 (TABH) as supporting electrolyte to yield 0.1 M ionic strength solution. $E_{1/2}$ values reported in this work were estimated from CV experiments as the average of the oxidative and reductive peak potentials $(E_{p,a} + E_{p,c})/2$.

X-ray Crystal Structure Determination. Crystal data for **7$^+$**, **8^{2+}** and **9^{3+}** were collected using an Oxford Diffraction SuperNova A diffractometer fitted with an Atlas detector. All the samples were measured with Mo–Kα (0.71073 Å). An at least

V

complete dataset was collected, assuming that the Friedel pairs are not equivalent. An analytical absorption correction based on the shape of the crystal was performed for all these crystals.[18] The structures were solved by direct methods using SHELXS-97[19] and refined by full matrix least-squares on F2 for all data using SHELXL-97. Their isotropic thermal displacement parameters were fixed to 1.2 times (1.5 times for methyl groups) the equivalent one of the parent atom. Anisotropic thermal displacement parameters were used for all non-hydrogen atoms.

Synthetic preparations

5: A mixture of Cs_2CO_3 (0.41 g, 1.257 mmols) and 1,4-diiodophthalazine (120 mg, 0.314 mmols) were placed into a 20 ml schlenk flask in a -15ºC bath (salt/ice). Several vacuum/argon cycles were applied. After that 4 ml of dried and argon-bubbled THF were added *via* canula. After degas the mixture and flush argon, bis-(triphenylphosphine)-palladium dichloride (22.05 mg, 0.031 mmols) and copper (I) iodide (6 mg, 0.031 mmols) are added. The flask is another time degassed and flushed with argon and finally Trimethylsilylacetylene (101 μl, 0.6912 mmols) is added. The mixture is stirred for 30 min at -15ºC and 4h at room temperature. The reaction mixture is poured in $H_2O:NH_3$ (30 ml, 2:1) and the product is extracted with ethyl acetate (20 ml). The organic fraction is washed with $H_2O:NH_3$ until no more blue color is observed. Finally it is washed with water (2x20 ml) and brine 2x100 ml and dried with anhydrous sodium sulphate. After evaporation of the solvents the solid residue is purified by silica chromatography in hexanes:ethyl acetate (98:2). (Yield: 22 mg, 20%) ^{1}H-NMR (500MHz, $CDCl_3$): δ = 8.31 (dd, 2H J_{7-8} = 6.3 Hz, $J_{7-8'}$ = 3.3 Hz, H7), 7.97 (dd, 2H, J_{8-7} = 6.3 Hz, $J_{8-7'}$ = 3.3 Hz, H8), 0.38 (s, 18H, H1). ^{13}C{^{1}H} NMR (500MHz, $CDCl_3$): δ = 145.30 (C4), 133.55 (C7), 126.98 (C6), 126.26 (C8), 106.12 (C2), 98.97 (C3), 0.00 (C1). ESI-MS (MeOH): *m/z* = 323.14 ([M]$^+$)

3a: MeN_3 was *in situ* generated stirring a mixture of Methyl iodide (76.7 μl, 1.2 mmols), sodium azide (240 mg, 3.69 mmols) and 7 ml of $THF:H_2O$ (50:50) in a microwave flask overnight at room temperature. After that time, **5** (75 mg, 0.233 mmols), $CuSO_4·5H_2O$ (23.22 mg, 0.093 mmols), sodium ascorbate (36.85 mg, 0.186 mmols) and K_2CO_3 (63.25 mg, 0.465 mmols) are added and the mixture is irradiated with a microwave reactor (100 W, 5 + 30 min, 100ºC). The reaction is poured in DCM (50 ml) and the organic fraction is washed with $H_2O:NH_3$ 2:1 (50 ml x 3, until no blue

copper color is observed), H_2O (50 ml x 2) and brine (50 ml x 2). Then is dried with anhydrous sodium sulphate and activated charcoal. After evaporation of the solvents a yellow powder is obtained. (Yield: 50 mg, 80 %). ^{1}H-NMR (500MHz, CDCl$_3$): $\delta = 9.73$ (dd, 2H, $J_{7-8} = 6.3$ Hz, $J_{7-8'} = 3.3$ Hz, H7), 8.70 (s, 2H, H2), 7.97 (dd, 2H, $J_{8-7} = 6.3$ Hz, $J_{8-7'} = 3.3$ Hz, H8), 4.28 (s, 6H, H1). ^{13}C{^{1}H} NMR (500MHz, CDCl$_3$): $\delta = 135.21$ (C8), 129.11 (C7), 128.59 (C2), 126.23 (C6), 37.36 (C1).

3b: **5** (100 mg, 0.31 mmols), CuSO$_4$·5H$_2$O (31 mg, 0.124 mmols), sodium ascorbate (50 mg, 0.248 mmols) and K$_2$CO$_3$ (284.32 mg, 0.62 mmols) and phenylazide (74 mg, 0.62 mmols) are added to a microwave sealed flask containing 7 ml of THF:H$_2$O (50:50). The mixture is irradiated with a microwave reactor (100 W, 5 + 30 min, 100ºC) and then poured in DCM (50 ml). The organic fraction is washed with H$_2$O:NH$_3$ 2:1 (50 ml x 3, until no blue copper color is observed), H$_2$O (50 ml x 2) and brine (50 ml x 2). It is dried with anhydrous sodium sulphate and activated charcoal. After evaporation of the solvents the solid residue is purified by silica chromatography in DCM:ethyl acetate (90:10). (30 mg, 20%). (Yield: 50 mg, 40 %).^{1}H-NMR (500MHz, CDCl$_3$): $\delta = 9.74$ (dd, 2H, $J_{7-8} = 6.3$ Hz, $J_{7-8'} = 3.3$ Hz, H7), 9.00 (s, 2H, H2), 8.09 (dd, 2H, $J_{8-7} = 6.3$ Hz, $J_{8-7'} = 3.3$ Hz, H8), 7.91 (d, 4H, J_{9-10}=8.30 Hz, H9), 7.62 (t, 4H, J_{9-10}=8.30 Hz, J_{10-11}=7.80 Hz, H10), 7.53 (t, 2H, J_{10-11}=7.80 Hz, H11). ^{13}C{^{1}H} NMR (500MHz, CDCl$_3$): $\delta = 149.51$ (C4), 147.61 (C3), 136.83 (C1), 133.10 (C8), 129.96 (C10), 129.22 (C11), 127.20 (C7), 125.32 (C6), 123.32 (C2), 120.72 (C9).

7$^+$: **3a** (10 mg, 0.034 mmols) and methyl iodide (13 μl, 0.200 mmols) were heated (80 ºC) in acetonitrile (7 ml) in a sealed tube for 24 h. Evaporation of the solvents and subsequent recrystallization with chloroform yielded yellow crystals. ^{1}H-NMR (500MHz, CD$_3$CN): $\delta = 10.0$ (d, 1H, J_{7-8}=8.57 Hz, H7), 9.74 (s, 1H, H2), 8.64 (s, 1H, H14), 8.40 (t, 1H, J_{7-8}=8.57 Hz, J_{8-9}=7.52 Hz, H8), 8.32 (d, 1H, J_{9-10}=8.30 Hz, H10), 8.23 (t, 1H, J_{9-10}=8.30 Hz, J_{8-9}=7.52 Hz, H9), 4.72 (s, 3H, H5), 4.40 (s, 3H, H15), 4.31 (s, 3H, H1).

8^{2+}: **3a** (10 mg, 0.034 mmols) and methyl triflate (40 μl, 0.34 mmols) were heated (45 ºC) in DCM (2 ml) in a sealed tube for overnight. The solution was filtrated and the solid residue was washed with fresh DCM and diethyl ether. Recrystallization with diethyl ether yielded brown crystals. ^{1}H-NMR (500MHz, CD$_3$CN): $\delta = 9.11$ (s, 1H, H14), 8.73 (s, 1H, H2$_2$), 8.64 (m, 2H, H7-8), 8.50 (m, 2H, H9-10), 4.69 (s, 3H, H5),

4.51 (s, 3H, H16), 4.49 (s, 3H, H15), 4.37 (s, 3H, H1). $^{13}C\{^{1}H\}$ NMR (500MHz, CD$_3$CN): δ = 153.82 (C4), 147.96 (C12), 140.30 (C8), 137.99 (C9), 134.22 (C14), 133.74 (C13), 133.50 (C3), 131.85 (C2), 131.55 (C7), 130.42 (C11), 127.77 (C6), 126.83 (C10), 52.00 (C5), 41.03 (C16), 40.33 (C15), 37.44 (C1).

9^{3+}: [RuCl$_3$(tpy)] (90 mg, 0.20 mmols) and LiCl (16 mg, 0.31 mmols) were dissolved in a solution of NEt$_3$ (57 μl, 0.41 mmols) and dry MeOH (30 mL). The mixture was stirred at room temperature for 20 min, and then **3a** (30 mg, 0.10 mmols) is added. The resulting solution was heated for overnight. The reaction mixture was filtered and then saturated aqueous NH$_4$PF$_6$ solution (1 mL) added to obtain a brown precipitate. The solid was collected, washed with cold water (3x5 mL) and diethyl ether (3 x 5 mL) and finally dried under vacuum to afford a mixture of complexes. Purification by alumina chromatography (DCM:MeOH 99:1) yielded pure **9(PF$_6$)$_3$** (Yield: 30 mg, 20%). ^{1}H NMR (400MHz, [D$_6$]acetone): δ = 9.94 (s, 2H, H2), 9.15 (dd, 2H, J$_{6\text{-}7}$ = 6.3 Hz, J$_{6\text{-}7'}$ = 3.3 Hz, H6), 8.67 (m, 8H, H14-8), 8.53 (d, 4H, J$_{11\text{-}10}$=7.80Hz H11), 8.47 (dd, 2H, J$_{7\text{-}6}$ = 6.3 Hz, J$_{7\text{-}6'}$ = 3.3 Hz, H7), 8.31 (t, 2H, J$_{15\text{-}14}$=9 Hz, H15), 8.00 (t, 4H, J$_{9\text{-}10}$=8.53 Hz, J$_{11\text{-}10}$=7.8 Hz, H10), 7.45 (t, 4H, J$_{9\text{-}10}$=7.8 Hz, J$_{9\text{-}8}$=6.3 Hz, H9), 4.14 (s, 6H, H1). $^{13}C\{^{1}H\}$ NMR (500MHz, [D$_6$]acetone): δ = 158.98 (C4), 158.65 (C13), 155.46 (C8), 153.52 (C5), 148.03 (C3), 139.43 (C10), 138.04 (C15), 136.44 (C7), 132.84 (C2), 128.51 (C9), 126.21 (C12), 125.96 (C6), 125.08 (C11), 123.76 (C14), 39.5 (C1). ESI-MS (MeOH): m/z = 1287.0 ([M-PF$_6$]$^{+}$).

10^{+}: obtained as a subproduct of the purification by alumina chromatography of **9^{3+}**. ^{1}H NMR (400MHz, [D$_6$]acetone): δ = 10.04, 9.45, 8.74, 8.69, 8.53, 8.35, 8.16, 8.03, 7.95, 7.80, 7.58, 7.53, 7.35, 4.76, 4.18.

V.5.   <u>References</u>

[1] R. Lalrempuia, N. McDaniel, H. Müller-Bunz, S. Bernhard, M. Albrecht, *Angew. Chem. Int. Ed.* **2010**, *49*, 9765–8; *Angew. Chem.* **2010**, *122*, 9959–62.

[2] a) P. L. Arnold, S. Pearson, *Coord. Chem. Rev.* **2007**, *251*, 596; b) M.Albrecht, *Chem. Commun.* **2008**, 601; c) O. Schuster, L. Yang, H. G.Raubenheimer, M. Albrecht, *Chem. Rev.* **2009**, *109*, 3445.

[3] For biruthenium catalysts, see: a) S. W. Gersten, G. J. Samuels, T. J. Meyer, *J. Am. Chem. Soc.* **1982**, *104*, 4029; b) C. Sens, I. Romero, M. Rodriguez, A. Llobet, T. Parella, J. Benet-Buchholz, *J. Am. Chem. Soc.* **2004**, *126*, 7798; c) R. Zong, R. P. Thummel, *J. Am. Chem. Soc.* **2005**, *127*, 12802; d) Z. Deng, H. Tseng, R. Zong, D. Wang, R. Thummel, *Inorg. Chem.* **2008**, *47*, 1835. For tetrametallic systems, see: e) A. Sartorel, M. Carraro, G. Scorrano, R. De Zorzi, S. Geremia, N. D. McDaniel, S. Bernhard, M. Bonchio, *J. Am. Chem. Soc.* **2008**, *130*, 5006; f) Y. V. Geletii, B. Botar, P. Koegerler, D. A. Hillesheim, D. G. Musaev, C. L. Hill, *Angew. Chem.* **2008**, *120*, 3960; *Angew. Chem. Int. Ed.* **2008**, *47*, 3896; g) A. Sartorel, P. Miro, E. Salvadori, S. Romain, M. Carraro, G. Scorrano, M. Di Valentin, A. Llobet, C. Bo, M. Bonchio, *J. Am. Chem. Soc.* **2009**, *131*, 16051.

[4] Xu, Y; Fischer, A; Duan, L; Tong, L; Gabrielsson, E; Akermark, B; Sun, L. *Angew. Chem. Int. Ed.* **2010**, *49*, 8934 –8937.

[5] Xu, Y; Akermark, T; Gyollai, V.; Zou, D; Eriksson, L.; Duan, L; Zhang, R.; Akermark, B; Sun, L. *Inorg. Chem.* **2009**, *48*, 2717-2719.

[6] Sens, C.; Romero, I.; Rodríguez M.; Llobet A.; Parella, T.; Benet-Buchholz, J. *J. Am. Chem. Soc.* **2004**, *126*, 7798-7799.

[7] P. Mathew, A. Neels, M. Albrecht, *J. Am. Chem. Soc.* **2008**, *130*, 13534. (b) Schuster, O.; Yang, L.; Raubenheimer, H.G.; Albrecht, M. *Chem. Rev.*, **2009**, *109* (8), 3445–3478. (c) Albrecht, M. *Science*, **2009**, *326*, 532-533. (d) Krüger, A.; Albrecht, M. *Chemistry-A European Journal*, 2012, 18. (e) Mercs, L.; Neels, A.; Stoeckli-Evans, H.; Albrecht, M. *Inorg. Chem.*, **2011**, *50,* 8188-8196. (f) Albrecht, M.; Cavell, K.J. *Organ. Chem.*, **2009** *35* :47-61.

[8] Chinchilla R.; Nájera C. *Chem. Soc. Rev.* **2011**, *40*, 5084-5121

[9] Gottardo, C.; Kraft, T.M.; Hossain, M.S.; Zawada, P.V.; Muchall, H.M. *Can. J. Chem.*, **2008**, *86*, 410-415

[10] Bosdet, Michael J.D.; Piers, Warren E.; Sorensen, Ted S.; Parvez, M. *Can. J. Chem.* **2010**, *88*, 426–433.

[11] Lehmann-Lintz, T., Stenkamp, D., Roth, G.J., Mueller, S.G., Kley, J., Heckel, A., Rudolf, K., Schindler, M., Lotz, R., Tielmann, P., Preparation of New Pyridazine Derivatives with MCH Antagonistic Activity. 2008071646, Jun 19, 2008

[12] Hirsch, A.; Orfphanos, D.G. *Can. J. Chem.*, **1966**, *44(13)*, 1551-4.

[13] Barral, K.; Moorhouse, A.D.; Moses, J.E. *Org. Lett.*, **2007**, *9(9)*, 1809–1811

[14] Fletcher, J.T.; Bumgarner, B.J.; Engels, N.D.; Skoglund, D.A. *Organometallics*, **2008**, *27 (21)*, 5430–5433.

[15] Reich, H.J. University of Wisconsin, **2010**.

[16] Heck, R. F. *Palladium Reagents in Organic Synthesis*; Academic Press: London, **1985**.

[17] Sullivan, B.P.; Calvert, J.M.; Meyer, T.J. *Inorg. Chem.* **1980**, *19*, 1404.

[18] Spek, A. L. *J. Appl. Cryst*. 2003, **36**, 7.

[19] Sheldrick, G. M. *Acta Cryst.* 2008, **A64**, 112.

V.6.   <u>Supporting Information</u>

- NMR
- ESI-MS
- X-ray

V

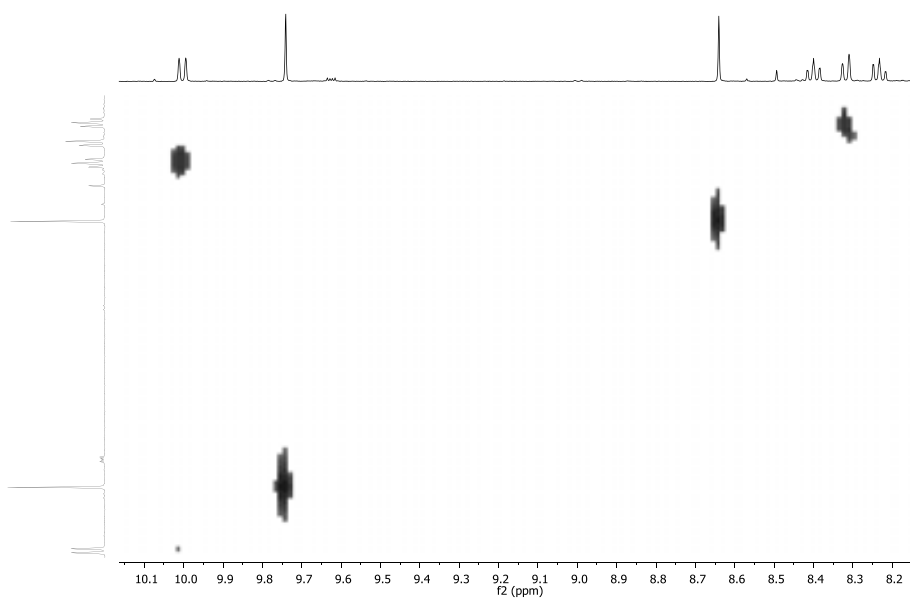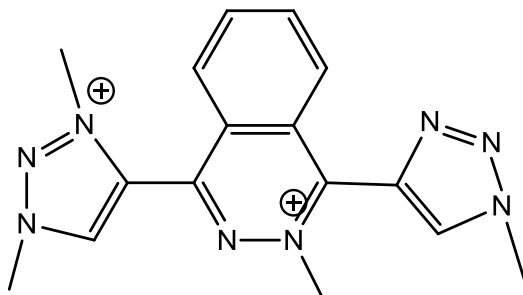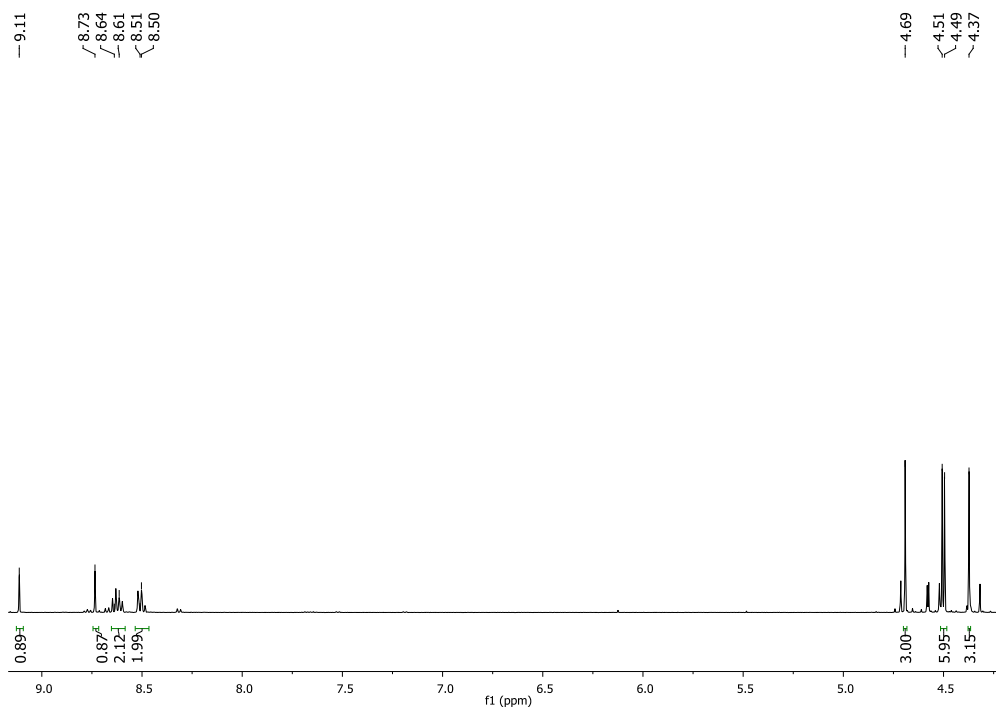**Figure S1.** 1D and 2D NMR spectra (500 MHz, 298 K, CDCl$_3$) for **5**: (a) **5** schematic representation (b) ^{1}H-NMR, (c) COSY, (d) ^{13}C-{^{1}H}-NMR, (e) HSQC-NMR (aromatic region) (f) HMBC-NMR (aromatic region).

a)
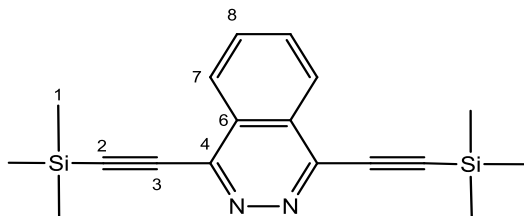
b)
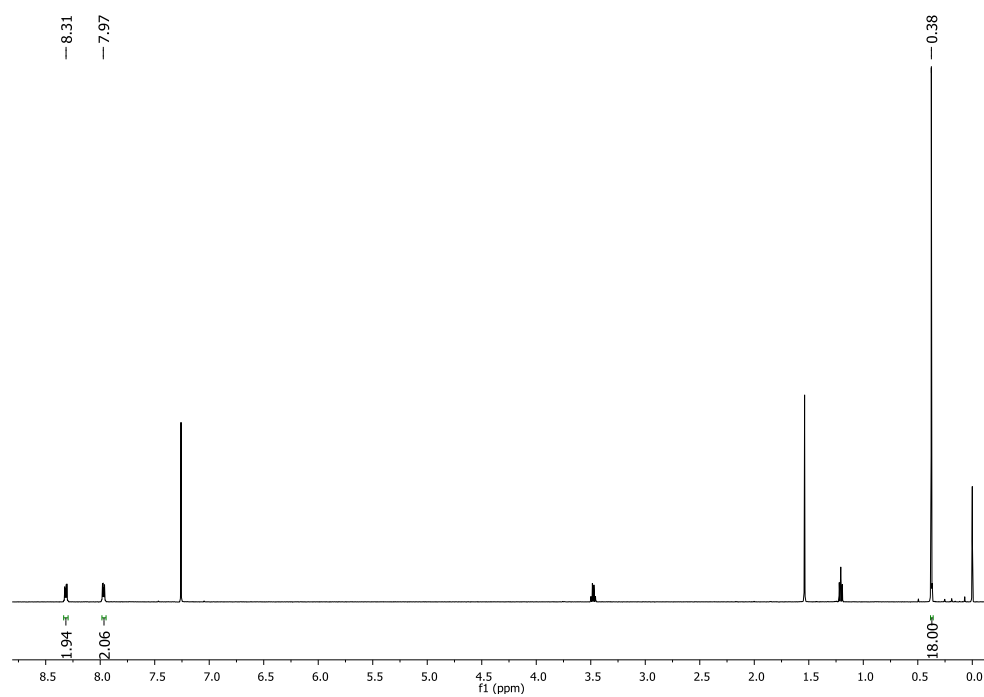
c)
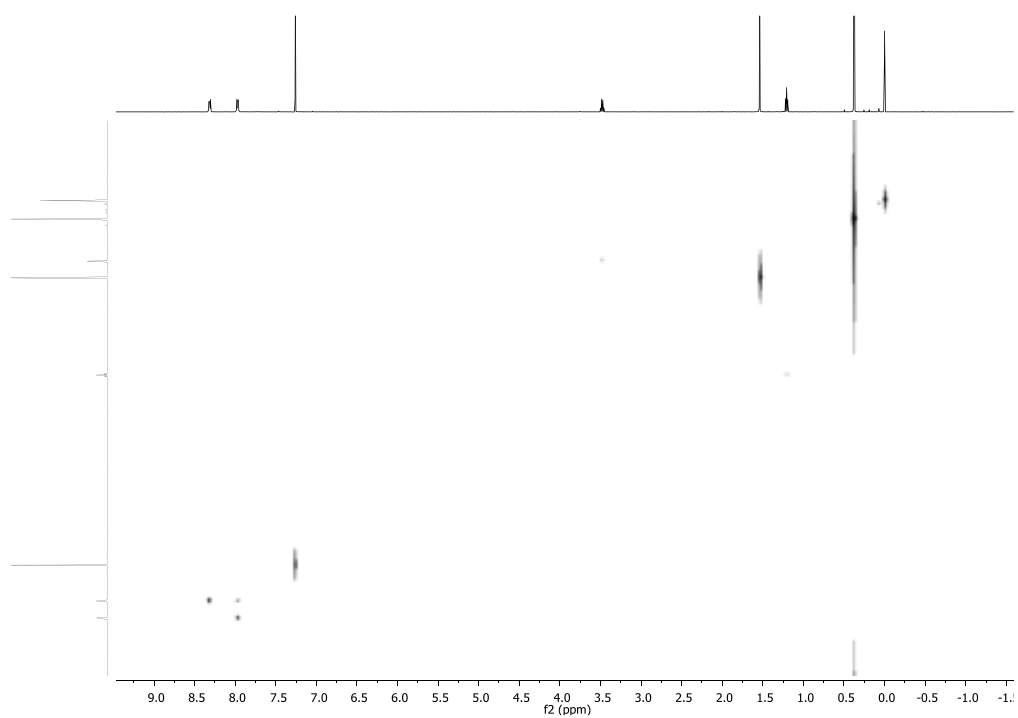
d)
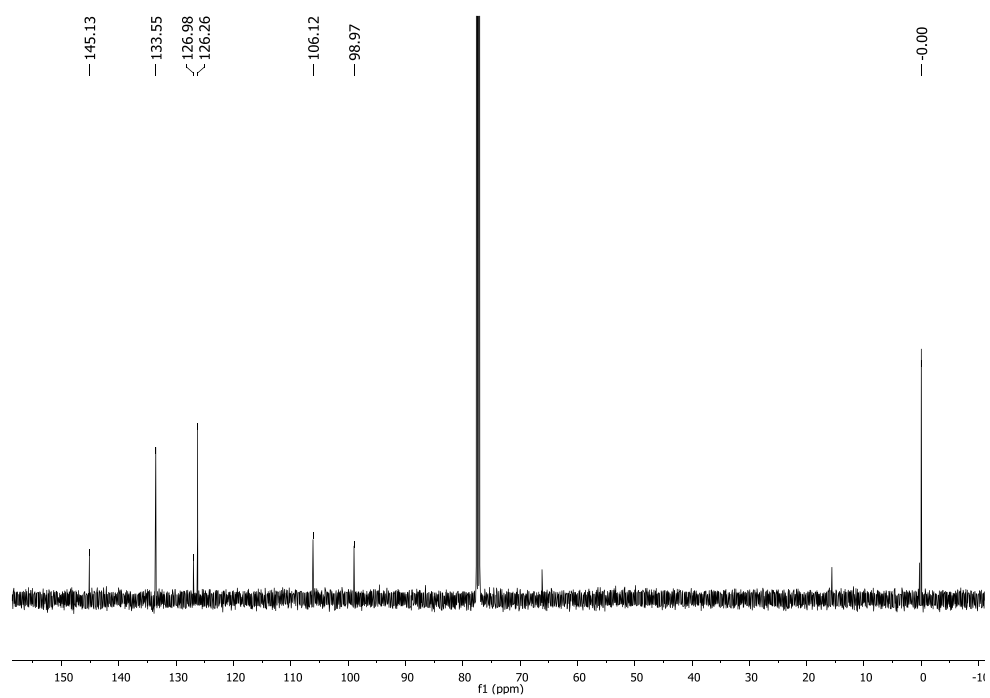
e)
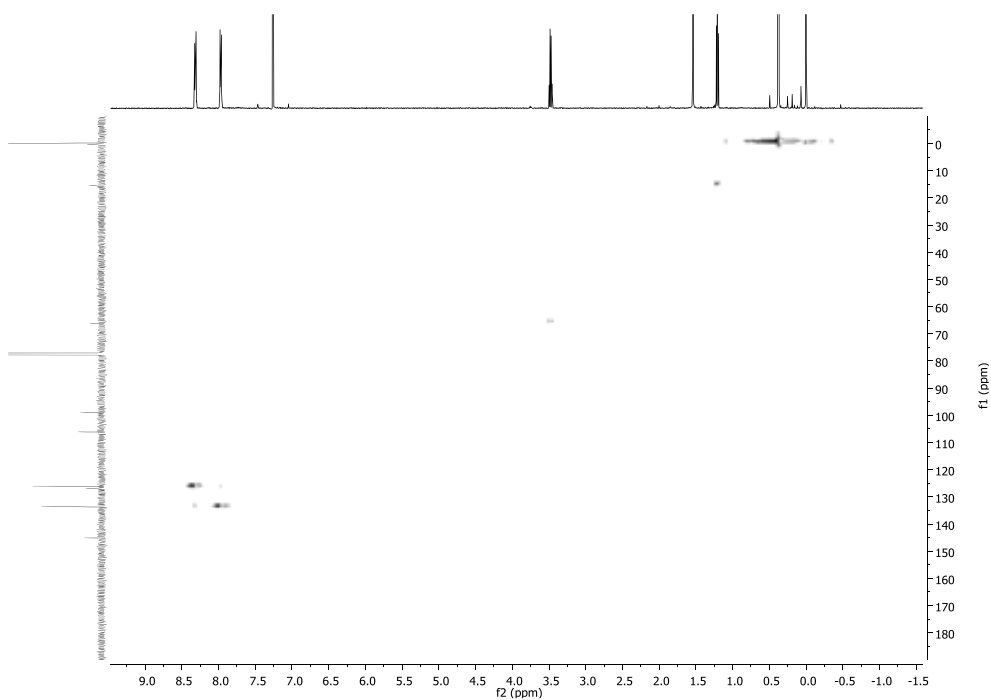
f)
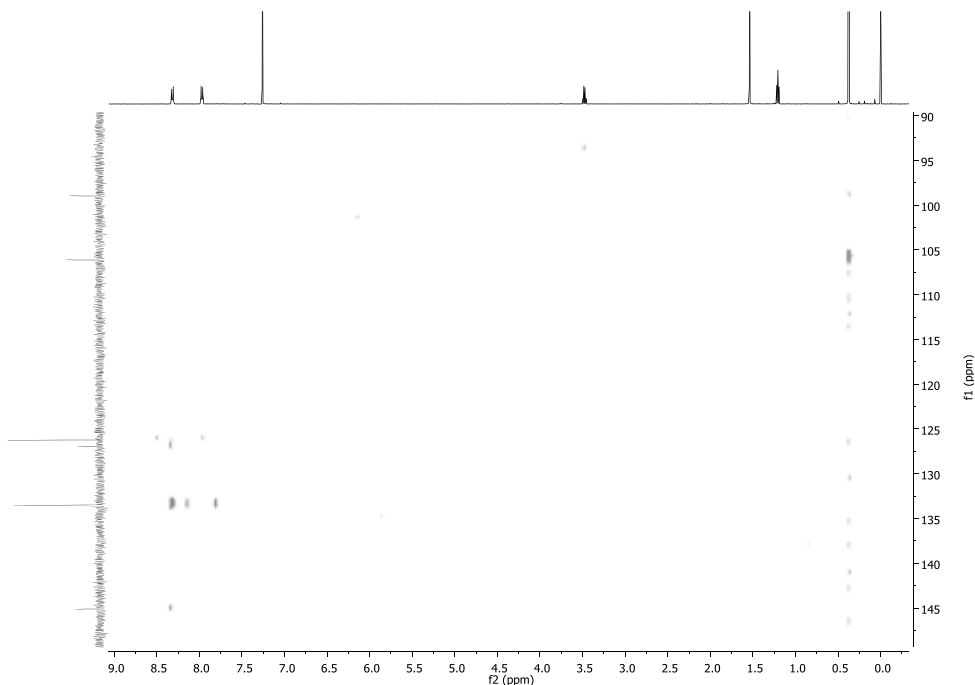
Figure S2. 1D and 2D NMR spectra (500 MHz, 298 K, CDCl$_3$) for **3a**: (a) **3a** schematic representation (b) ^{1}H-NMR, (c) COSY, (d) ^{13}C-{^{1}H}-NMR, (e) HSQC-NMR (aromatic region).

(a)
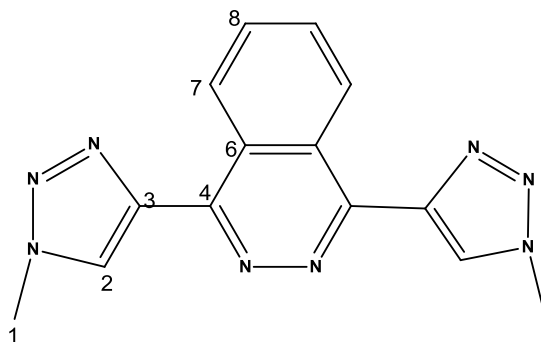
(b)
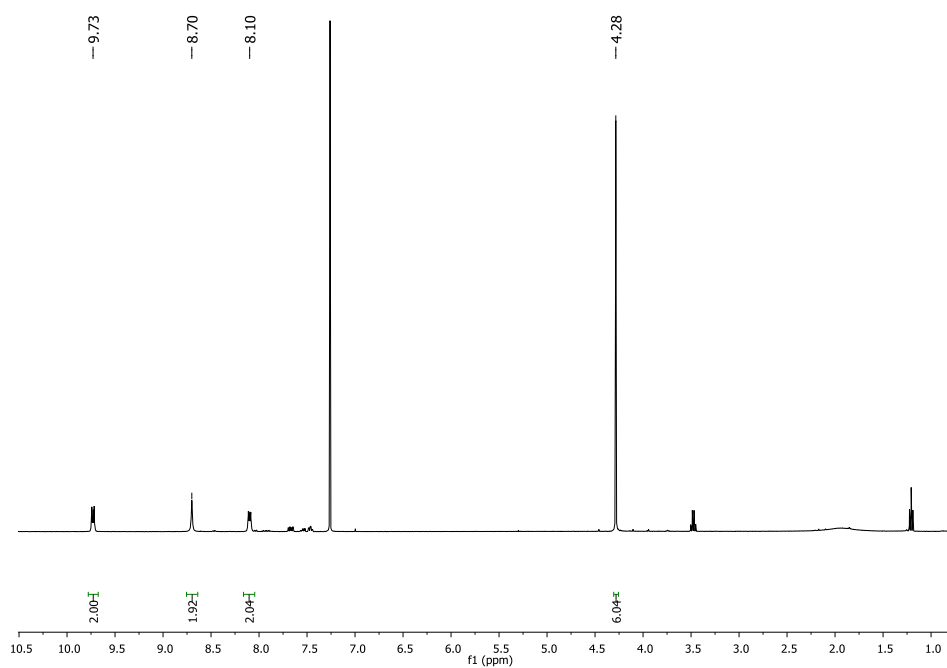
(c)
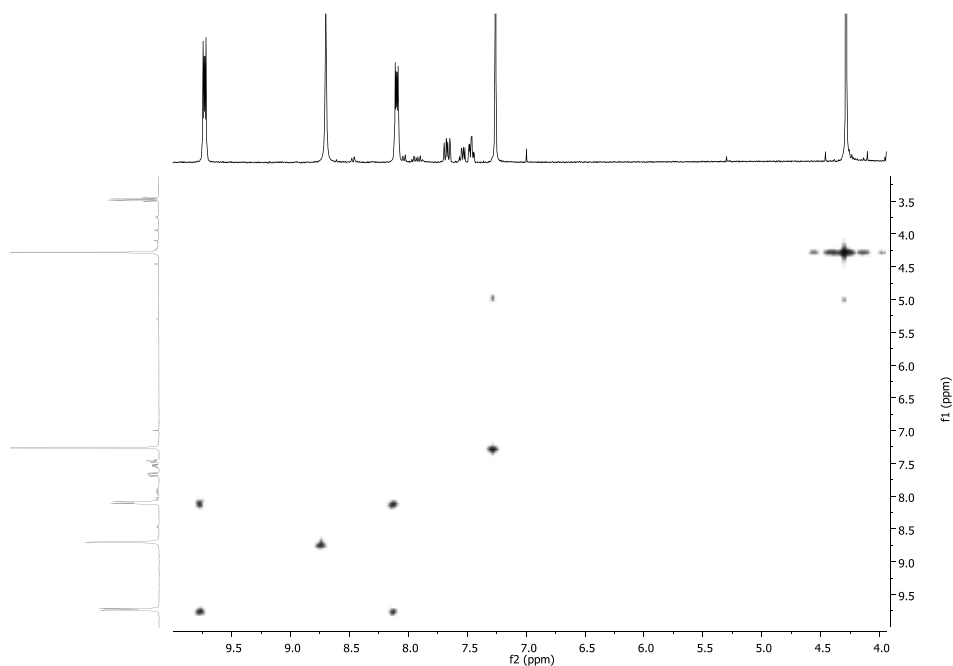
(d)
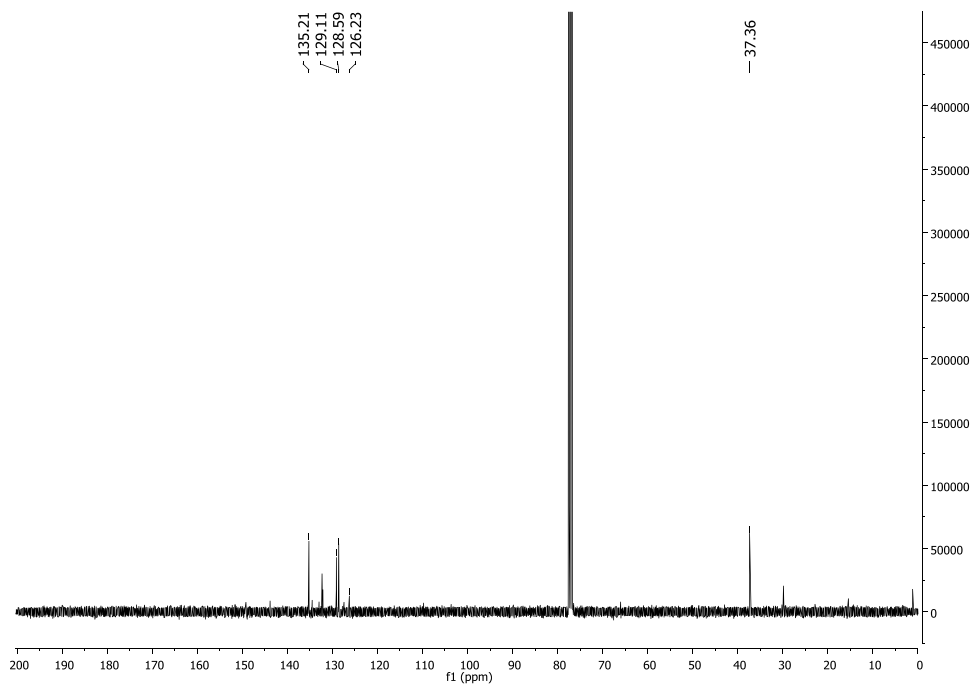
(e)
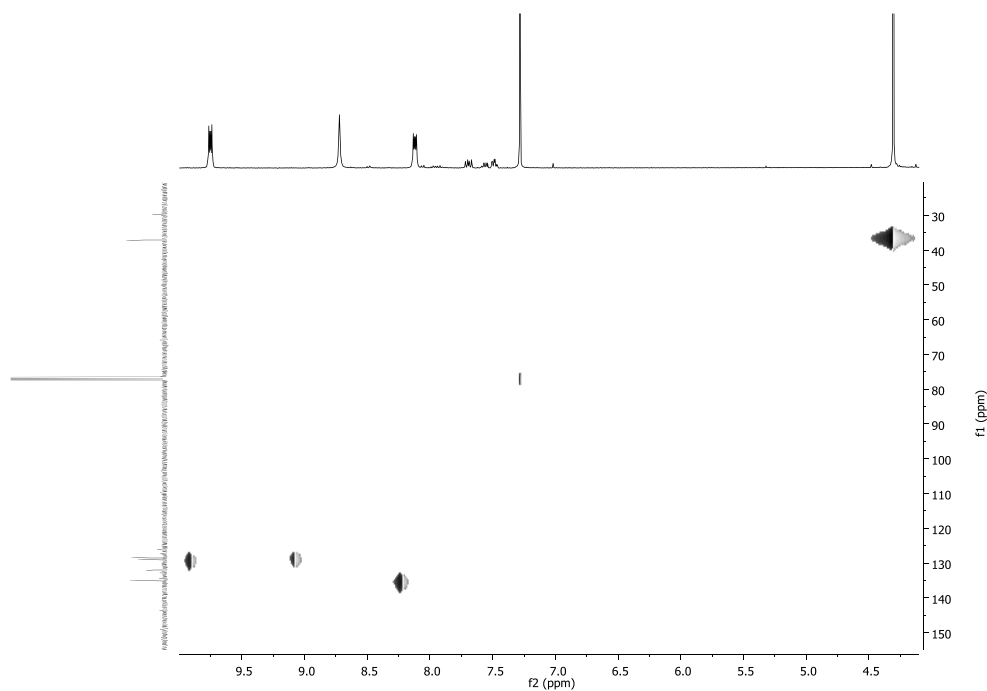
Figure S3. 1D and 2D NMR spectra (500 MHz, 298 K, CDCl$_3$) for **3b**: (a) **3b** schematic representation (b) ^{1}H-NMR, (c) COSY, (d) ^{13}C-{^{1}H}-NMR, (e) HSQC-NMR (aromatic region), (f) HMBC-NMR (aromatic region).
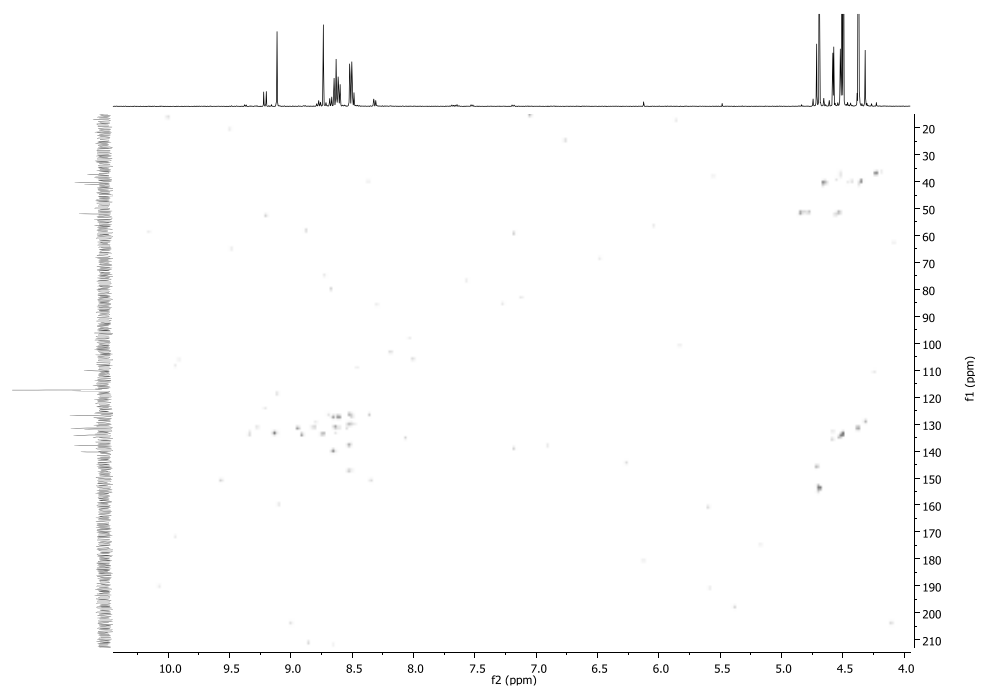
(a)

V
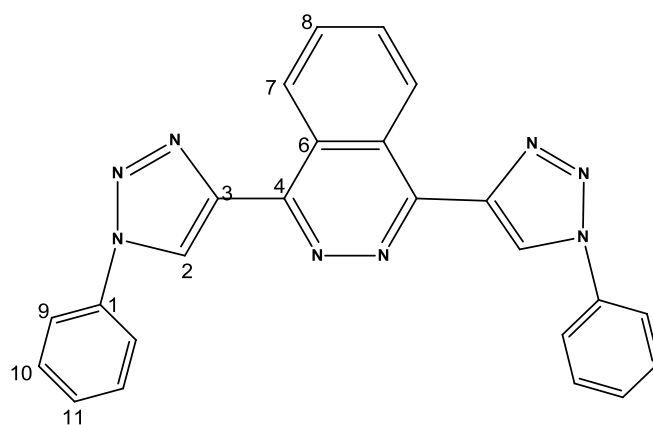
(b)
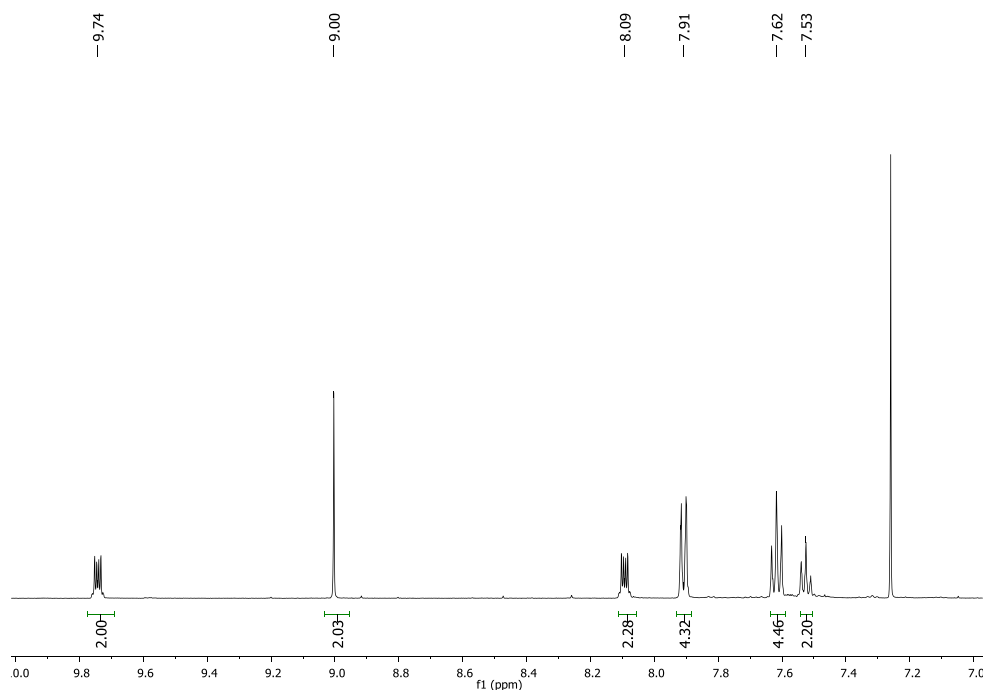
(c)
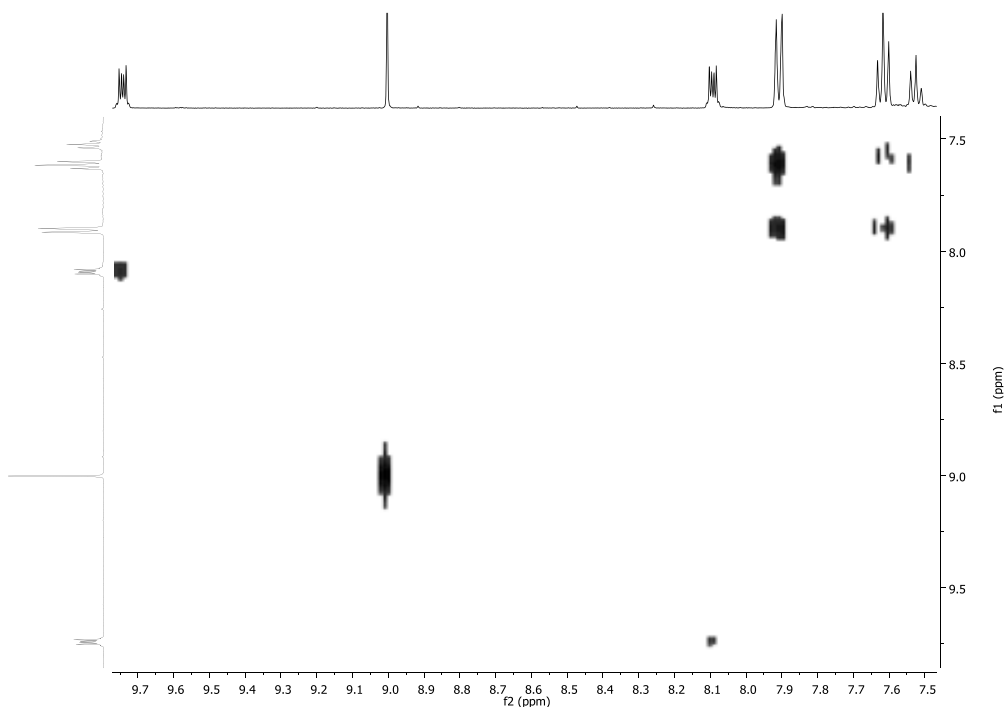
(d)
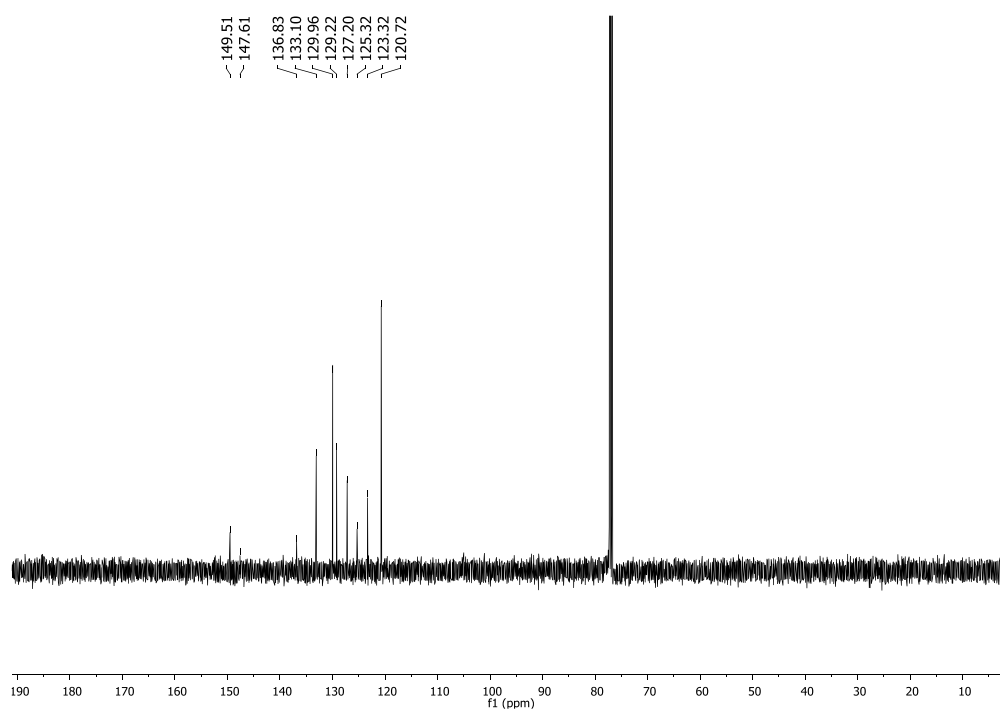
(e)
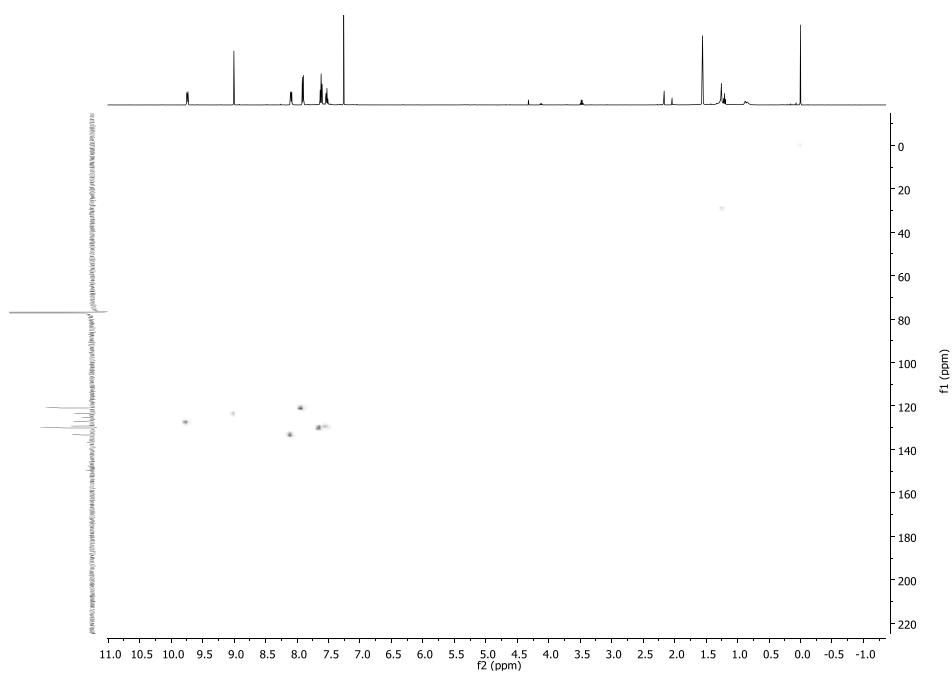
(f)
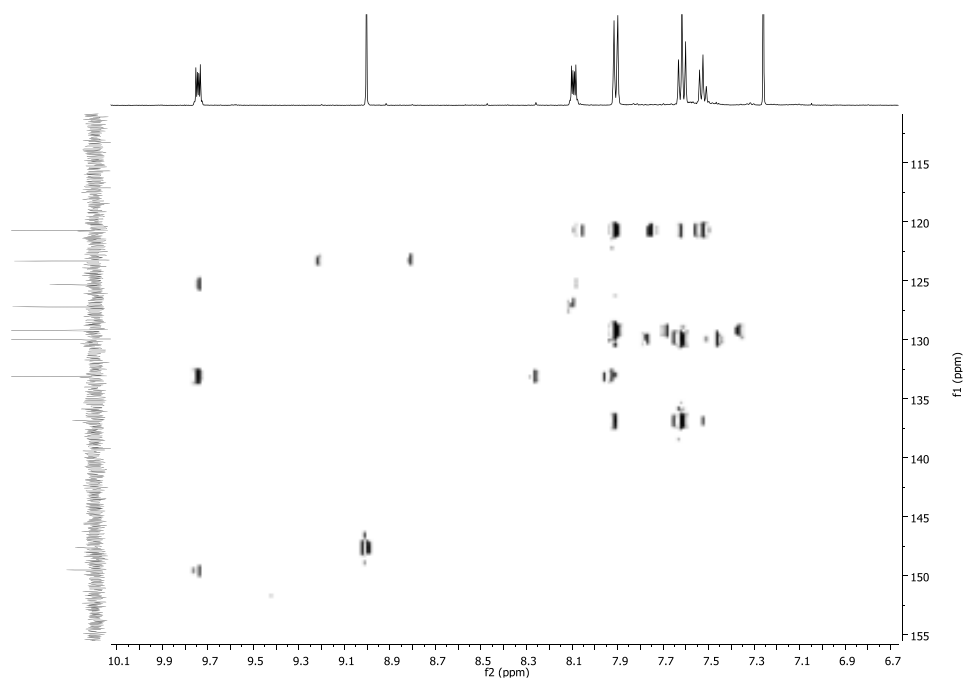
Figure S4. 1D and 2D NMR spectra (500 MHz, 298 K, CDCl$_3$) for **7$^+$**. (a) **7$^+$** schematic representation (b) ^{1}H-NMR, (c) COSY.

(a)
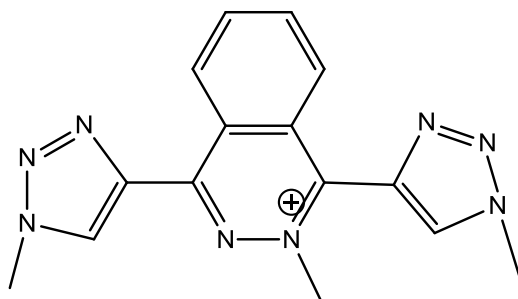
(b)
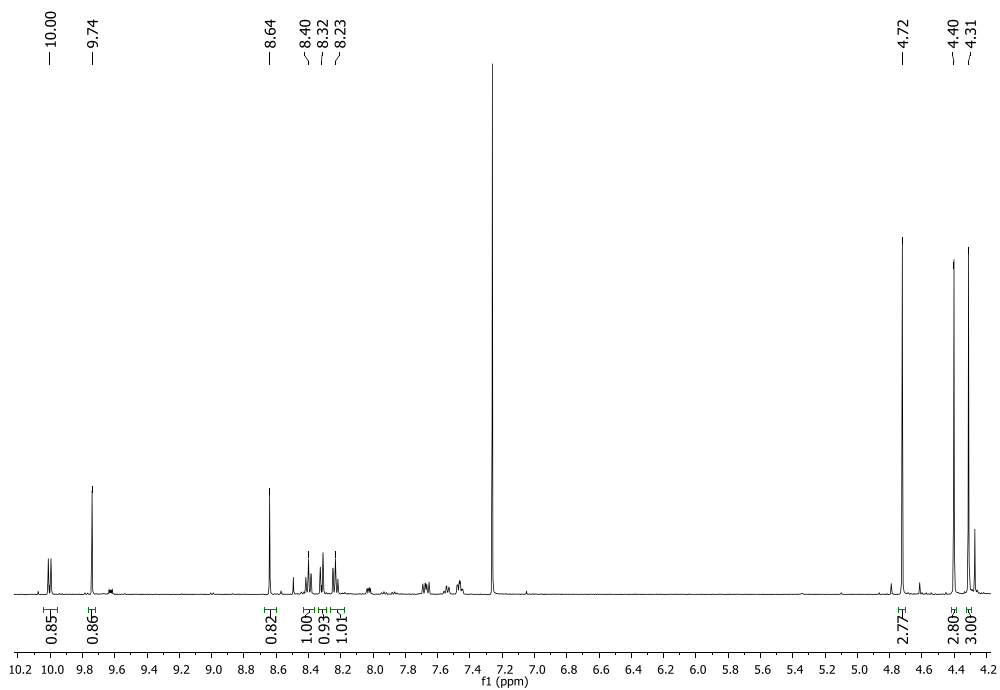
(c)

Figure S5. 1D and 2D NMR spectra (500 MHz, 298 K, CD_3CN) for $\mathbf{8^{2+}}$: (a) $\mathbf{8^{2+}}$ schematic representation (b) ^{1}H-NMR, (c) COSY, (d) ^{13}C-{^{1}H}-NMR, (e) HSQC-NMR (aromatic region), (f) HMBC-NMR (aromatic region).

(a)

(b)

(c)

(d)

V
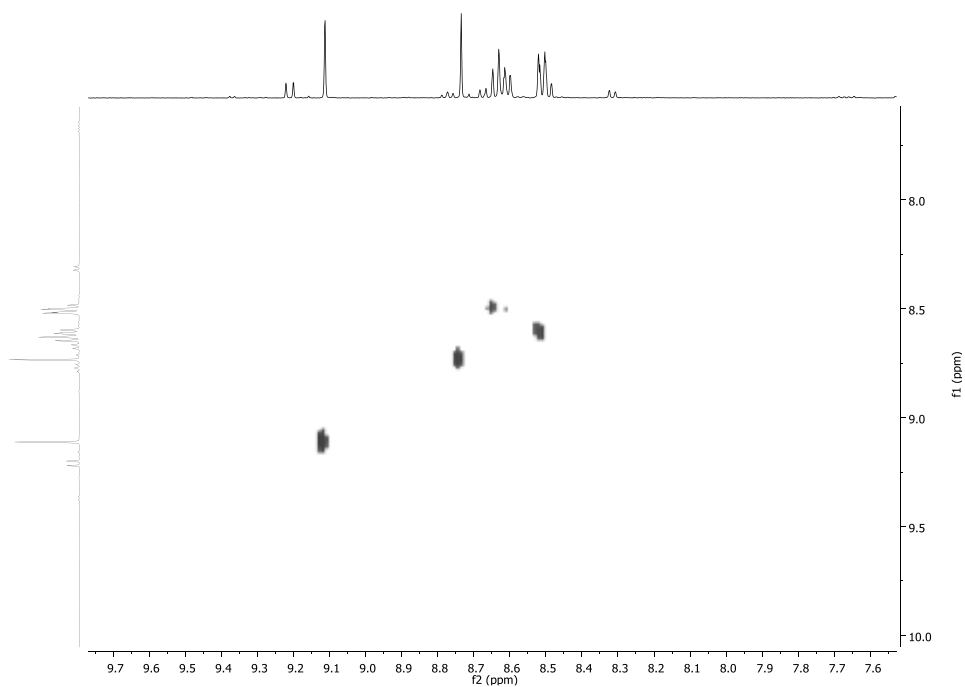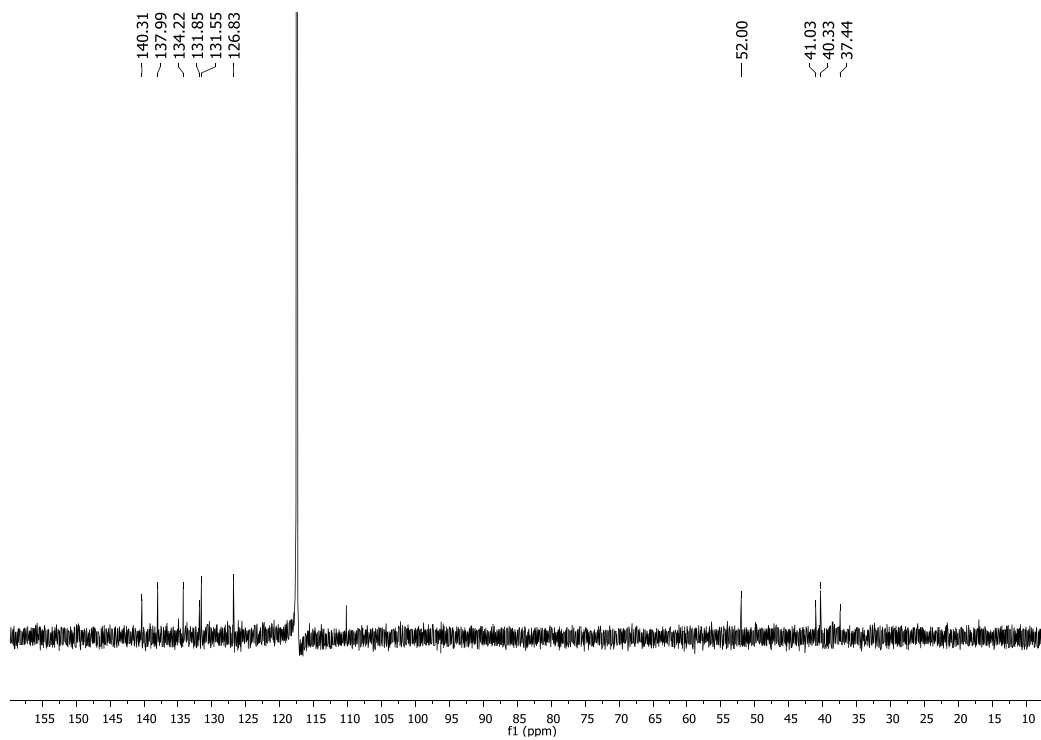
(e)
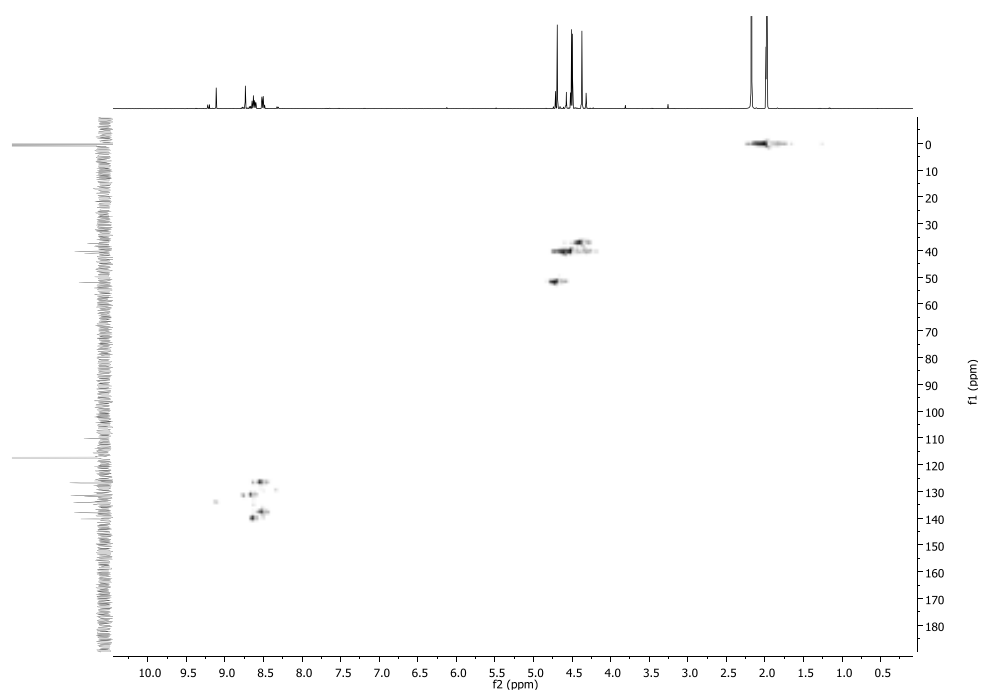
(f)

Figure S6. 1D and 2D NMR spectra (500 MHz, 298 K, Acetone-d6) for **9³⁺**: (a) ¹H-NMR, (b) COSY, (c) ¹³C-{¹H}-NMR, (d) HSQC-NMR (aromatic region), (e) HMBC-NMR (aromatic region).
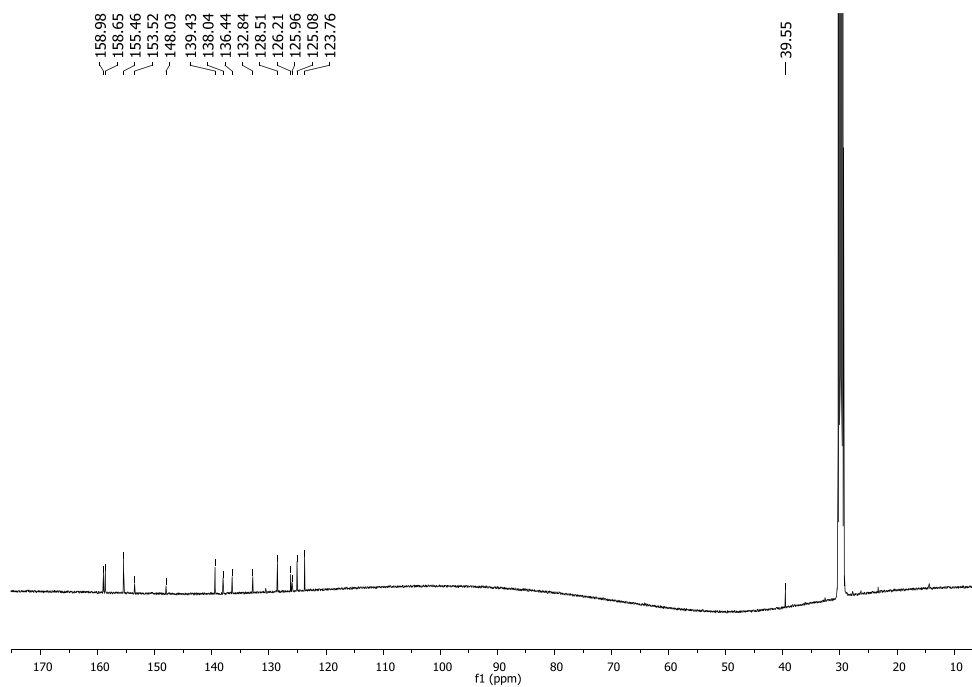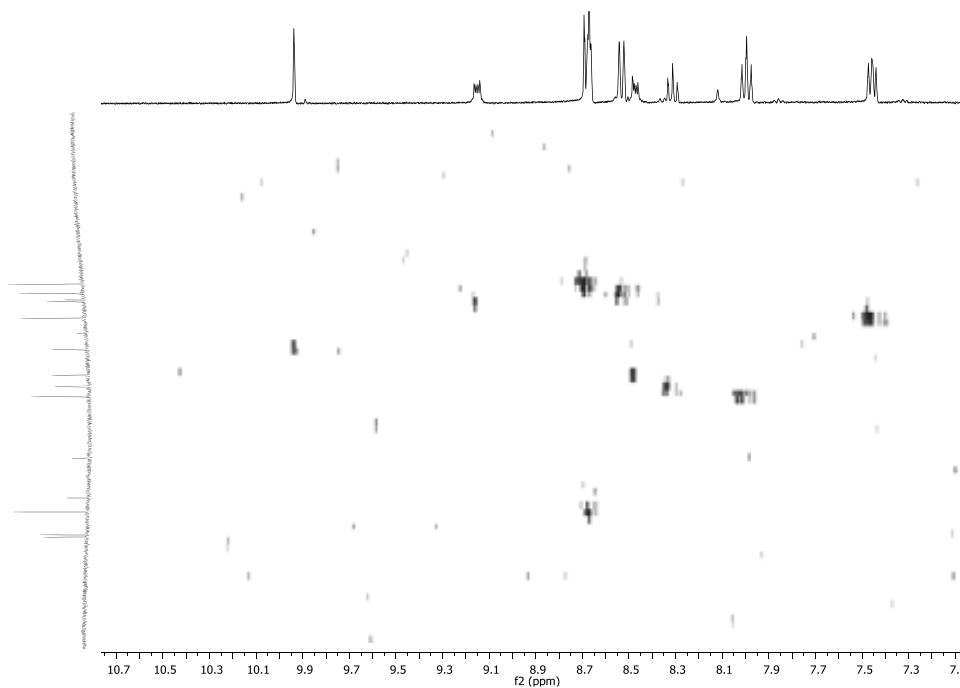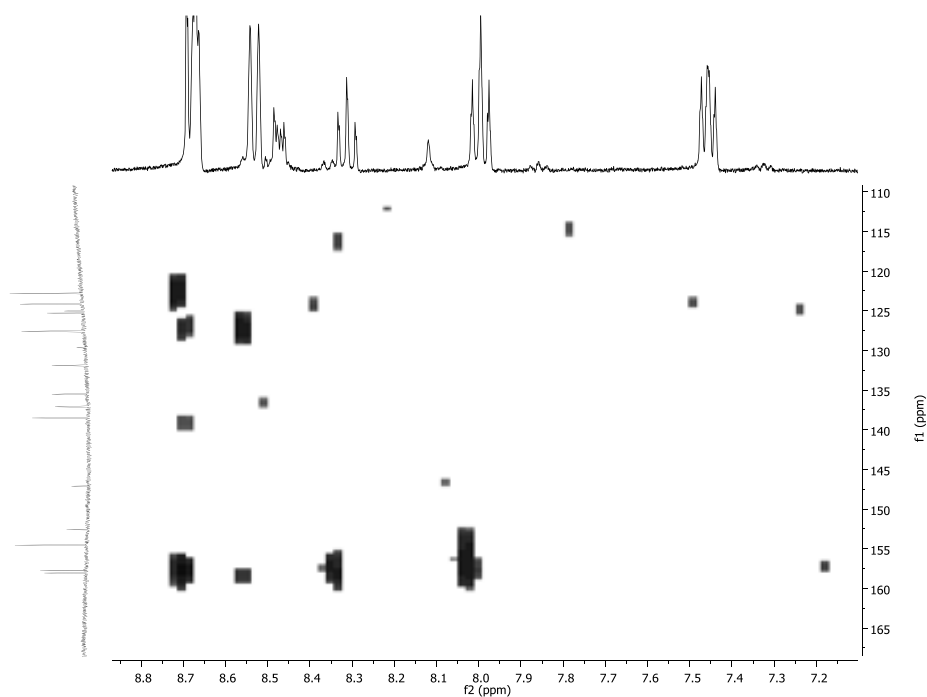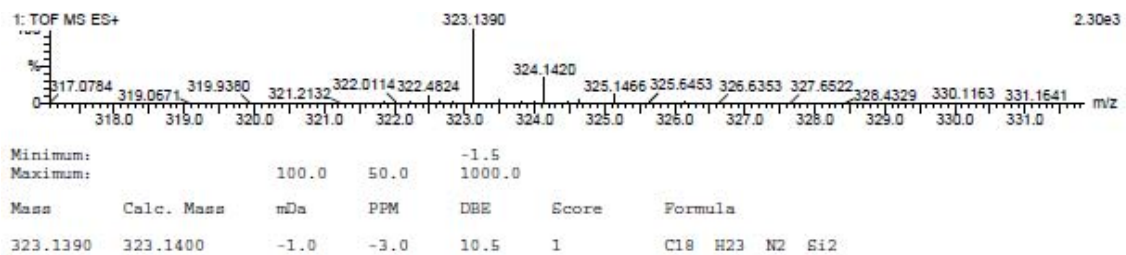
(a)
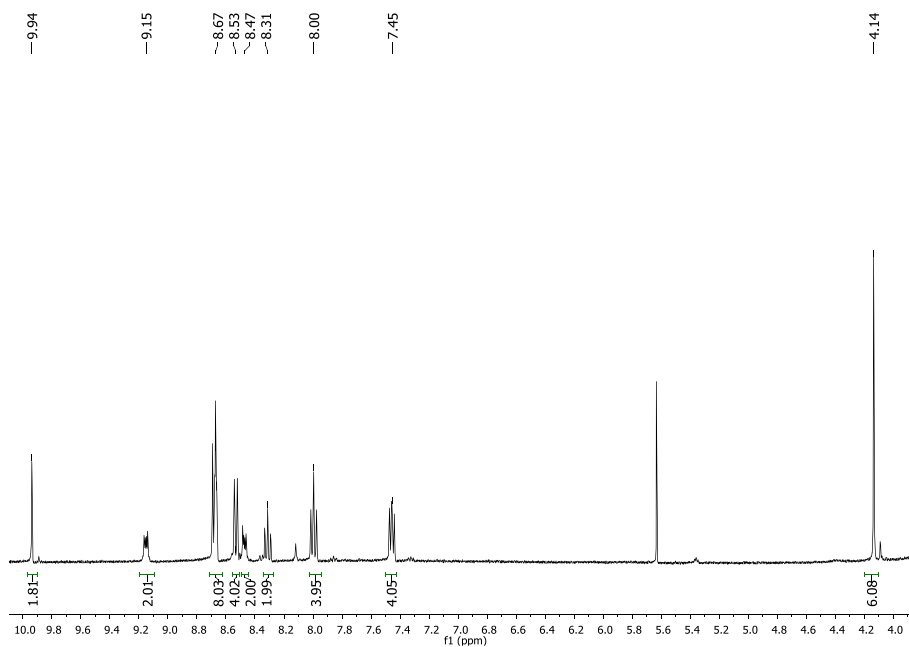
(b)
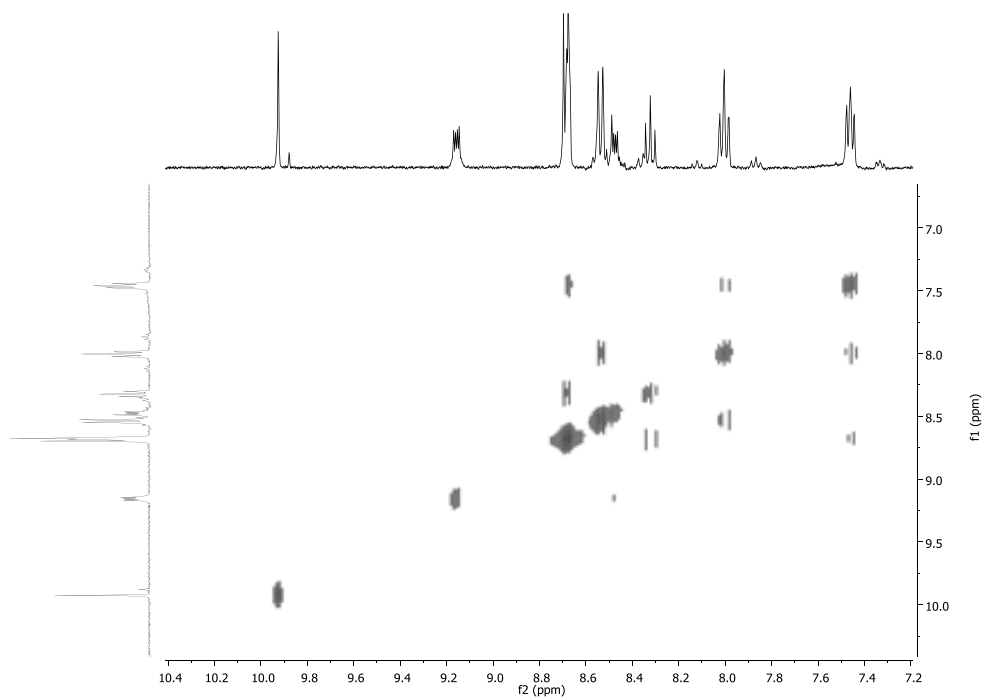
(c)
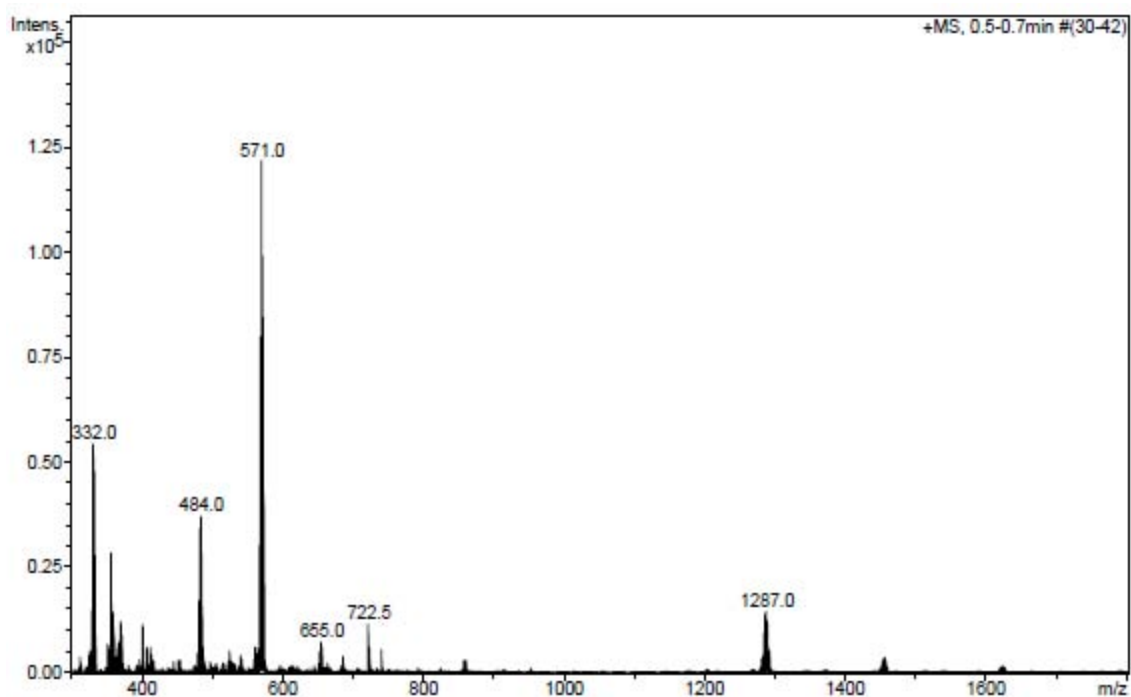
(d)

(e)

Figure S7 Mass Spectrum for **5**.

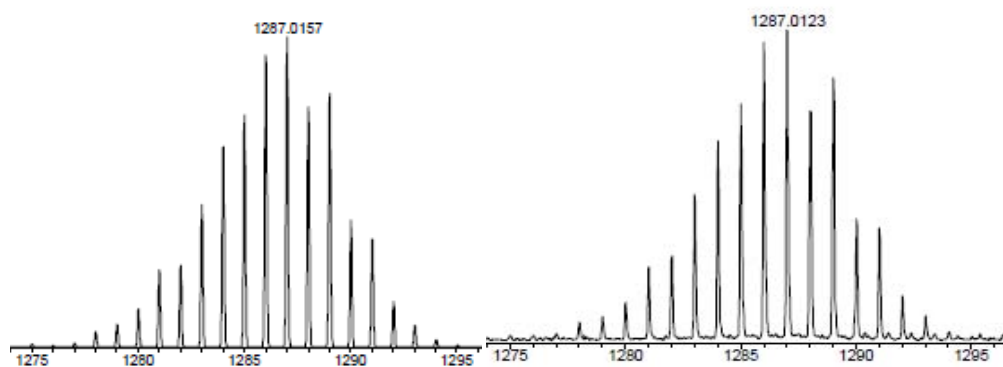**Figure S8** Mass Spectrum for complex **9³⁺**

Figure S9 Experimental (right side) and theoretical zoom (left side) Mass Spectra for complex **9³⁺**.

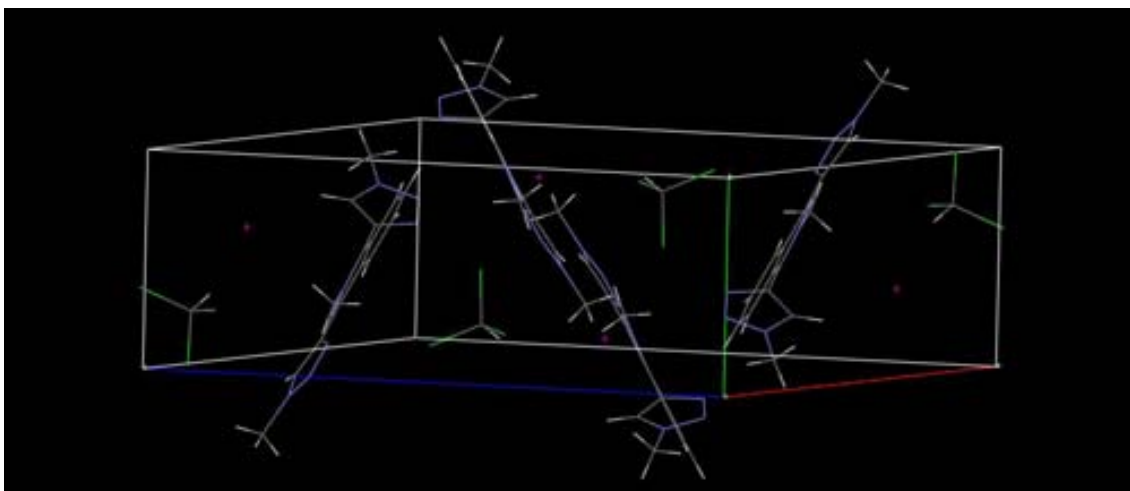**Figure S10** Stereoscopic view of **7**⁺ unit cell.

Figure S11 Stereoscopic view of **7**⁺ with the triazole torsion angle.

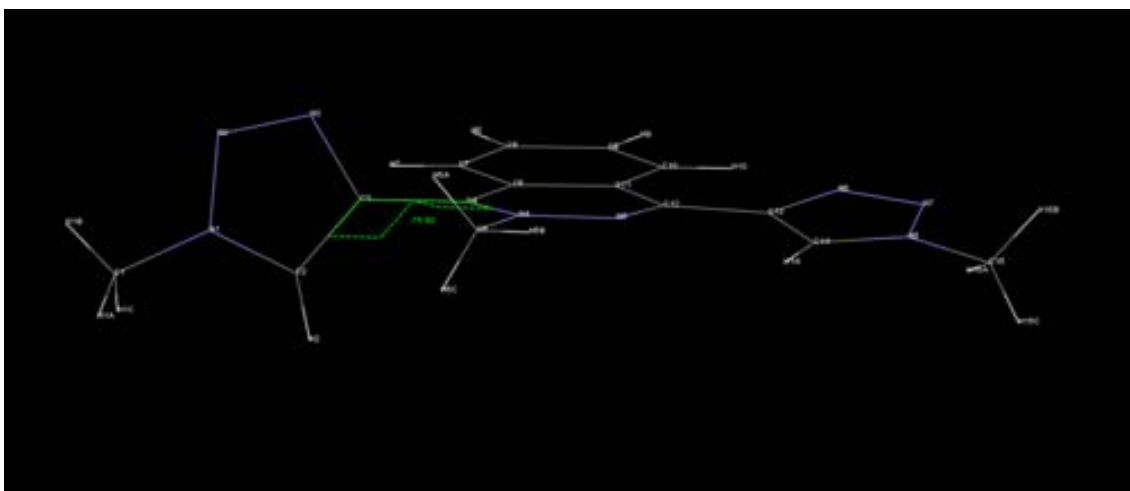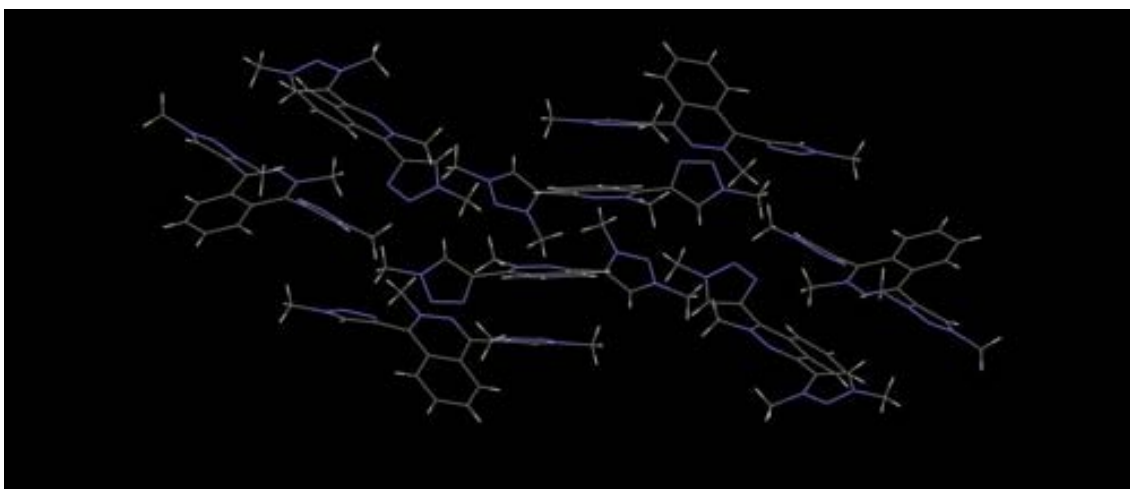**Figure S12** Stereoscopic view of 8^{2+} unit cell.

Figure S13 Stereoscopic view of 8^{2+} with the triazole torsion angles.
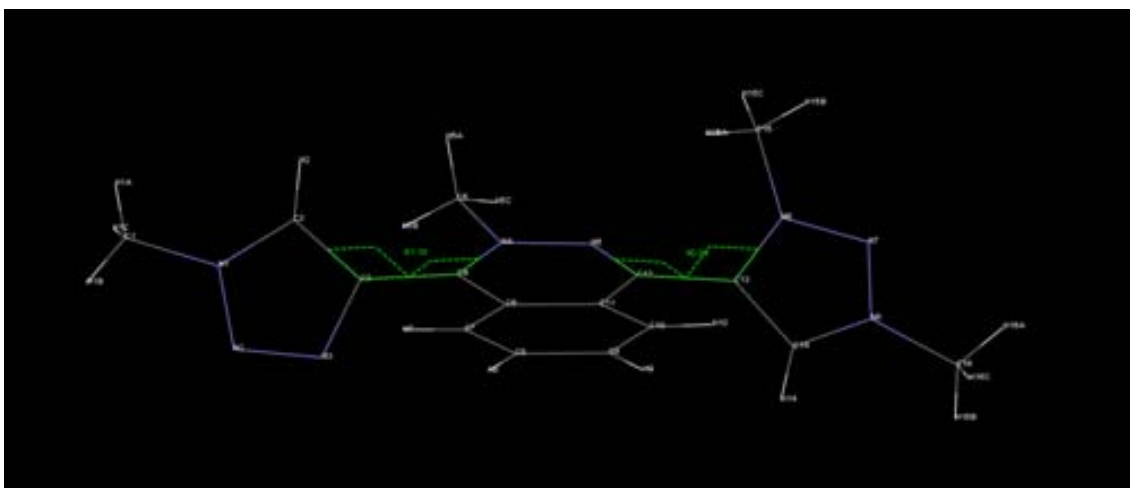
Figure S14 Stereoscopic views of **9**$^{3+}$ unit cell.

V
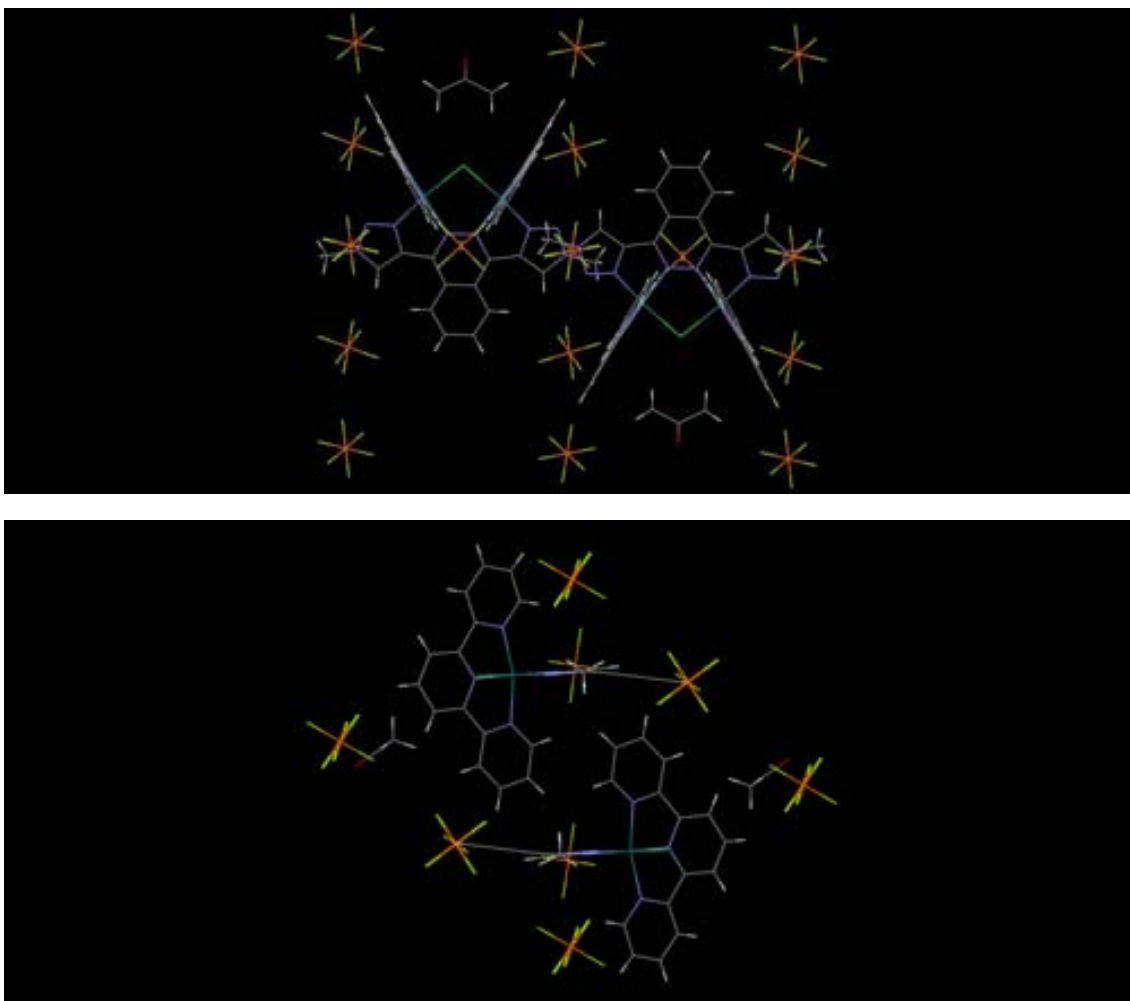
Table S1. Crystallographic data for **7**$^{+}$.

Formula	C15 H15 N8, C H Cl3, I
Formula Weight	553.62
Crystal System	Monoclinic
Space group	P21/c (No. 14)
a, b, c [Angstrom]	16.5447(6) 6.8596(3) 19.1037(8)
V [Ang**3]	2119.32(15)
alpha, beta, gamma [deg]	90 102.175(4) 90
Z	4
D(calc) [g/cm**3]	1.735
Mu(MoKa) [/mm]	1.909
F(000)	1088
Crystal Size [mm]	0.08 x 0.10 x 0.18
Temperature (K)	100
Radiation [Angstrom]	MoKa 0.71073
Theta Min-Max [Deg]	3.3, 24.1

Dataset	-18: 18 ; -7: 7 ; -21: 21
Tot., Uniq. Data, R(int)	15714, 3351, 0.054
Observed data [I > 2.0 sigma(I)]	2791
Nref, Npar	3351, 256
R, wR2, S	0.0288, 0.0638, 1.06
w = 1/[\s^2^(Fo^2^)+(0.0197P)^2^+2.5839P] where P=(Fo^2^+2Fc^2^)/3	
Max. and Av. Shift/Error	0.00, 0.00
Min. and Max. Resd. Dens. [e/Ang^3]	-0.39, 0.79

Table S2. Crystallographic data for 8^{2+}.

Formula	C16 H18 N8, 2(C F3 O3 S)
Formula Weight	620.54
Crystal System	Orthorhombic
Space group	Pbca (No. 61)
a, b, c [Angstrom]	23.156(1) 8.0465(3) 26.901(1)
V [Ang**3]	5012.3(3)
Z	8
D(calc) [g/cm**3]	1.645
Mu(MoKa) [/mm]	0.310
F(000)	2528
Crystal Size [mm]	0.00 x 0.00 x 0.00
Temperature (K)	293
Radiation [Angstrom]	MoKa 0.71073
Theta Min-Max [Deg]	3.4, 22.0
Dataset	-24: 24 ; -8: 8 ; -28: 28
Tot., Uniq. Data, R(int)	20946, 3069, 0.056
Observed data [I > 2.0 sigma(I)]	2844
Nref, Npar	3069, 365
R, wR2, S	0.0869, 0.1660, 1.20
w = 1/[\s^2^(Fo^2^)+(0.0000P)^2^+42.4684P] where P=(Fo^2^+2Fc^2^)/	
Max. and Av. Shift/Error	0.01, 0.00
Min. and Max. Resd. Dens. [e/Ang^3]	-0.39, 0.43

Table S3. Crystallographic data for complex 9^{3+}.

Formula	C44 H34 Cl N14 Ru2, 3 (F6 P), 2 (C3 H6 O)
Formula Weight	1547.51
Crystal System	Monoclinic
Space group	P21/m (No. 11)
a, b, c [Angstrom]	11.8427(5) 21.0984(7) 12.933(1)
alpha, beta, gamma [deg]	90 103.303(6) 90
V [Ang**3]	3144.8(3)
Z	2
D(calc) [g/cm**3]	1.573

Mu(MoKa) [/mm]	1.573
F(000)	1480
Crystal Size [mm]	0.03 x 0.13 x 0.26
Temperature (K)	100
Radiation [Angstrom]	MoKa 0.71073
Theta Min-Max [Deg]	3.4, 24.1
Dataset	-13: 13 ; -24: 24 ; -14: 13
Tot., Uniq. Data, R(int)	14563, 5106, 0.054
Observed data [I > 2.0 sigma(I)]	3837
Nref, Npar	5106, 423
R, wR2, S	0.0485, 0.1298, 1.04
w = 1/[\s^2^(Fo^2^)+(0.0701P)^2^+1.1102P] where P=(Fo^2^+2Fc^2^)/3	
Max. and Av. Shift/Error	0.00, 0.00
Min. and Max. Resd. Dens. [e/Ang^3]	-0.52, 1.03

V

CHAPTER VI

Mononuclear Ru(II) Complexes Containing the PY4Im Ligand: Synthesis, Characterization and Oxidative Catalysis

VI
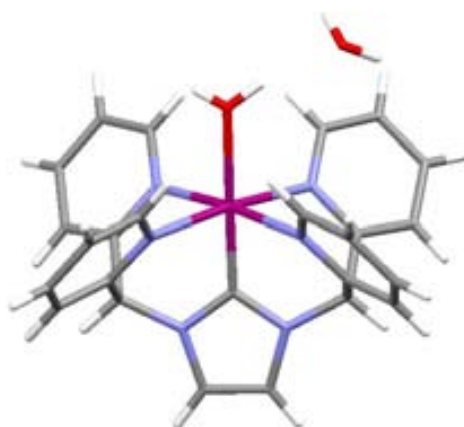
In this chapter we present the synthesis and the spectroscopical and electrochemical characterization of a new family of complexes with general formula $[Ru^{II}(PY4Im)(X)]^{n+}$ (X = Cl, n = 1 or X = H_2O, n = 2), where PY4Im is the pentadentate 1,3-bis(bis(2-pyridyl)methyl)imidazol-2-ylidene ligand. These results together with the performance of the new species towards the oxidation of water and alkenes will be thoroughly discussed in the present chapter.

CHAPTER VI. Mononuclear Ru(II) Complexes Containing the PY4Im Ligand: Synthesis, Characterization and Oxidative Catalysis

VI

VI.1.   <u>**Introduction**</u>

Since 2008, when contributions from the groups of Thummel and Meyer[1] pointed out that polypyridyl Ru complexes with only one active site were also capable (in addition to the well known activity of dinuclear species) to mediate the multiple proton electron transfer processes needed for water oxidation, an important number of publications within this field have appeared.[2]

Pentadentate ligands that coordinate metals in a square pyramidal fashion are able to both enforce an octahedral geometry around the metal center as well as restrict the metal substitution chemistry to a single coordination site. An archetypical example of them is the PY5R$_2$ family (Chart 1), which usually binds the metal ion through one axial and four equatorial pyridine donors.[3] However, a wide range of variations of this PY5R$_2$ skeleton, including the exchange of the axial unit by a thiofuran[4] scaffold or the substitution of the four equatorial pyridine units by imidazole,[5] amine,[6] hydroxide[7] or phosphine[8] units, have been reported. Recently, several works have emerged taking advantage of the interesting properties of this scaffold. Therefore, for instance, Berlinguette et al reported the first tetravalent Co complex stabilized by PCET by employing the Py5 ligand (Chart 1).[9] This pentadentate ligand ensure: (a) one single free coordination site to accommodate the aqua ligand and thus allow the PCET processes, (b) a rugged environment non-susceptible to oxidation (c) the stabilization of the coordination site trans to the M-O bond, thus preventing common degradation processes. On the other hand, Fukuzumi et al reported several catalytic oxidation systems, including PCET processes to generate the active metal-oxo active species.[10] The latest includes the coordination of the pentadentate ligand N4Py shown in Chart 1, with interesting results in terms of its electrochemistry and a possible seven coordination in the Ru metal.[11] Finally, in 2010, Long *and co-workers* reported the synthesis and characterization of a series of first row metal complexes containing the PY4Im ligand shown in Chart 1.[12] The PY4Im scaffold is clearly related to the PY5R$_2$ ligand commented above, with the axial pyridine replaced by a NHC (*N*-heterocyclic carbene) moiety.

Taking into account the above mentioned interesting properties of pentadentate ligands to coordinate metals centers and thus potentially achieve stable high oxidation states *via* PCET, in this chapter we present the synthesis and the spectroscopical and

VI

electrochemical characterization of a new family of complexes with general formula $[Ru^{II}(PY4Im)(X)]^{n+}$ (X = Cl, n = 1 or X = H_2O, n = 2), where PY4Im is the 1,3-bis(bis(2-pyridyl)methyl)imidazol-2-ylidene ligand. These results together with the performance of the new species towards the oxidation of water and alkenes will be thoroughly discussed in the present work.
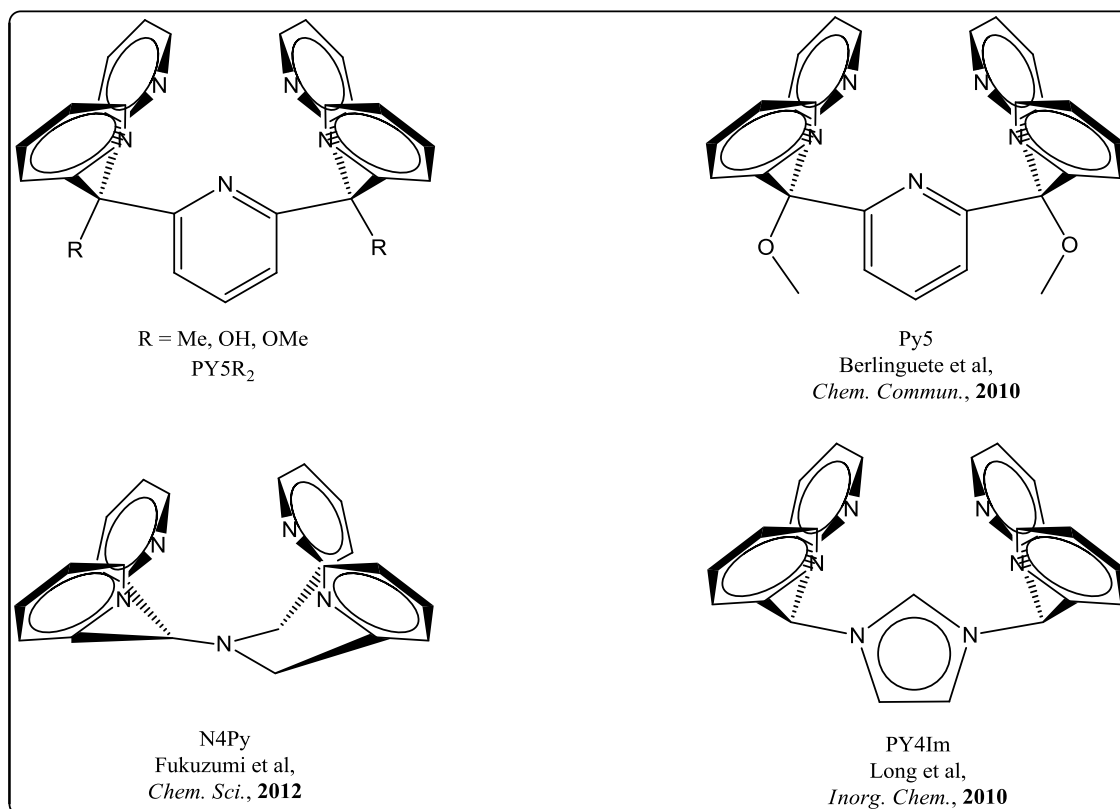

R = Me, OH, OMe
PY5R$_2$

Py5
Berlinguete et al,
Chem. Commun., **2010**

N4Py
Fukuzumi et al,
Chem. Sci., **2012**

PY4Im
Long et al,
Inorg. Chem., **2010**

Chart 1. Pentadentate coordinating fashion ligands discussed in this work.

VI.2.   Results & Discussion

VI.2.1.   Synthesis of PY4Im Ligand

The synthesis of the PY4Im ligand has been carried out by following the reported procedure depicted in Scheme 1.[12] 2-methylpyridine with 2-fluoropyridine *via* litiation in hexanes afforded 2-(2-pyridylmethyl)pyridine.[13] The latest yielded the bis(2-pyridyl)bromomethane when was fastly (5 minutes reaction) brominated as reported in the literature.[14]
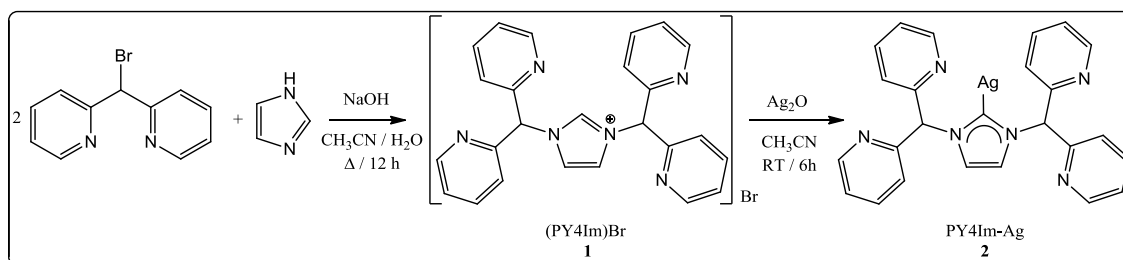

Scheme 1.   Synthetic pathway followed to obtain the PY4Im-Ag (**2**) ligand.

Despite **2** was reported to be obtained from the reaction of (PY4Im)Br with Ag_2O in dichloromethane, only when the reaction was performed in acetonitrile the desired product could be isolated as a pure white powder.

VI.2.2.   Synthesis and Characterization of 3(Cl) and 4(BF$_4$)$_2$

After several unfruitful attempts of coordinating the PY4Im-Ag ligand, **2**, to Ruthenium by using different solvents and the usual metal precursors: $Ru^{III}Cl_3 \cdot 3H_2O$ and $Ru^{II}Cl_2(dmso)_4$, the reaction conditions depicted in Scheme 2 were established.
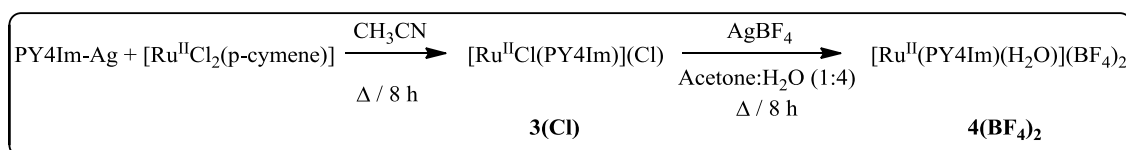
Scheme 2.   Synthetic strategy for the obtention of **3(Cl)** and **4(BF$_4$)$_2$**.

Therefore, the chlorido complex **3(Cl)** was obtained by reacting PY4Im-Ag with $Ru^{II}Cl_2$(p-cymene)$_2$ in acetonitrile and the subsequent precipitation of the product in the reaction media as a pure yellowish powder . Comparison of its ESI-MS spectrum with the theoretically expected (Figure S6) confirmed its stoichiometry and discarded the potential coordination of MeCN (the reaction solvent) to the metal centre. The latter was

VI

also corroborated by the absence of ^{1}H-NMR signals corresponding to coordinated acetonitrile. The synthesis of the aqua complex **4(BF$_4$)$_2$** involved the presence of silver tetrafluorborate as scavenger for the chlorido anion, that allowing the coordination of the water molecule. After AgCl filtration, slow evaporation of the acetone solvent yielded nice yellow crystals suitable for X-ray diffraction analysis.

The most relevant results of the structural, spectroscopic and electrochemical characterization of complexes **3(Cl)** and **4(BF$_4$)$_2$** will be discussed in the following sections. Further information about ESI-MS spectra is depicted in the Supporting Information (Figures S6-S7).

VI.2.2.1. *NMR spectroscopy*

Nuclear Magnetic Resonance experiments have been carried out for the diamagnetic compounds **3(Cl)** and **4(BF$_4$)$_2$** (Figures 1-2 and Figures S1-S2 in the Supporting Information). Both 1D (^{1}H and ^{13}C $\{^1$H$\}$) and 2D (COSY, HSQC and HMBC) experiments have proven to be mandatory tools in order to structurally characterize **3$^+$** and **4^{2+}** in solution. Both chlorido and aqua compounds display C$_{2v}$ symmetry in solution, with one symmetry plane passing through the chlorido/oxygen, the C(14) of the central imidazole and the Ru atom and bisecting the C(12)-C(13) bond thus interconverting the two sides of the complex. Moreover, one symmetry plane (perpendicularly bisecting the former) contains the imidazole ring and the Ru and chloro/aqua atoms, thus interconverting the other two pyridine rings.
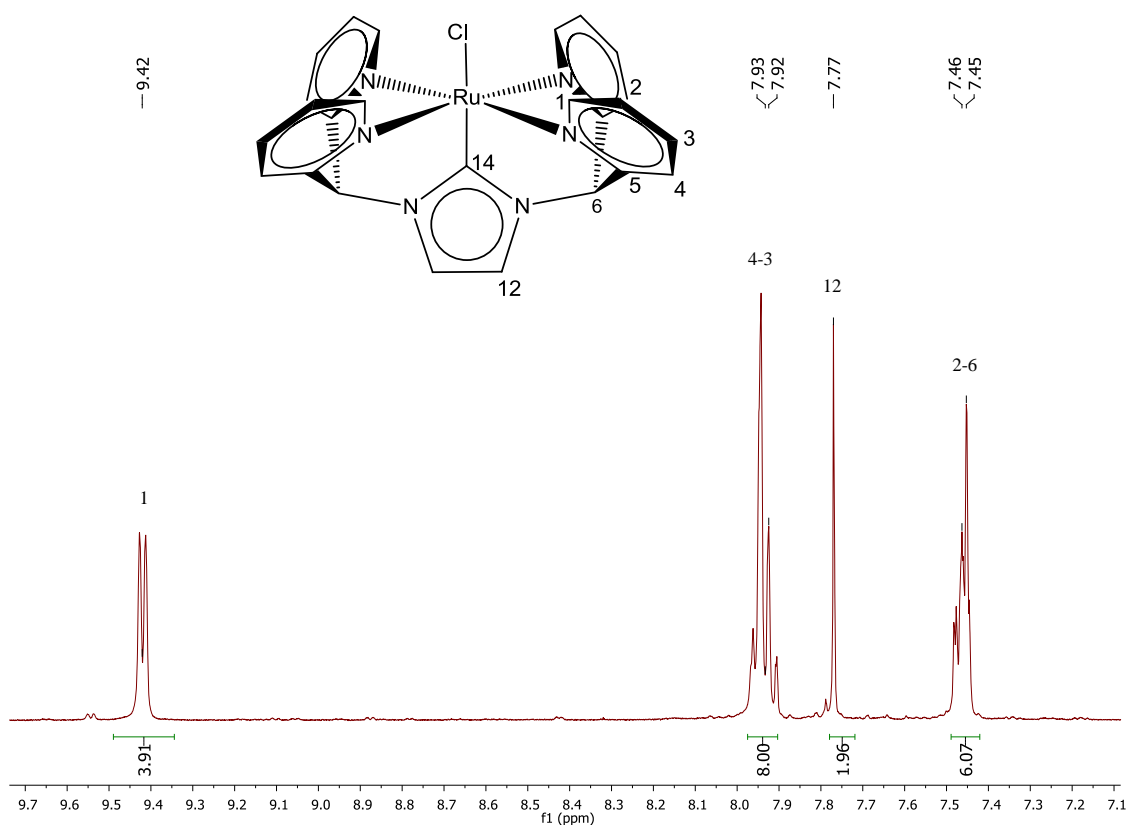
Figure 1. ^{1}H-NMR (400 MHz, DMSO-d$_6$) and resonance assignment for **3**$^+$

It is worth to mention at this point the characteristic chemical shift (down-field shifted) of the doublet corresponding to H1 probably due to H bonding interaction between these protons in alpha to the nitrogen atoms of each pyridyl ring and the chlorido/oxygen coordinated to the ruthenium ion. HMBC experiments have been mandatory to unambiguously assign H12 and H6 singlets as well as all quaternary carbon resonances.
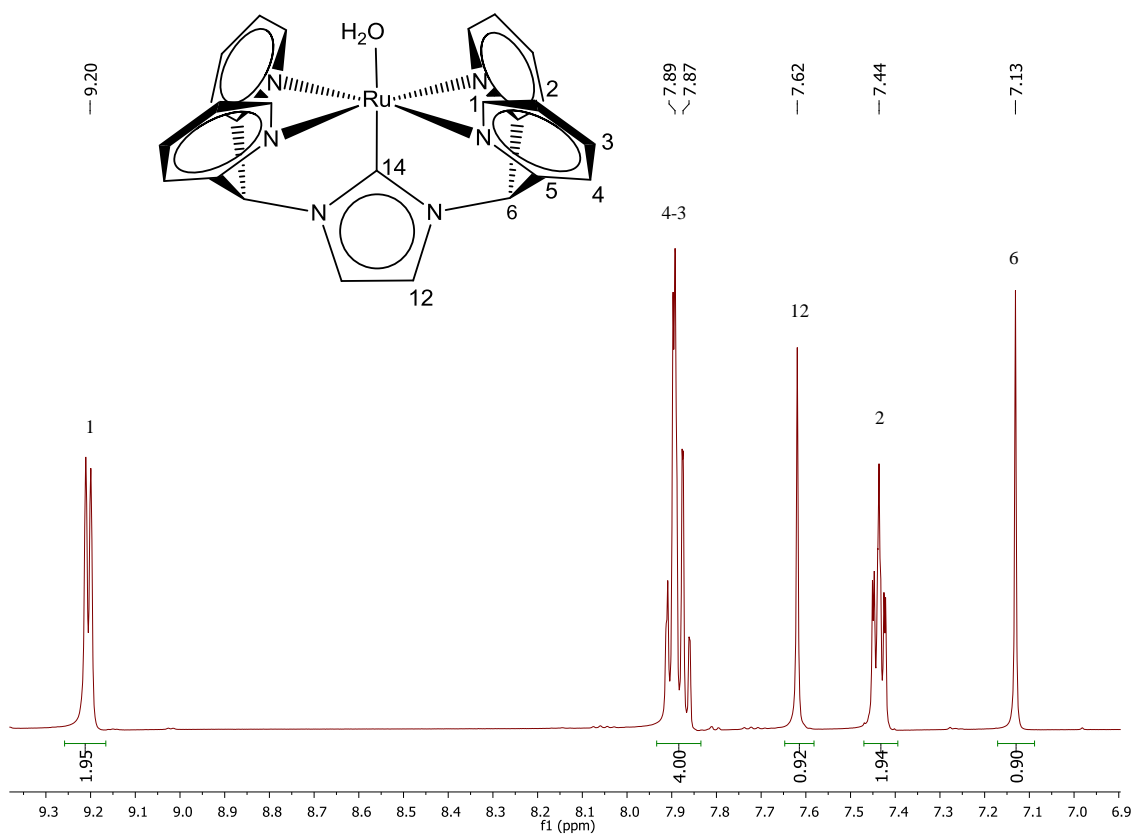
VI

Figure 2. ^{1}H-NMR (400 MHz, D$_2$O) for **4^{2+}**.

VI.2.2.2. X-ray Crystal Structures

Suitable crystals for X-Ray diffraction analysis of **4(BF$_4$)$_2$** were obtained after the slow evaporation of an acetone:water saturated solution of the complex. Figure 3 displays an Ortep plot for the cationic moiety of this complex together with its corresponding atom labeling scheme. Acquisition and crystallographic data is reported as Supporting Information (Table S1).
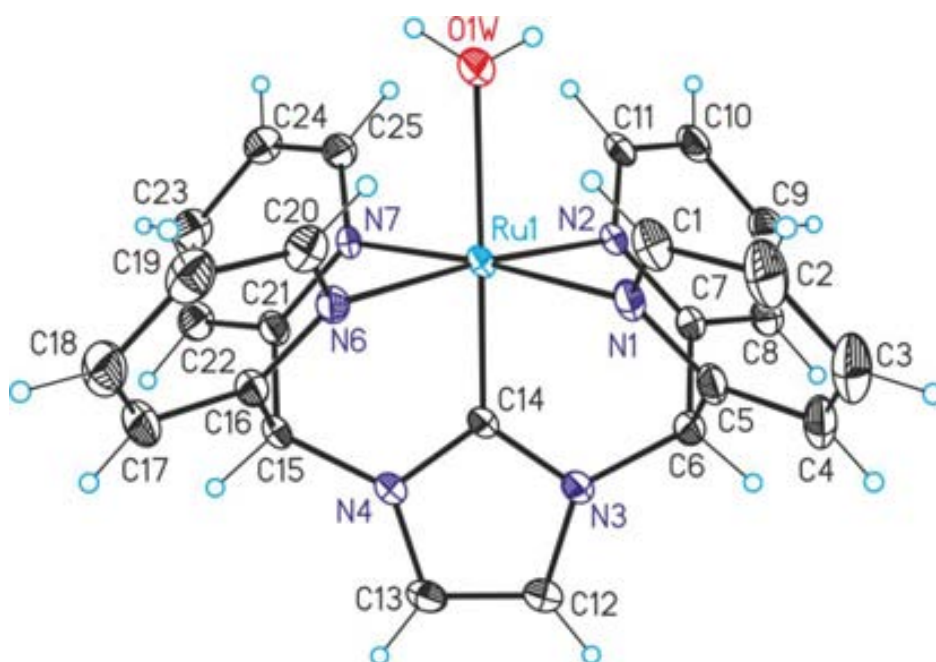
Figure 3.   Ortep plot (ellipsoid at 50% probability) of the cationic moiety of 4^{2+} with its corresponding labeling scheme.

4^{2+} crystallizes in a cell containing four $[Ru(PY4Im)(H_2O)]^{2+}$ cationic units, sixteen water molecules and eight tetrafluorborate anions, which is in agreement with an oxidation state value of two for the Ru metal ion. As shown in Figure S8, the four cations interact two by two *via* pyridyl π-stacking interactions. The asymmetric unit contains one molecule of the cationic complex with a coordinated water molecule, two $(BF_4)^-$ anions and four non-coordinated water molecules. One of the $(BF_4)^-$ anions and three of the water molecules are disordered in two positions. The Ruthenium metal displays an octahedral coordination with the four equatorial positions occupied by the pyridylic nitrogen atoms and the axial by the NHC and the aqua group. Bond distances and angles are in the expected range. A comparison of their more relevant values for 4^{2+} with the ones corresponding to the related Ru-OH$_2$ complex $[Ru(PY5Me_2)(H_2O)]^{2+}$, which contains the penta-pyridilic pentadentate ligand PY5Me$_2$ (Chart 1, top left, R = Me), is displayed in Table 1.[*] For the better understanding of this section, Figure 4 shows a view of the $[Ru(PY5Me_2)(H_2O)]^{2+}$ cationic unit with its corresponding labeling scheme.

VI

---

[*] X-ray data related to $[Ru(PY5Me_2)(H_2O)]^{2+}$ is still not reported in the literature, thus it has been gently provided by Ms. Jordan C. Axelson from Prof. J.R. Long research group (University of California, Berkeley).

Table 1. Selected interatomic distances (Å) and angles (º) for complex **4^{2+}** and the related $[Ru(PY5Me_2)(H_2O)]^{2+}$ complex.

ENTRY	BOND DISTANCES	4^{2+}	$[Ru(PY5Me_2)(H_2O)]^{2+}$ ¡Error! Marcador no definido.
1	Ru-N(1)	2.090(3)	2.0846(14)
2	Ru-N(2)	2.085(3)	2.0624(14)
3	Ru-X_{ax} [a]	1.892(3)	2.0008(14)
4	Ru-N(7)	2.090(3)	2.0688(14)
5	Ru-N(6)	2.096(3)	2.0699(14)
6	Ru-O(1)	2.195(3)	2.1228(13)
7	O(1)-H(1)	2.837	2.836
8	O(1)-H(11)	2.823	2.600
9	O(1)-H(20)	2.853	2.563
10	O(1)-H(25)	2.795	2.757
	ANGLES		
11	N(1)-Ru-N(7)	174.37(10)	177.80(6)
12	N(2)-Ru-N(6)	174.14(10)	177.94(6)
13	O(1)-Ru-X_{ax}	179.24(12)	178.13(5)
14	O(1)-Ru-N(1)	93.40(11)	93.23(6)
15	O(1)-Ru-N(2)	93.11(10)	89.97(5)
16	O(1)-Ru-N(7)	92.07(10)	88.36(6)
17	O(1)-Ru-N(6)	92.60(10)	91.20(5)

[a] X_{ax} represents either C14 for $[Ru(PY4Im)(H_2O)]^{2+}$ or N3 for $[Ru(PY5Me_2)(H_2O)]^{2+}$.

All Ru-N bond distances are similar for both complexes. The Ru-X_{ax} distance (entry 3, Table 1) is shorter for **4^{2+}** (1.892 Å) than for the related $[Ru(Py5Me_2)(H_2O)]^{2+}$ (2.000 Å) due to the much stronger σ-donor character of the carbene moiety (C14) with regards to the pyridyl scaffold. This feature will have dramatic effects in the acidity of the aqua group, as will be discussed in next section. Despite of the different coordinating atom in *trans* to the aqua group, Ru-O(1) distances (entry 6) are similar for both species. Angles O(1)-Ru-N(x) (where X = 1, 2, 7 and 6) give an idea about the position of the metal with respect to the plane formed by the 4 pyridylic nitrogen atoms. Values close to 90º (Table 1 entries 14-17), indicate that the Ru metal lies on the same plane than those nitrogen atoms. Finally, it is worth to point out at this moment, that the distances O(1)-H(x) (where X = 1, 11, 20 and 25, table 1 entries 7-10) are suitable for H bonding interaction between the protons in alpha to the nitrogen atoms of each pyridyl ring and

the oxygen of the aqua group coordinated to the ruthenium ion. These interactions will be key in order to understand some of the spectroscopic and electrochemical features of the complex that will be discussed later on.
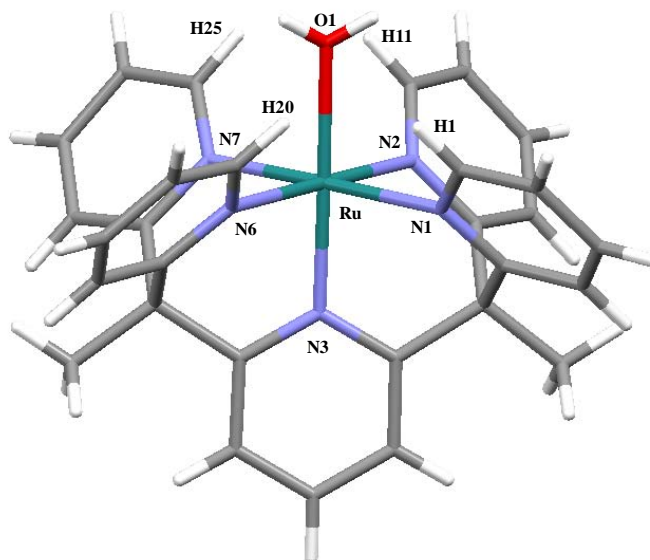

Figure 4. X-ray structure of the $[Ru(PY5Me_2)(H_2O)]^{2+}$ complex with its corresponding labeling scheme.

VI.2.2.3. *Electrochemistry and UV-vis features*

The redox properties of the complexes **3(Cl)** and **4(BF$_4$)$_2$** have been investigated in terms of CV and DPV. The CV of **3$^+$** in methanol (Figure S3) exhibits a unique reversible wave at $E_{1/2} = 0.85$ V, ($\Delta E = 75$ mV) corresponding to the following process:

$$[Ru^{III}(Cl)(PY4Im)]^{2+} + 1e^- \quad \rightarrow \quad [Ru^{II}(Cl)(PY4Im)]^+ \quad (0.84 \text{ V}) \qquad (1)$$

The electrochemical properties of the aqua complex **4^{2+}** were also extensively investigated by means of CV and DPV in aqueous solutions (pH from 0 to 14) in order to better understand the redox behavior of the complex. At pH=2, the unique reversible wave observed in the CV shown in Figure 5 is assigned to the following process (see the corresponding DPV in Figure S4):
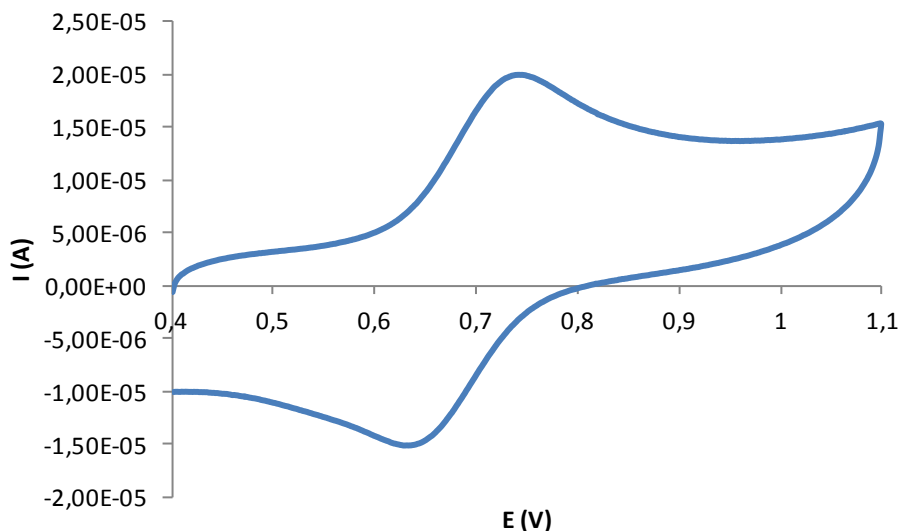
$$[Ru^{III}(PY4Im)(H_2O)]^{3+} + 1e^- \rightarrow \quad [Ru^{II}(PY4Im)(H_2O)]^{2+} (0.66 \text{ V}) \qquad (2)$$

VI

Figure 5.   Cyclic Voltammetry for the aquo complex **4^{2+}** in water pH=2 (phosphate buffer) at 100 mV/s scan rate. Glassy carbon electrode is used as working electrode and the potential is measured *vs.* SSCE.

At pH=8, two redox processes are observed in the DPV shown in Figure 6 (see the corresponding CV in Figure S5) and assigned to the following electrochemical reactions:

$$[Ru^{III}(PY4Im)(OH)]^{2+} + 1e^- + 1H^+ \rightarrow \quad [Ru^{II}(PY4Im)(H_2O)]^{2+} \ (0.56 \text{ V}) \quad (3)$$

$$[Ru^{IV}(PY4Im)(O)]^{2+} + 1e^- + 1H^+ \quad \rightarrow \quad [Ru^{III}(PY4Im)(OH)]^{2+} \ (0.71 \text{ V}) \quad (4)$$

For aqua complexes such as **4^{2+}**, the presence of aqua groups enables PCET (proton coupled electron transfer) processes as the ones shown in Equations 3 and 4, which occur at relatively low and narrow potentials.[15] The easy access to higher oxidation states as Ru^{IV} is due to the simultaneous removal of electrons and protons which does not allow the buildup of high Columbic charges in the complex and also due to the σ and π-donor nature of the oxido group bound to the ruthenium metal centre. The redox assignment of the mentioned processes (Eq. 3 and 4) has been carried out by comparison with the parent and extensively studied analogue $[Ru^{II}(tpy)(bpy)(H_2O)]^{2+}$.[16]
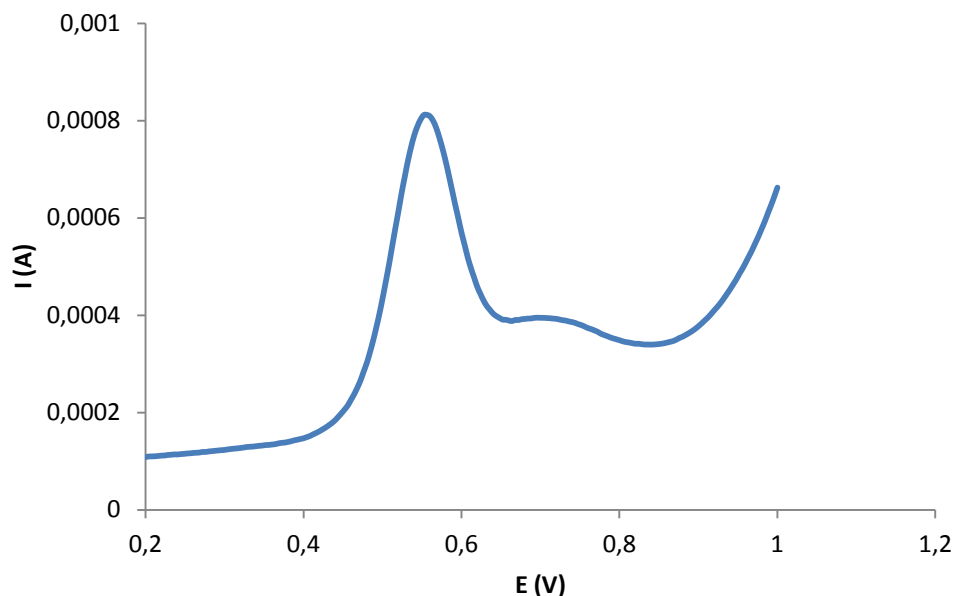
Figure 6.   Differential Pulse Voltammetry for the aqua complex **4^{2+}** in water pH=8.2 (phosphate buffer) at 100 mV/s scan rate. Glassy carbon electrode is used as working electrode and the potential is measured *vs.* SSCE.

The Pourbaix diagram (representation of E$_{1/2}$ *vs.* the pH) of the complex **4^{2+}** is depicted in Figure 7, indicating the different zones of thermodynamic stability of the corresponding species with a different degree of protonation and/or oxidation. The Pourbaix diagram allows us to tentatively assign the values of pK$_{a1}$ and pK$_{a2}$ for the aqua group coordinated to the Ru center, as follows (PY4Im ligand omitted for the sake of clarity):
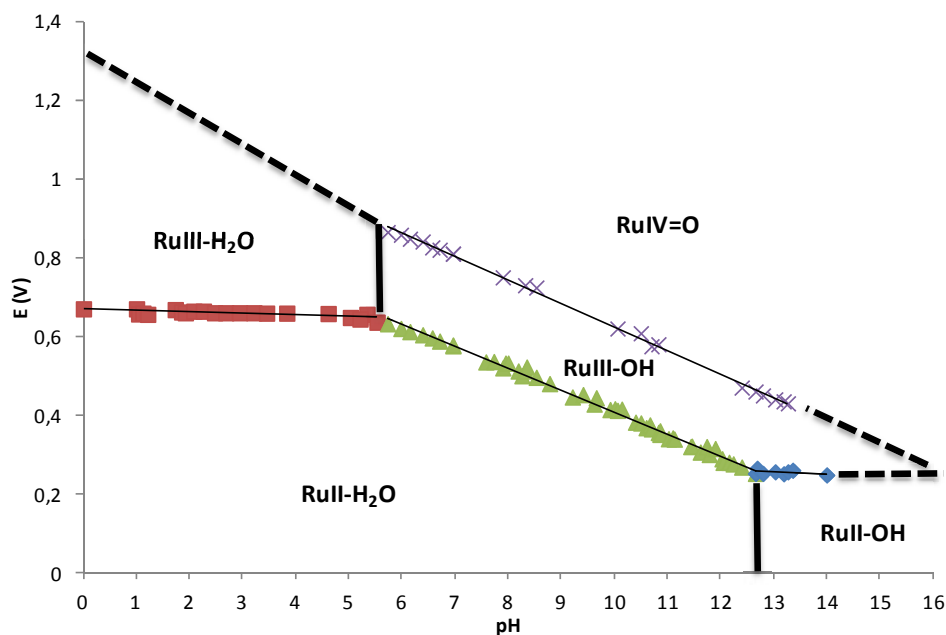
$$Ru^{III}H_2O \quad \rightarrow \quad Ru^{III}OH \quad (pK_{a1}\ 5.3)$$

$$Ru^{II}H_2O \quad \rightarrow \quad Ru^{II}OH \quad (pK_{a2}\ 12.7)$$

VI

Figure 7.   Pourbaix diagram for the $[Ru^{II}(PY4Im)(H_2O)]^{2+}$ complex, **4^{2+}**. Continuous line: experimental data. Dashed line: hypothetical data. $E_{1/2}$ *vs.* SSCE.

Table 2 reports a comparison of the data extracted from the Pourbaix diagram of **4^{2+}** and from reported values for the paradigmatic Ru-N5 complex $[Ru(tpy)(bpy)(H_2O)]^{2+}$, for purposes of comparison.

Table 2.   Redox   potentials   (*vs.*   SSCE)   for $[Ru^{II}(PY4Im)(H_2O)]^{2+}$ and $[Ru(tpy)(bpy)(H_2O)]^{2+}$.

	RuIII/RuII		RuIV/RuIII			*Ref*
	pH 1[b]	pH 7[c]	pH 7	pK_{a1} (Ru^{III})	pK_{a2} (Ru^{II})	
4^{2+}	0.67	0.58	0.8	5.3	12.7	*a*
$[Ru(tpy)(bpy)(H_2O)]^{2+}$	0.80	0.49	0.62	1.7	9.7	*16*

a This work. *b* 0.1 M triflic acid aqueous solution. *c* Phosphate buffer in aqueous solution.

As can be observed in Table 2 the redox potentials of the III/II couple measured in water at pH = 1 are shifted cathodically by 130 mV for **4^{2+}** with respect to $[Ru^{II}(trpy)(bpy)]^{2+}$. This shift is a clear consequence of the strong sigma donating character of the carbene unit present in **4^{2+}**. The sigma donation of the carbene is still more evident when comparing the pK_a values of these species. The acidity of both $Ru^{III}(H_2O)$ and $Ru^{II}(H_2O)$ protons is decreased by 3 and 4 units, respectively, in the PY4Im complex with regard to the related $[Ru^{II}(trpy)(bpy)]^{2+}$. On the other hand, the

RuIII/RuII and RuIV/RuIII redox processes are separated 220 mV at pH=7 in **4^{2+}**, meanwhile this separation is only of 130 mV in $[Ru^{II}(trpy)(bpy)]^{2+}$. This difference points out the higher stability of the Ru(III)-OH species in **4^{2+}** than in $[Ru^{III}(OH)(trpy)(bpy)]^{2+}$, potentially due to hydrogen bonding interactions between the hydroxo group and the hydrogen atoms in alpha to the pyridylic nitrogens of the pentadentate ligand (see Figure 4 above for a better understanding of this statement).

The UV-vis spectrum of **4^{2+}** has been recorded in H_2O at pH=8 (phosphate buffer) and is displayed in Figure 8. Two regions can be observed: one between 220 nm and 300 nm with very intense bands due to intraligand $\pi \rightarrow \pi*$ transitions and a second between 300 nm and 500 nm, where unsymmetrical broad typical metal-to-ligand charge transfer (MLCT) bands appear.[17]
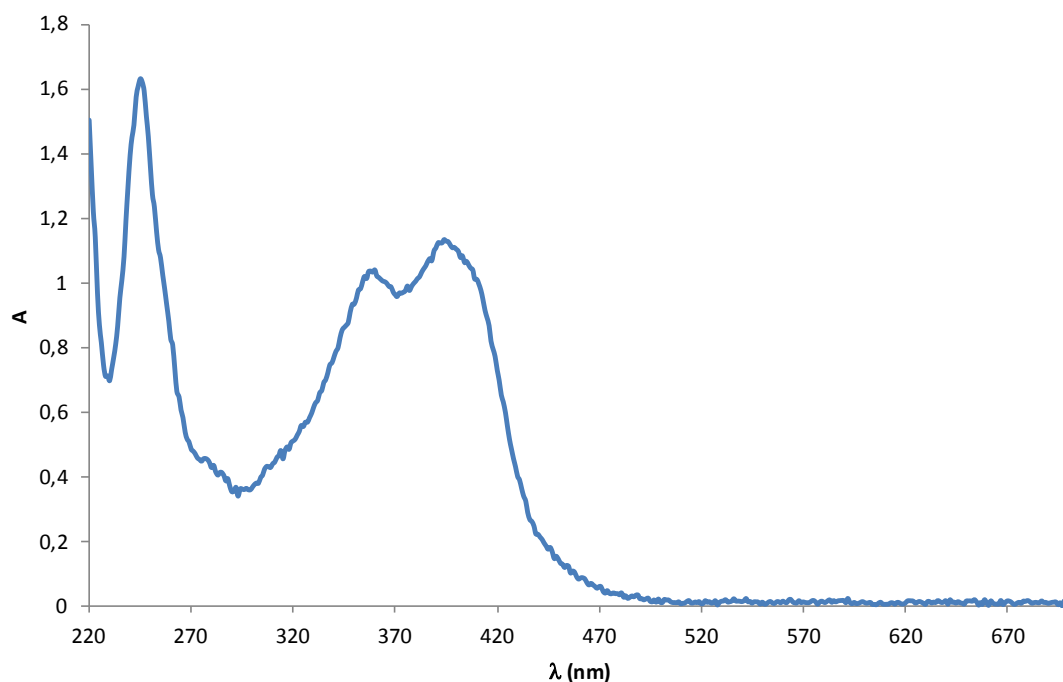

Figure 8.   UV-vis spectra for **4^{2+}** in H_2O at pH=8 (phosphate buffer).

Once electrochemically generated, the RuIII and RuIV oxidation states of **4^{2+}** have also been characterized in terms of its electronic spectra. Therefore, when applying a fixed potential of 0.65 V *vs.* SSCE to a pH 8 phosphate buffer solution of **4^{2+}** for 20 min, the initial RuII species was oxidized to RuIII as shown in Figure 9a. The four nice isosbestic points observed at 238, 257, 324 and 452 nm suggests the net generation of the latter. A plot of the absorbance at $\lambda = 292$ nm *vs.* the electrolysis time is depicted in Figure S9 (Supporting Information). The charge passed after UV-vis stabilization

VI

corresponds to a 1e⁻ oxidation process. Subsequent electrolysis at E_{app} = 0.9 V *vs.* SSCE during c.a. 20 min. to the same solution generates the corresponding Ru(IV)=O species, typically featureless in the visible region, as shown in Figure 9b. Despite nice isosbestic points were here again observed (240, 257, 320 and 437 nm), much higher charge values than the expected for a RuIII-RuIV 1e⁻ oxidation process were observed, thus suggesting the presence of a chemical reaction coupled to the RuIV generation. The oxidation of water to dioxygen by means of the Ru(IV)=O species could be this coupled process; accordingly, it will be thoroughly discussed in the next section.
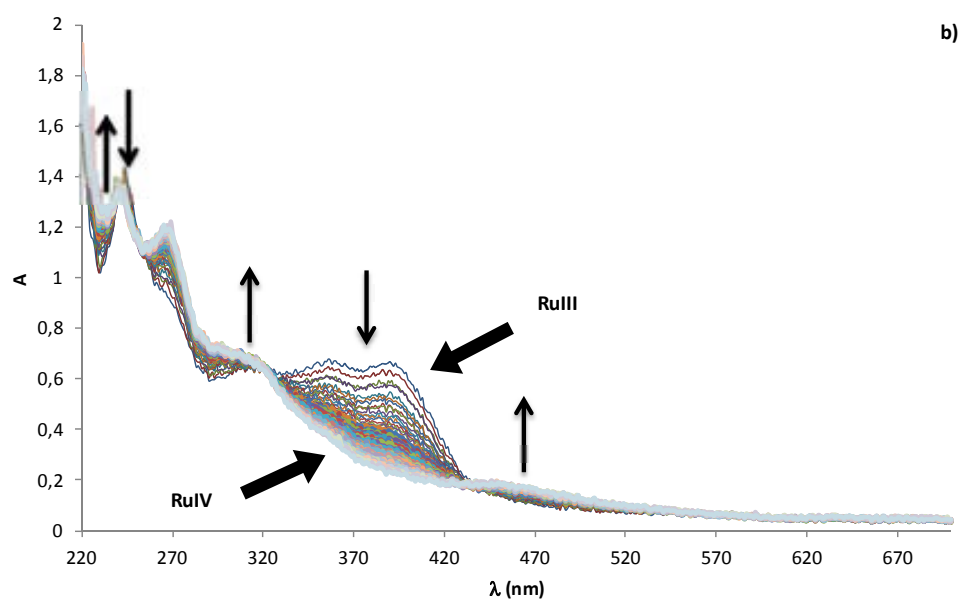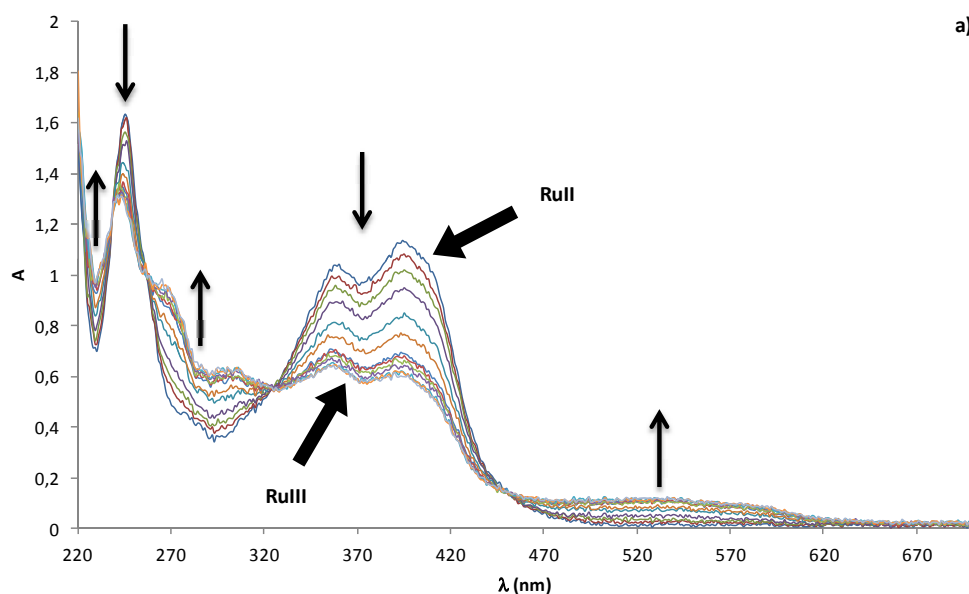
Figure 9.   Spectrochemical generation of higher oxidation state species derived from **4²⁺** in aqueous solution pH = 8.2 (phosphate buffer): (a) from Ru^{II} to Ru^{III} at E$_{app}$ = 0.65 V; (b) from Ru^{III} to Ru^{IV} at E$_{app}$ = 0.90 V. All redox potentials applied *vs.* SSCE.

VI.2.3.   Water Oxidation Catalysis

[Ru^{II}(PY4Im)(H$_2$O)]$^{2+}$, **4²⁺**, has been tested as a potential water oxidation catalyst by using both chemical and electrochemical oxidants:

a) Using Ce(IV) as chemical sacrificial oxidant.

The catalytic properties of complex **4²⁺** together with those for [Ru^{II}(Py5Me$_2$)(H$_2$O)]$^{2+}$ [†] were tested with regard to its capacity to oxidize water using Ce(IV) as oxidant, and the gases evolved were monitored by *online* manometry and MS. In all cases the following conditions were used: catalyst (**4²⁺** or [Ru^{II}(Py5Me$_2$)(H$_2$O)]$^{2+}$) 1 mM / Ce((IV) 100 mM / 0.1M triflic acid in 2 ml total volume at 25 ºC). The most relevant results regarding these experiments are reported in Figures 10 and 11.
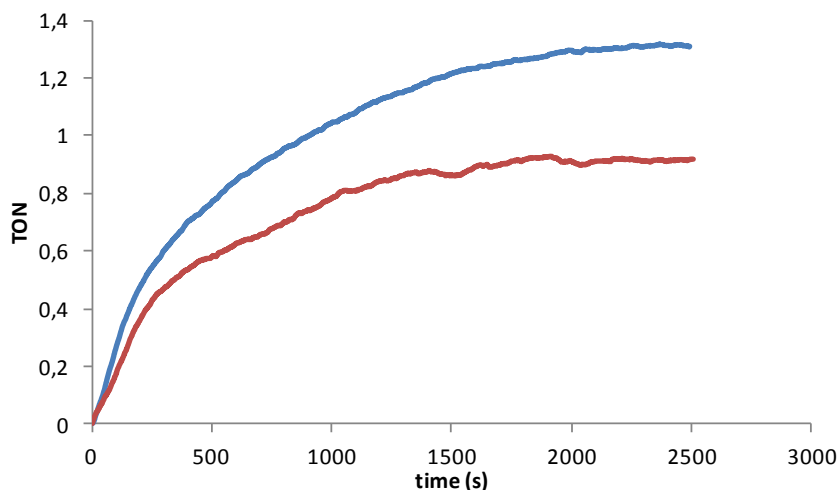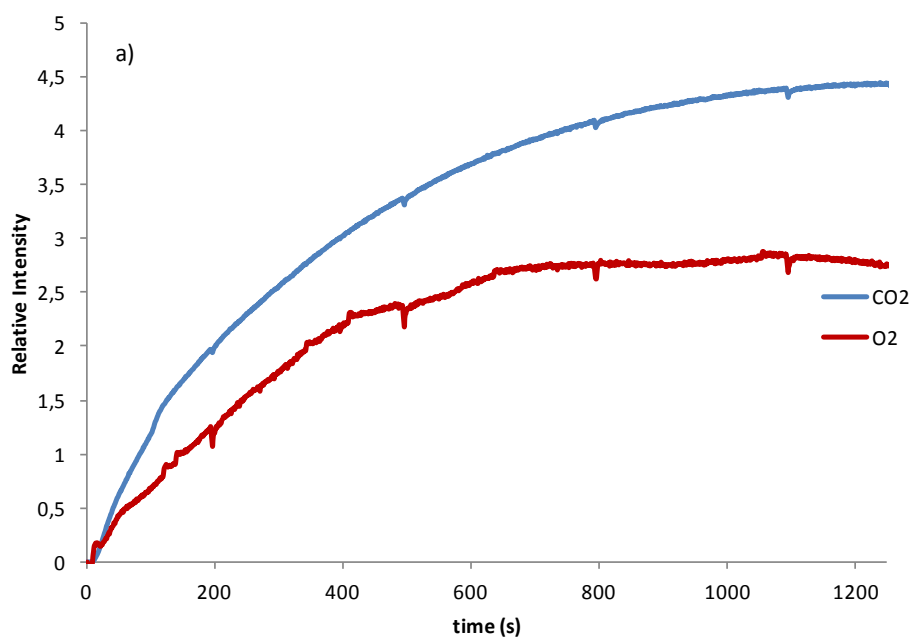

Figure 10.   Manometric monitoring of gas evolution *vs.* time for complexes **4²⁺** (blue line) and [Ru^{II}(Py5Me$_2$)(H$_2$O)]$^{2+}$ (red line), (1 mM) at pH =1.0 in 0.1M triflic acid solution in the presence of (NH$_4$)$_2$Ce^{IV}(NO$_3$)$_6$ (100 mM).

[†] [Ru^{II}(PY5)(H$_2$O)]$^{2+}$ was gently provided by Ms. Jordan C. Axelson from Prof. J.R. Long research group (University of California, Berkeley).

Both complexes resulted to be poor towards the generation of oxygen as the low manometry values demonstrate in Figure10. However, it is interesting to point out the different composition of the gas evolved for the two catalysts tested; while the MS experiment for $[Ru^{II}(Py5Me_2)(H_2O)]^{2+}$ (Figure 11b) shows just trace amounts of CO_2, 4^{2+} (Figure 11a) generate a 5,5:1 mixture of $CO_2:O_2$. These results clearly manifest the different behavior and robustness of both species under the catalytic conditions. In fact, the presence of the carbene moiety and the CH linkage between the carbene and the pyridines rings in 4^{2+} seems to be the *Achilles heel* of the system, due to it is the unique difference regarding the related five pyridines complex, $[Ru^{II}(Py5Me_2)(H_2O)]^{2+}$.
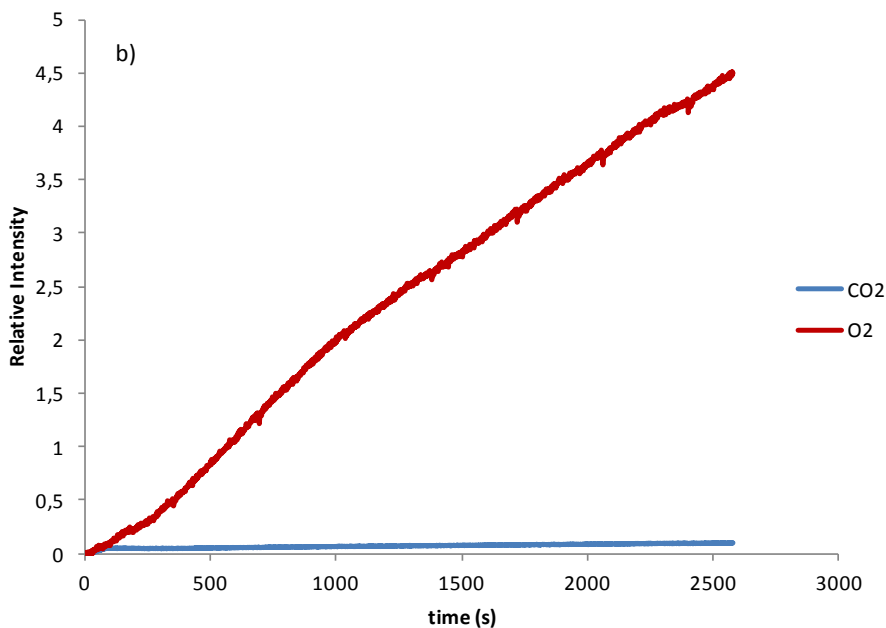
Figure 11. On-line MS monitoring of oxygen (red line) and carbon dioxide (blue line) evolution *vs.* time for complexes **4^{2+}** (a) and $[Ru^{II}(Py5Me_2)(H_2O)]^{2+}$ (b) (1 mM) at pH =1.0 in 0.1M triflic acid solution in the presence of $(NH_4)_2Ce^{IV}(NO_3)_6$ (100 mM).

b) Electrochemically-triggered O_2 generation.

While registering CVs and DPVs for the construction of the above displayed Pourbaix diagram of **4^{2+}** (Figure 7), nice electrocatalytic waves such as the one shown in Figure 12 were observed. The important increase observed on the anodic current suggested the potential electrocatalytic activity of **4^{2+}** towards the oxidation of water, result in agreement with the large charge value obtained when studying the RuIII/IV process by means of CPE (see above).
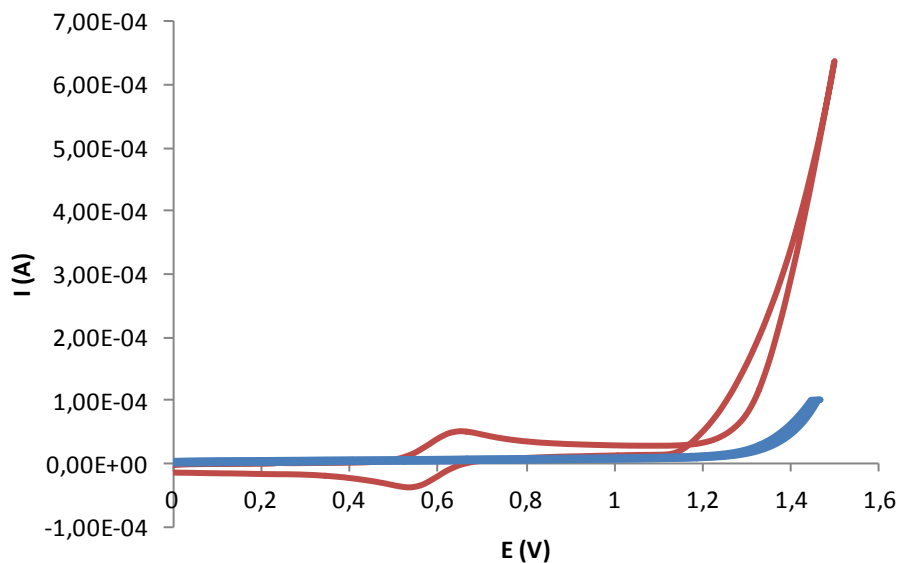
VI

Figure 12. Cyclic Voltammetry for the aqua complex **4²⁺** in water pH=8 (phosphate buffer) at 100 mV/s scan rate (red line) and the corresponding blank (blue line). FTO used as working electrode and potential measured *vs.* Ag/AgCl.

In order to confirm this potential catalytic activity of **4²⁺** with regards to the oxidation of water, a CPE electrolysis connected with a Clark electode in the gas phase was set up. Therefore a potential of 1.35 V *vs.* SSCE was applied for 8h to pH 8 aqueous solution of **4²⁺** (0.53 mM). Figure 13 displays the measured charge during the CPE and that of the corresponding blank experiment.
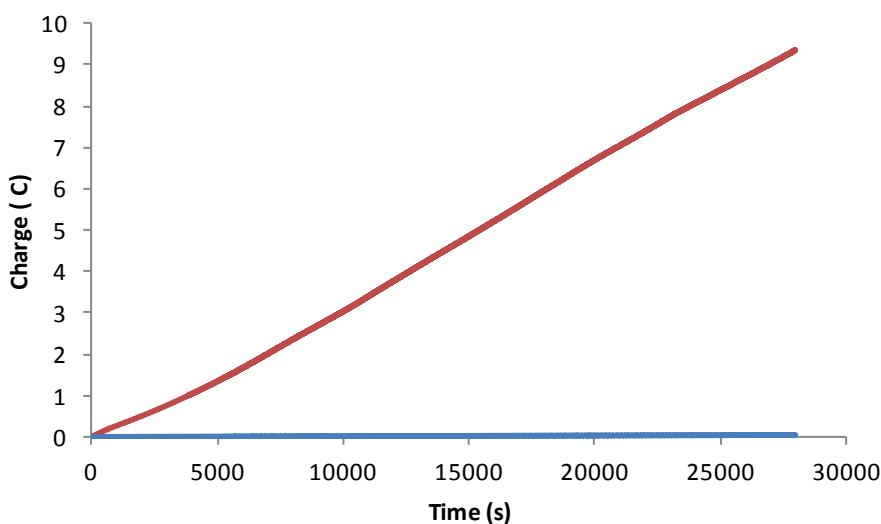

Figure 13. Charge *vs.* time representation for the CPE (E_{app} = 1.35V *vs.* SSCE) of a blank (blue line) and an aqueous solution of **4²⁺** ((53 mM, pH 8) red line) .

From the measured charge (around 10 C) and supposing a 100 % Faradaic efficiency a value of 10.6 TON was obtained. The real activity of the catalyst was calculated from the measurement of the generated oxygen with a Clark electrode in the gas phase as shown in Figure 14. The evolution of oxygen confirmed the water oxidation activity of our system under these conditions. However, the measured Faradaic efficiency was low (about 25%), thus evidencing the use of most part of the charge consumed on side reaction such as, for instance, the oxidative degradation of the catalytically active species.
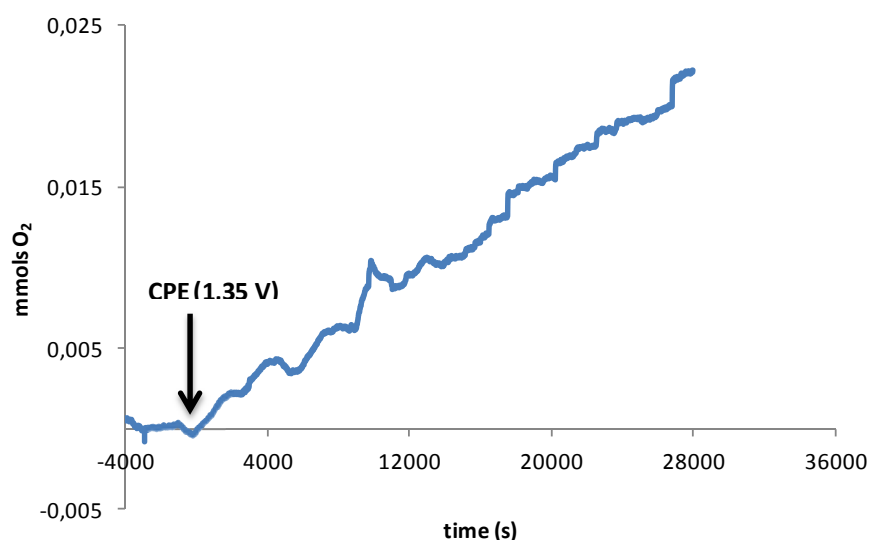

Figure 14. Clark probe profile during CPE (1.35 V vs. SSCE) of a pH 8 0.53 mM aqueous solution of **4^{2+}**.

In order to analyze the stability of the catalytic system under CPE conditions and confirm the degradation observed in terms of CO_2 formation, cyclic voltammetries before and after CPE were recorded (Figure 15 and Figure S10). The final waves appear shifted and non-reversible, clearly indicating the presence of new species with different coordination environment with regards to **4^{2+}**. It is also worth to mention the clear reduction in the electrocatalytic activity of the catalyst observed in the important decrease of the anodic current (Figure 15).
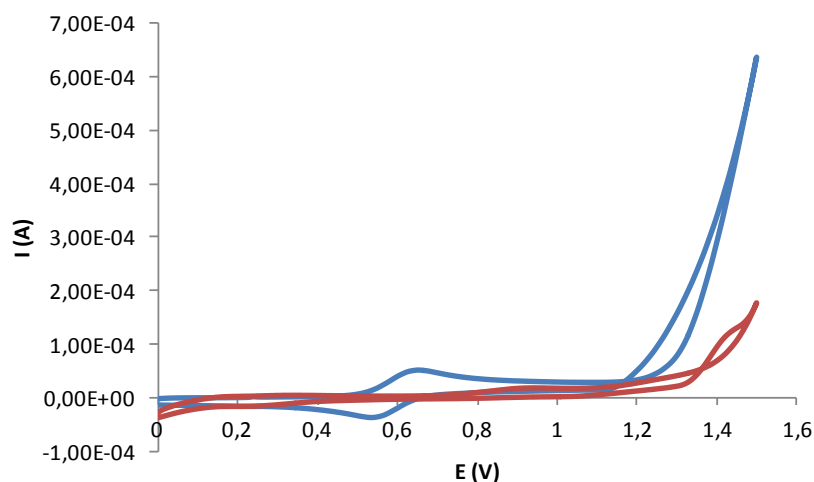
VI

Figure 15. Cyclic voltammetry of 4^{2+} before (blue line) and after (red line) CPE at pH = 8 (phosphate buffer in water). FTO used as working electrode and potential measured *vs.* Ag/AgCl.

VI.2.4. Epoxidation Catalysis

4^{2+} has also been tentatively tested with regards to its ability to oxidize alkenes to epoxides as shown in Scheme 3. The catalytic reactions have been carried out following the conditions exposed in Table 3, which have been already mentioned in Chapter 2.
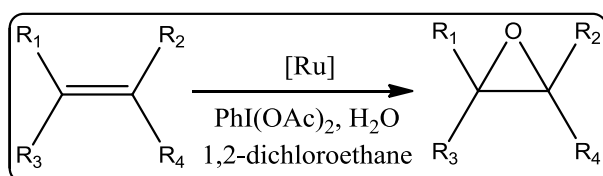
Scheme 3. Catalytic epoxidation of alkenes by Ruthenium complexes.

Table 3. Reaction conditions for the epoxidation of alkenes. Final volume $\approx$ 1.47 ml.

Specie	mmols	Concentration (M)	Ratio cat:X
4^{2+}	2,5E-03	1,70E-03	-
Alkene	2,5	1,7	1000
Dodecane	1	0,7	800
(diacetoxyiodo)benzene	5	3,4	2000
Water	5	3,4	2000

A vial containing 1 ml of 1,2-dichloroethane as solvent, (diacetoxyiodo)benzene as oxidant, dodecane as internal standard, catalyst **4^{2+}**, and water, was initially stirred for 120 min. This "incubation" period before substrate addition was observed to be key in order to improve the rate of the catalytic reaction. Finally, the substrate was added to the previous mixture. The excess of water is mandatory to ensure the generation of PhIO from PhI(OAc)$_2$.[18] Figure 16 summarizes the set of reactions that take place during the catalytic epoxidation of alkenes for the proposed system.
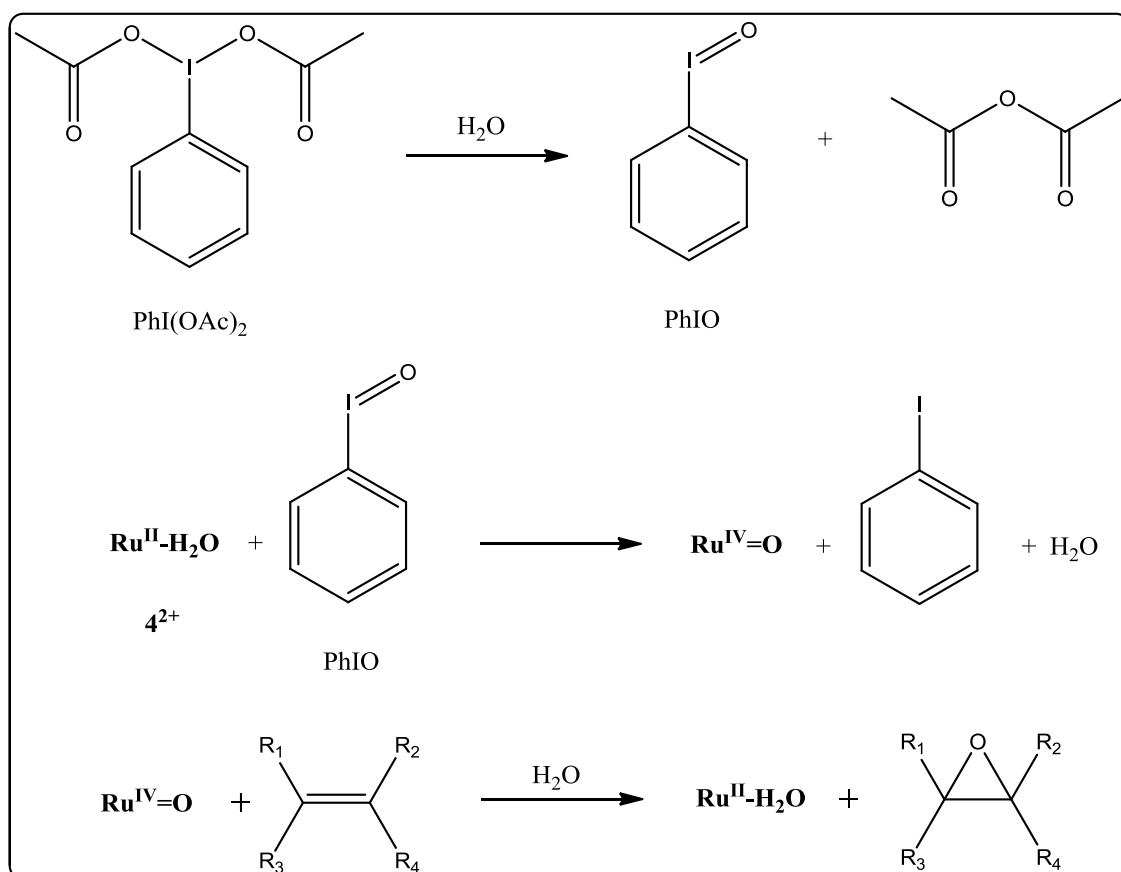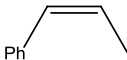

Figure 16.   Summary of the reactions taking place in the catalytic epoxidation of alkenes with **4^{2+}** as catalyst and the reaction conditions shown in Table 3.

The catalytic activity of **4^{2+}** towards the epoxidation of alkenes has been tested for the oxidation of *cis*-β-methylstyrene and the reaction evolution monitored by GC and GC-MS. As it can be observed the system: **4^{2+}** 1.70 mM/*cis*-β-methylstyrene 1.7 M/PhI(OAc)$_2$ 3.4 M/H$_2$O 3.4 M in DCE gives 0.63 M *cis*-β-methylstyrene epoxide that represents 350 turnover numbers (TONs) with regard to the initial catalyst in 20h. After this time the conversion of the initial substrate is 62% and thus represents an epoxide selectivity of 66%.

Table 4.   Catalytic performance of **4**$^{2+}$ for the epoxidation of alkenes using PhI(OAc)$_2$ as oxidant in DCE (Cat:Sub:Ox. 1:2000:4000).[a]

Entry	Substrate		Substrate conversion (%)[b]	[Epoxide], M; (Selectivity, %)[c]	TON/TOF$_i$[d]
1	*cis*-β-methylstyrene	Ph⟋⟍	100	0.63; (66)[e]	350/73

[a] Reaction conditions: **4(PF$_6$)$_2$** (1.8 mg, 2.5 E^{-3} mmols, final concentration 1.7 mM) in DCE (1 ml), substrate (2.5 mmols, 1.7 M), PhI(OAc)$_2$ (5 mmols, 3.4 M), H$_2$O (5 mmols, 3.4 M), dodecane (1 mmol, 0.68 M); final volume ≈ 1.47 ml. [b] Substrate conversion = {([substrate]$_i$ − [substrate]$_f$)/[substrate]$_i$}·100. [c] Epoxide selectivity = {[epoxide]$_f$/([substrate]$_i$ − [substrate]$_f$)}·100. [d] TON with regard to epoxide; TOF$_i$ = TON/min. [e] 100% *cis* epoxide.

VI.3.   <u>Conclusions</u>

In this chapter we have prepared and thoroughly characterized a novel family of complexes with general formula [Ru^{II}(PY4Im)(X)]$^{n+}$ (X = Cl, n = 1 or X = H$_2$O, n = 2), which represent the first class of ruthenium complexes containing a pentadentate ligand bearing an NHC scaffold on its axial position. Moreover, both Ru^{III}(OH) and Ru^{IV}(O) high oxidation state species have been electrochemically generated and spectroscopically characterized. The strong σ-donor character of the carbene ligand is clearly manifested in **4**$^{2+}$ by both, the important reduction of the redox potentials and the clear increase of the pKa values when comparing this data with that of the paradigmatic Ru-N$_5$ complex [Ru(trpy)(bpy)(H$_2$O)]$^{2+}$. In addition, the use of a pentadentate moiety likewise PY4Im provides interesting hydrogen bonding interactions between the H in alpha to the nitrogen atoms in the equatorial pyridines and the hydroxo group of the Ru^{III}(OH) species, thus stabilizing them towards its oxidation to Ru^{IV}(O). In addition, the catalytic activity of [Ru^{II}(PY4Im)(H$_2$O)]$^{2+}$ as water oxidation catalyst has been tested by using both chemical (Ce(IV)) and electrochemical (CPE) sacrificial oxidants. Degradation of the initial catalyst, potentially due to intermolecular catalyst-catalyst oxidative degradation processes, has been observed with both methodologies. However, much more promising preliminary results has been achieved when employing **4**$^{2+}$ as catalyst for the epoxidation of alkenes. 0.66 mM of *cis*-β-methylstyrene oxide were generated and full conversion of the substrate after 20h. This results and the

performance of this catalyst towards other substrates will be further investigated in our laboratory.

VI.4. <u>Experimental Section</u>

Materials: All reagents used in the present work were obtained from Aldrich Chemical Co. and were used without further purification. Reagent-grade organic solvents were obtained from Scharlab. $RuCl_3 \cdot 3H_2O$ was supplied by Alfa Aesar and was used as received. All synthetic manipulations were routinely performed under nitrogen atmosphere using Schlenk tubes and vacuum-line techniques.

Instrumentation and Measurements: UV-Vis spectroscopy was performed by a HP8453 spectrometer using 1 cm quartz cells. NMR spectroscopy was performed on a Bruker DPX 250 MHz, DPX 360 MHz or a DPX 400 MHz spectrometer or in a Varian NMR System 500MHz or 300MHz. Samples were run in acetone-d_6 with internal references. Electrospray ionization mass spectrometry (ESI-MS) experiments were carried out on an HP298s gas chromatography (GC-MS) system from the CAS-UAB. Cyclic voltammetry and Differential pulse voltammetrys experiments were performed on an Ij-Cambria HI-660 potentiostat using a three-electrode cell. A glassy carbon electrode (2 mm diameter) was used as working electrode, platinum wire as auxiliary electrode and a SSCE as a reference electrode. Working electrodes were polished with 0.05 micron Alumina paste washed with distillated water and acetone before each measurement. The chlorido complex was dissolved in methanol containing the necessary amount of n-Bu$_4$NPF$_6$ (TABH) as supporting electrolyte to yield 0.1 M ionic strength solution. The $E_{1/2}$ values reported in this work were estimated from CV experiments as the average of the oxidative and reductive peak potentials $(E_{p,a} + E_{p,c})/2$. All the controlled potential electrocatalysis (CPE), electrocatalysis and CV's before and after the catalytic process were performed in a two compartment/three electrodes cell using a Bio-logic potentiostat/galvanostat and EC-Lab software. In these cases a FTO slide (1 cm2) connected to a tin wire was used as working electrode, platinum grid as the auxiliary electrode and an aqueous Ag/Ag+ (KCl 3 M) as the reference electrode. Online manometry measurements were carried out on a Testo 521 differential pressure manometer with an operating range of $1 - 100$ hPa and accuracy within 0.5% of the measurement, coupled to thermostatted reaction vessels for dynamic monitoring of the headspace pressure above each reaction. The secondary ports of the manometers were

connected to thermostatically controlled reaction vessels that contained the same solvents and headspace volumes as the sample vials. Online monitoring of the gas evolution was performed on a Pfeiffer Omnistar GSD 301C mass spectrometer. Typically, 16.04 mL degassed vials containing a suspension of the catalysts in a0.1 M triflic acid (1.5 mL) were connected to the apparatus capillary tubing. Subsequently, the `previous degassed solution of cerium(IV) (0.5 mL) at pH=1 (triflic acid, 200 equiv.) was introduced using a Hamilton gastight syringe, and the reaction was dynamically monitored. A response ratio of 1:2 was observed when equal concentrations of dioxygen and carbon dioxide, respectively, were injected and thus was used for calculation of their relative concentrations. For the CPE, the oxygen concentration of the headspace of the compartment containing the working electrode was monitored with a Clark's fast-response oxygen micro-electrode needle sensor (OX-N, 40 mm needle length, 1.1 mm diameter, 90% response time <10 s) commercialized by Unisense A/S.

X-ray Crystal Structure Determination. Data collection was made on a Bruker-Nonius diffractometer equipped with an APPEX II 4K CCD area detector, a FR591 rotating anode with Mo Kα radiation, Montel mirrors as a monochromatic and a Kryoflex low-temperature device (T = -173ºC). Full-sphere data collection was used with w and f scans. Programs used: data collection APPEX II,[19] data reduction, Bruker Saint V/.60A;[20] absorption corrections, SADABS.[21]

Structure and Refinement. For this, SHELXTL[22] was used.

Synthetic preparations

[Ru^{II}(Cl)(PY4Im)]$^+$ **(3(Cl)).** [PY4ImAg]Br (0.062 g, 0.202 mmol) and [Ru(Cl)$_2$(p-cymene)]$_2$ (0.062 g, 0.101 mmols) were dissolved in a flask containing acetonitrile (25 ml) and the resulting solution heated for overnight. After that time a yellow precipitate appeared which was filtered and dried with diethyl ether. Yield: 94 mg (86%).^{1}H-NMR (400MHz, DMSO): δ = 9.42 (d, 4H, J$_{1-2}$=5.67 Hz, H1), 7.93 (d, 4H, H4), 7.92 (t, 4H, H3), 7.77 (s, 2H, H12), 7.46 (t, 4H, H2), 7.45 (s, 2H, H6). ^{13}C{^{1}H} NMR (400MHz, DMSO): δ = 194.78 (C14), 155.63 (C1), 154.91 (C5), 137.20 (C4), 125.67 (C3), 124.40 (C2), 120.51 (C12), 65.19 (C6). ESI-MS (MeOH): *m/z*= 541.04 ([M-Cl]$^+$)

[Ru^{II}(PY4Im)(H$_2$O]$^{2+}$ **(4(BF$_4$)$_2$).** **3(Cl)** (0.060 g, 0.103 mmols) and AgBF$_4$ (0.061 g, 0.309 mmols) were dissolved in the darkness in a flask containing acetone:water (10 ml,

1:4). The resulting solution was stirred and heated for overnight. After cool down to room temperature the solution was filtered removing the formed AgCl. Slow evaporation of the acetone yielded nice yellow crystals, which were filtered and dried over air. Yield: 60 mg (84%). ^{1}H-NMR (400MHz, D_2O): δ = 9.20 (d, 4H, J_{1-2}=5.60 Hz, H1), 7.89 (d, 4H, H4), 7.87 (ddd, 4H, H3), 7.62 (s, 2H, H12), 7.44 (ddd, 4H, J_{2-3}=7.73 Hz, J_{2-1}=5.60 Hz, J_{2-4}=2.12 Hz, H2), 7.13 (s, 2H, H6). ^{13}C{^{1}H} NMR (400MHz, D_2O): δ = 195.18 (C14), 154.24 (C1), 153.26 (C5), 137.15 (C4), 125.46 (C3), 124.00 (C2), 119.64 (C12), 66.07(C6). UV/vis (aqueous solution at pH = 8, phosphate buffer): λ_{max} (ε)= 245 (1027), 360 (6549), 394 (7140). ESI-MS (MeOH): *m/z*= 239.0 ([M-2PF$_6$]$^{2+}$).

Acknowledgements

VI

VI.5. <u>**References**</u>

[1] (a) Tseng, H.; Zong, R.; Muckerman, J.T.; Thummel, R. *Inorg. Chem*. **2008**, *47*, 11763-11773. (b) Concepción J.J.; Jurss, J.W.; Templeton, J.L.; Meyer, T.J. *J. Am. Chem. Soc*. **2008**, *130*, 16462-16463.

[2] (a) Duan, L.; Bozoglian, F.; Mandal, S.; Stewart, B.; Privalov, T.; Llobet, A.; Sun, L. *Nat. Chem.* **2012**, *4*, 418. (b) Roeser, S.; Farras, P.; Bozoglian, F.; Martinez-Belmonte, M.; Benet-Buchholz, J.; Llobet, A. *ChemSusChem* **2011**, *4*, 197. (c) Duan, L.; Xu, Y.; Gorlov, M.; Tong, L.; Andersson, S.; Sun, L. *Chem.Eur.J.* **2010**, *16*, 4659. (d) S. Masaoka, K. Sakai, *Chem. Lett.* **2009**, *2*, 182-183; (e) D. J. Wasylenko, C. Ganesamoorthy, B. D. Koivisto, M. A. Henderson, C. P. Berlinguette, *Inorg. Chem.* **2010**, *49*, 2202-2209.

[3] (a) de Vries, M. E.; La Crois, R. M.; Roelfes, G.; Kooijman, H.; Spek, A. L.; Hage, R.; Feringa, B. L. *Chem. Commun.* **1997**, 1549. (b) Klein Gebbink, R. J. M.; Jonas, R. T.; Goldsmith, C. R.; Stack,T. D. P. *Inorg. Chem.* **2002**, 41, 4633.

[4] Fazio, O.; Gnida, M.; Meyer-Klaucke, W.; Frank, W.; Kläui, W.Eur. J. *Inorg. Chem*. **2002**, 2891.

[5] Tamagaki, S.; Kanamaru, Y.; Ueno, M.; Takagi, W. *Bull. Chem. Soc.Jpn.* **1991**, *64*, 165.

[6] (a) Grohmann, A.; Knoch, F. *Inorg. Chem.* **1996**, *35*, 7932. (b) Grohmann, A.; Knoch, F. *Dalton Trans.* **2010**, *39*, 1432 and references cited therein.

[7] Schmidt, S.; Omn_es, L.; Heinemann, F. W.; Kuhnigk, J.; Kr€uger, C.;Grohmann, A. *Z. Naturforsch. B* **1998**, *53*, 946.

[8] (a) Zimmermann, C.; Heinemann, F. W.; Grohmann, A. *Eur. J.Inorg. Chem.* **2005**, 3506. (b) Kohl, S. W.; Heinemann, F. W.; Hummert, M.;Weiβhoff, H.; Grohmann, A. *Eur. J. Inorg. Chem*. **2006**, 3901. (c) Kohl, S. W.;Heinemann, F. W.; Hummert, M.; Bauer, W.; Grohmann, A. *Chem.;Eur. J*. **2006**, *12*, 4313.

[9] (a) Wasylenko, D.J.; Ganesamoorthy, C.; Borau-Garcia, J.; Berlinguette, C.P. *Chem. Commun.*, **2011**, *47*, 4249-4251. (b) Sun, Y.; Sun, Y.; Long, J.R.; Yang, P.; Chang, C.J.; *Chem. Sci.*, **2013**, *4*, 118-124.

[10] (a) Hirai, Y.; Kojima, T.; Mizutani, Y.; Shiota, Y.; Yoshizawa, K.; Fukuzumi, S. *Angew. Chem., Int. Ed.*, **2008**, *47*, 5772; (b) Kojima, T.; Hirai, Y.; Ishizuka, T.; Shiota, Y.; Yoshizawa, K.; Ikemura, K.; Ogura, T.; Fukuzumi, S. *Angew. Chem., Int. Ed.*, **2010**, *49*, 8449. (c) Kojima, T.; Fukuzumi, S. *Angew. Chem., Int. Ed.*, **2011**, *50*, 3852.

[11] Ohzu, S.; Ishizuka, T.; Hirai, Y.; Jiang, H.; Sakaguchi, M.; Ogura, T.; Fukuzumi, S.; Kojima, T., *Chem. Sci.*, **2012**, *3*, 3421.

[12] Smith, J.M.; Long, J.R. *Inorg. Chem.* **2010**, *49*, 11223-11230.

[13] Dyker, G.; Muth, O. *Eur. J. Org. Chem.* **2004**, 4319-4322.

[14] Vedevnikov A.N.; Fettinger, J.C.; Mohr, F. *J. Am. Chem. Soc.* **2004**, *126*, 11160-11161.

[15] Huynh, M.H.V.; Meyer, T.J. *Chem. Rev.* **2007**, *107*, 5004-5064.

[16] Takeuchi, K.J.; Thompson, M.S.; Pipes, D.W.; Meyer, T.J. *Inorg. Chem.* **1984**, *23,*1845-1851.

[17] (a) Rodríguez, M.; Romero, I.; Llobet, A. *Inorg. Chem.* **2001**, 40, 4150-4156. (b) Takeuchi, K.J.; Thompson, M.S.; Pipes, D.W.; Meyer, T.J. *Inorg. Chem.* **1984**, 23, 1845-1851.

[18] In, J.-H.; Park, S.-E.; Song, R.; Nam, W. *Inorg. Chim. Acta* **2003**, *343*, 373.

[19] Data collection with: *Apex II*, versions v1.0-22, v2009.1-0 and v2009.1-02; Bruker AXS Inc.: Madison, WI, 2007.

[20] Data reduction with : *SAINT*, versions V.2.10 (2003), V/.60A and V7.60A; Bruker AXS Inc.: Madison, WI, 2007.

[21] *SADABS*, versions V.2.10 (2003): V2008 and V2008/1 (2001); Bruker AXS Inc.: Madison, WI, 2008. Blessing, R. H. *Acta Crystallogr.* **1995**, *A51*, 33-38.

[22] Sheldrick, G. M. Acta Crystallogr. **2008**, *A64*, 112-122 (SHELXTL, versions V6.12 and V6.14).
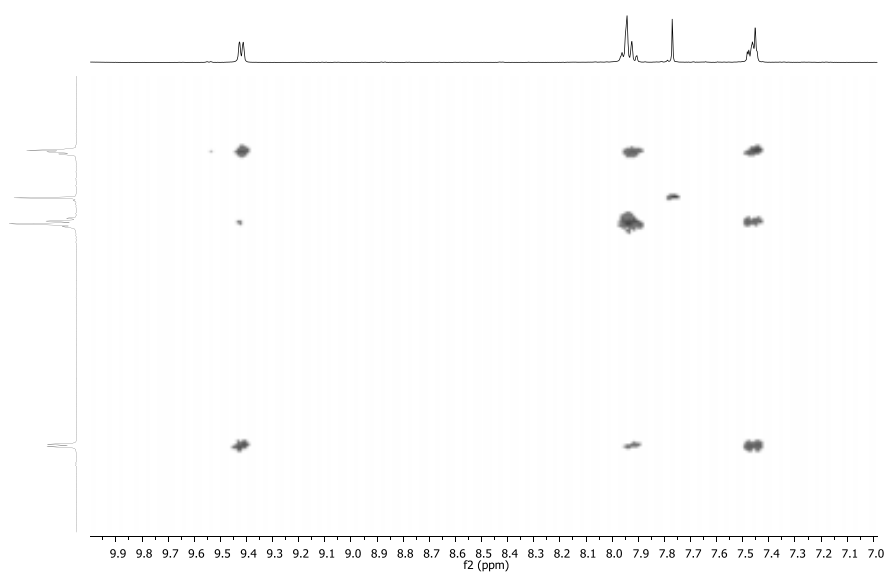
VI.6.   <u>Supporting Information</u>

- NMR
- Electrochemistry
- ESI-MS
- X-Ray
- PCE

VI

Figure S1. 1D and 2D NMR spectra (400 MHz, 298 K, DMSO) for **3**$^{+}$: (a) ^{1}H-NMR, (b) COSY, (c) ^{13}C-{^{1}H}-NMR, (d) HSQC NMR (aromatic region) (e) HMBC NMR (aromatic region).
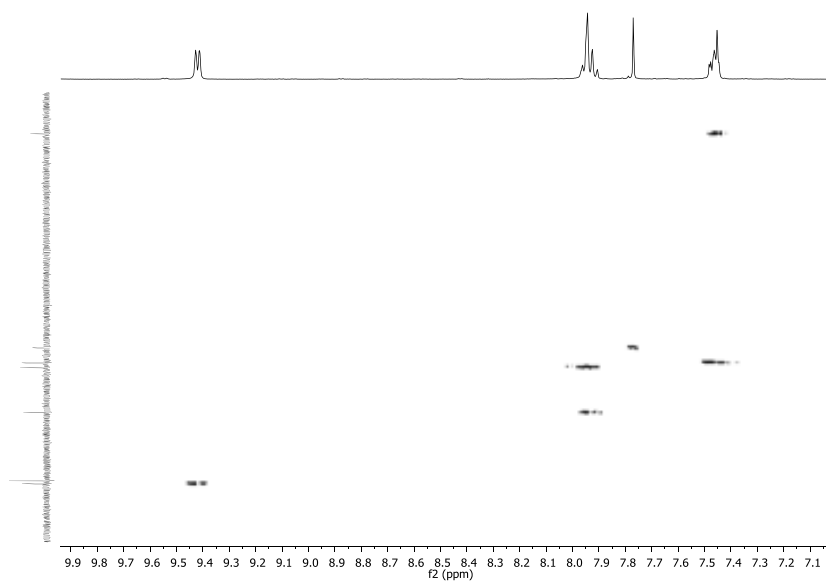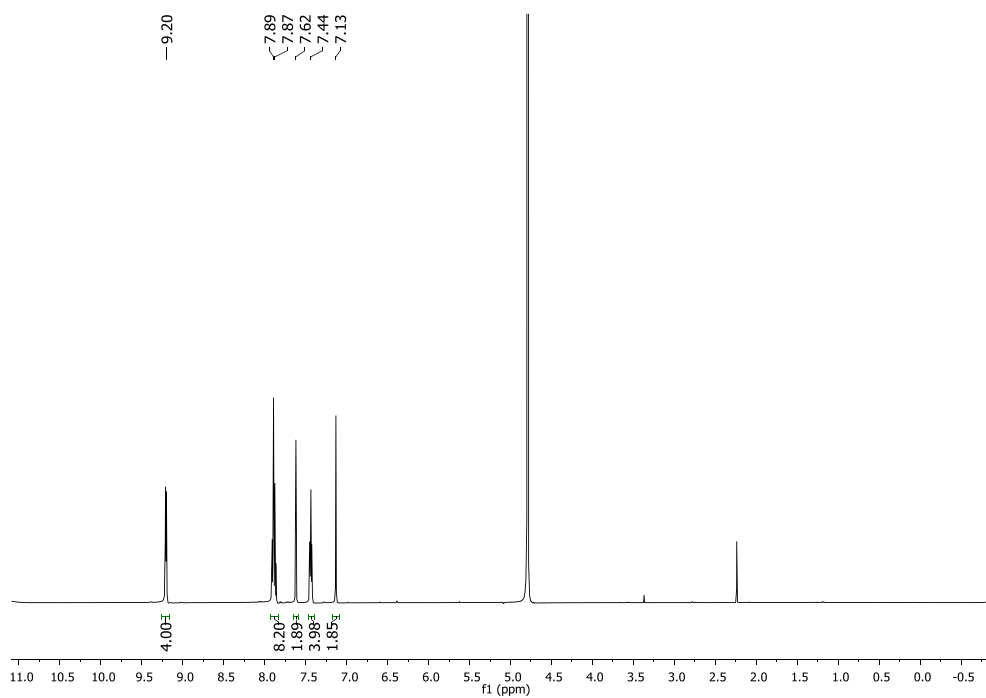
a)

b)

c)

d)

VI
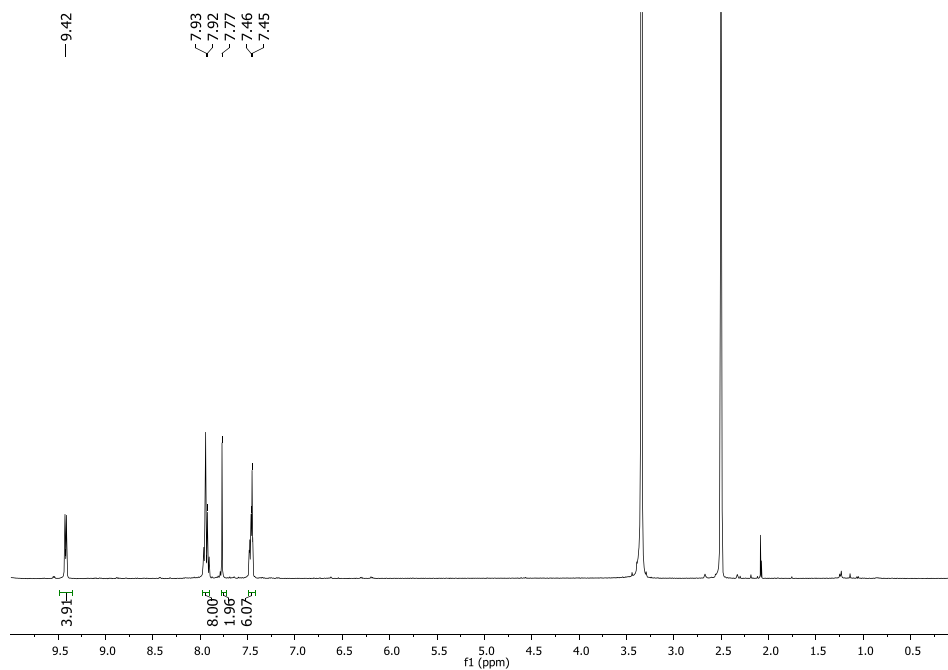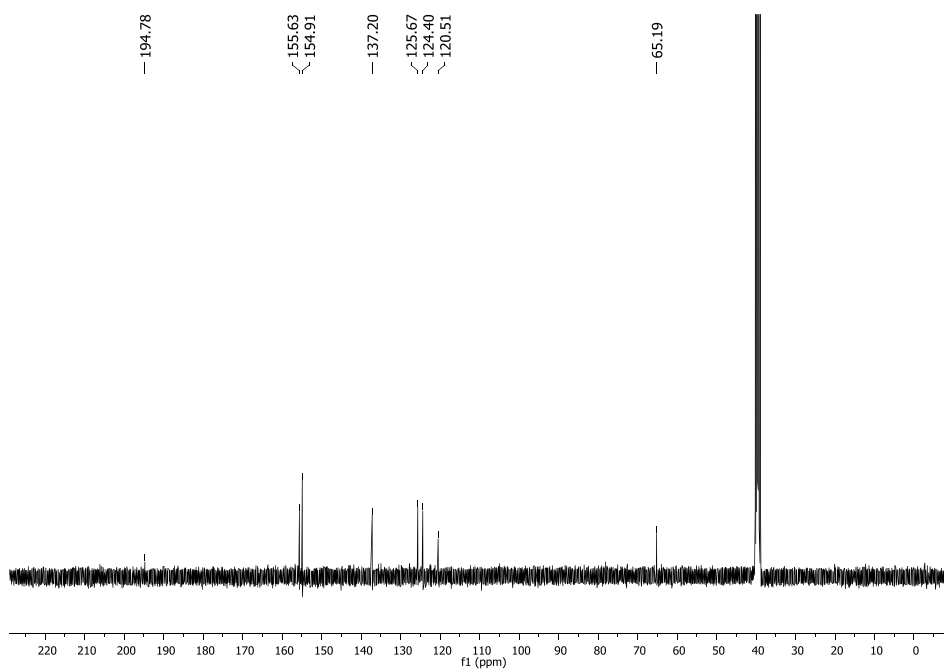
e)
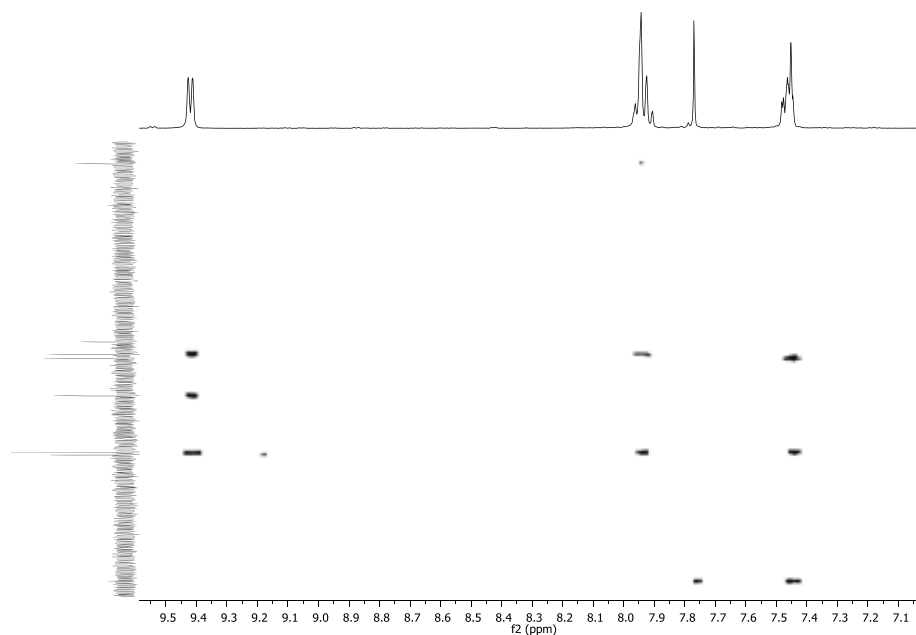
Figure S2. 1D and 2D NMR spectra (400 MHz, 298 K, D$_2$O) for complex **4^{2+}**: (a) ^{1}H-NMR, (b) COSY, (c) ^{13}C-{^{1}H}-NMR, (d) ^{13}C-{^{1}H}- DEPTQ135 (e) HSQC NMR (aromatic region) (f) HMBC NMR (aromatic region).
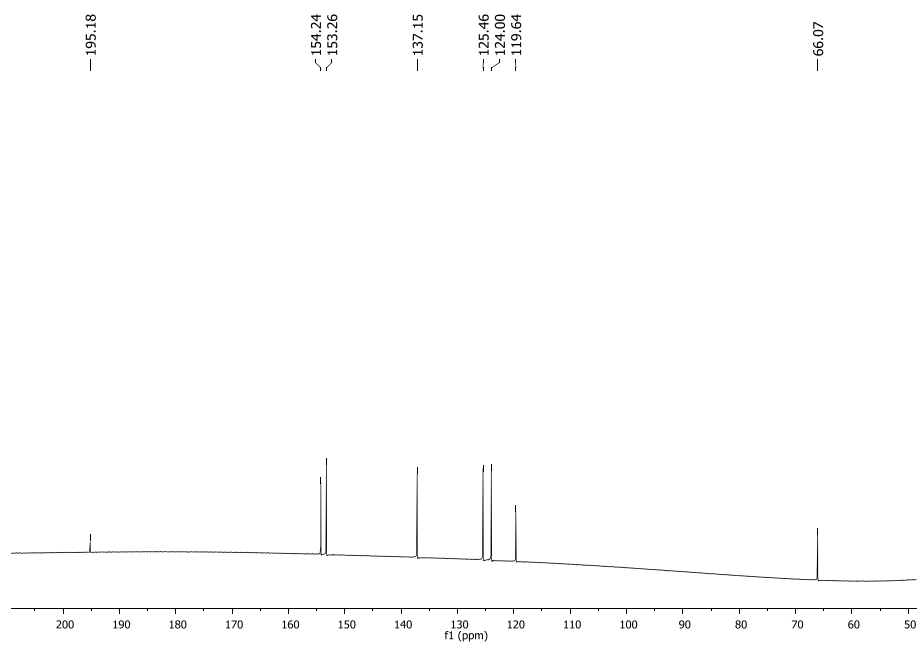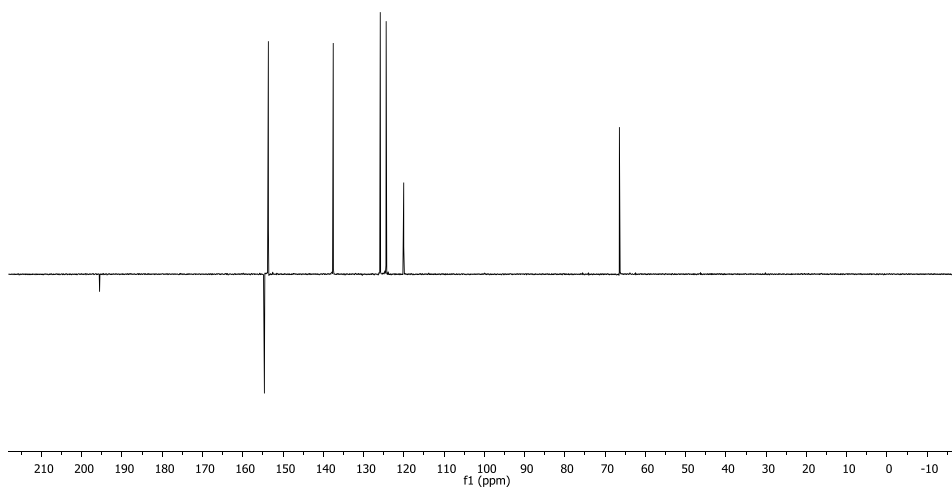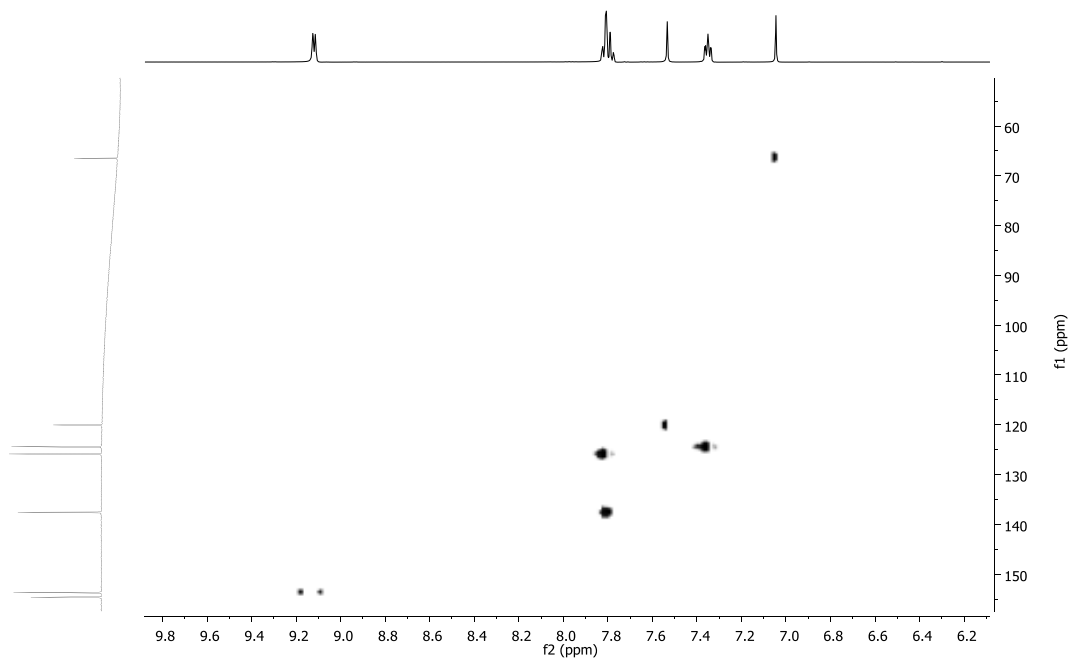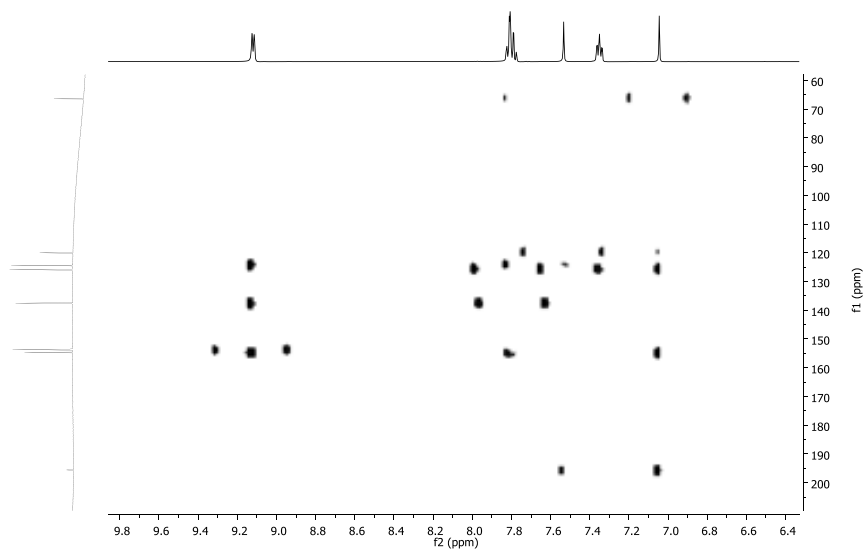
a)

b)

c)

VI
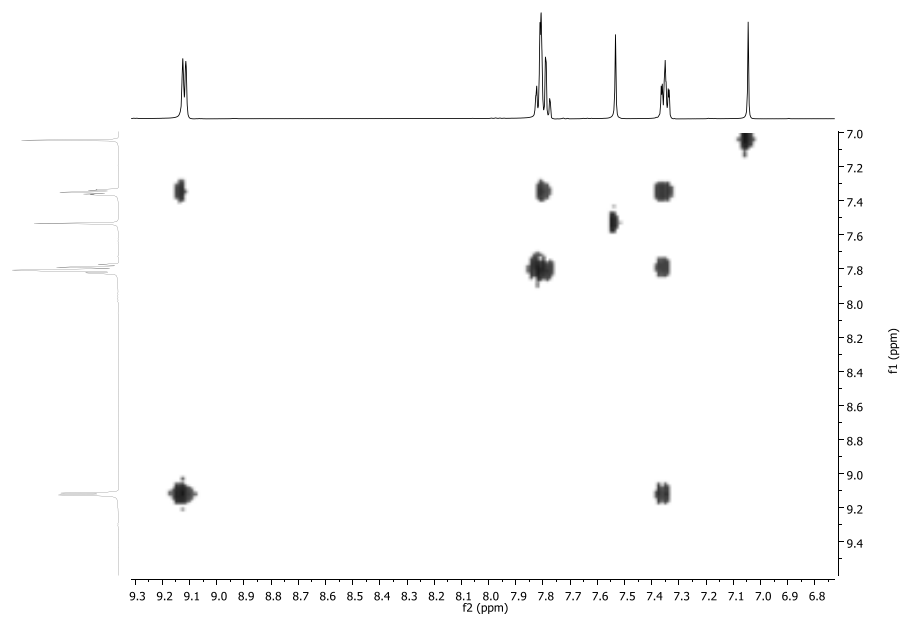
d)

e)

f)

Figure S3. Cyclic voltammogram for **3**[+] in 0.1 M n-Bu$_4$NPF$_6$ in methanol at 100 mV/s scan rate. Glassy carbon electrode is used as working electrode and the potential is measured *vs.* SSCE.
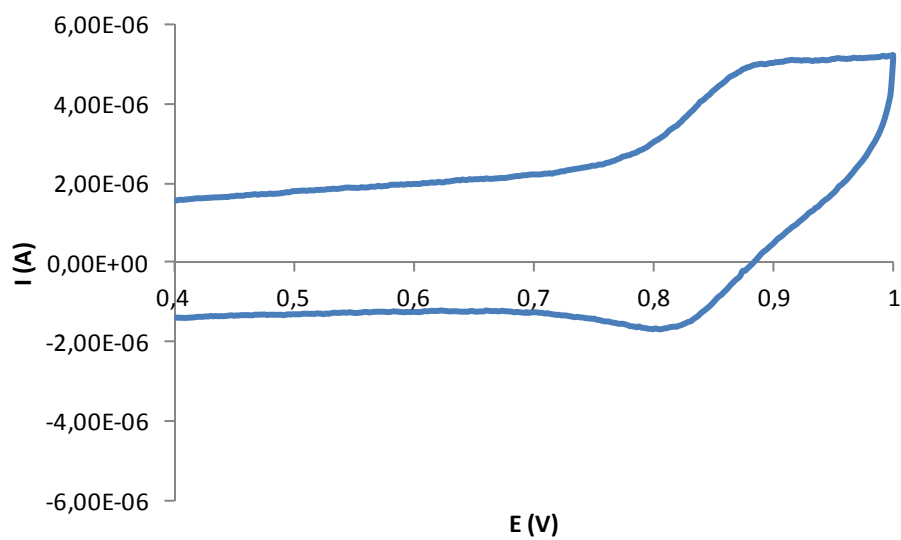

VI

Figure S4. Differential Pulse Voltammetry for the aqua complex **4²⁺** in water pH=2 (phosphate buffer) at 100 mV/s scan rate. Glassy carbon electrode is used as working electrode and the potential is measured *vs*. SSCE.

Figure S5. Cyclic voltammetry for the aqua complex **4²⁺** in water pH=8 (phosphate buffer) at 100 mV/s scan rate. Glassy carbon electrode is used as working electrode and the potential is measured *vs*. SSCE.
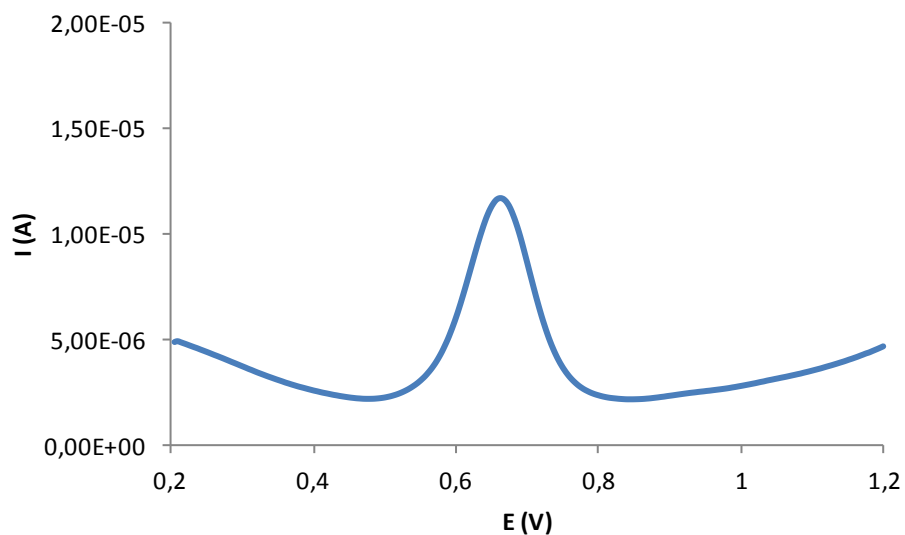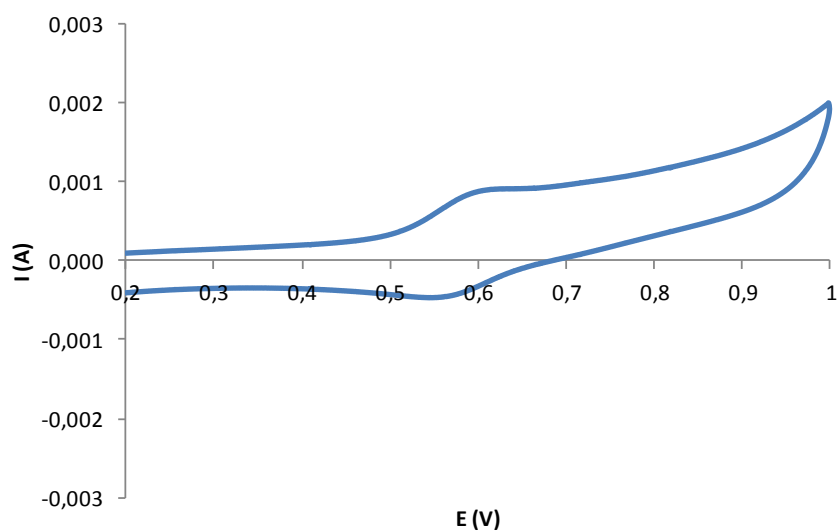
Figure S6. Experimental (right side) and theoretical zoom (left side) Mass Spectra for complex **3⁺**.
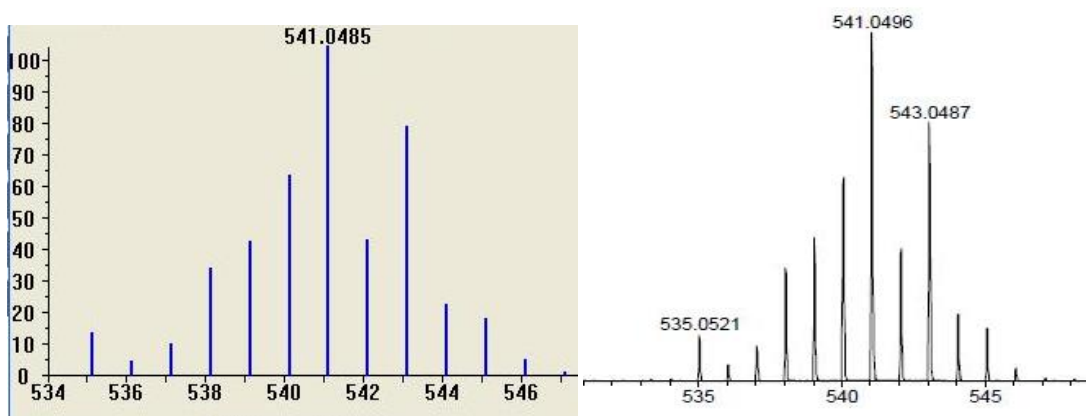

Figure S7. Experimental (right side) and theoretical zoom (left side) Mass Spectra for complex **4²⁺**.
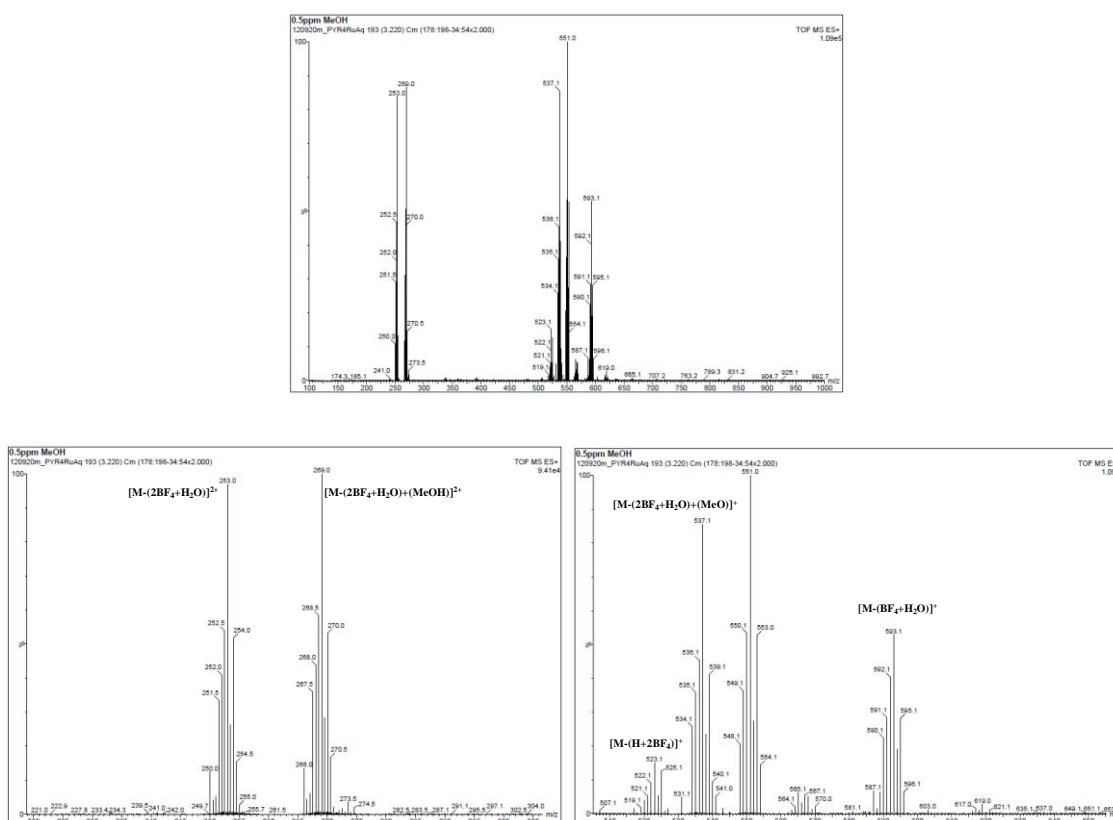

VI

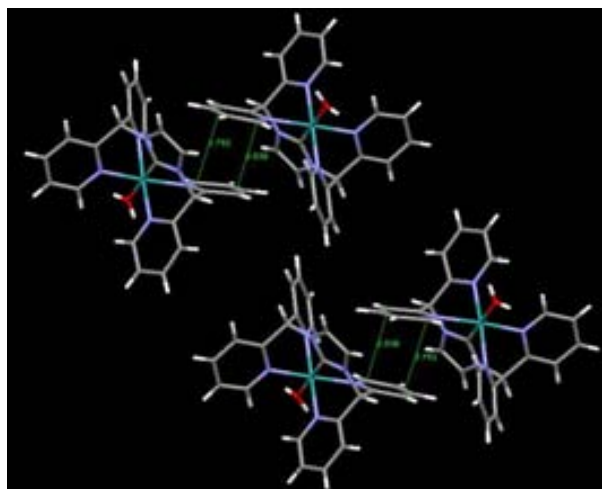**Figure S8.** Plot of the unit cell of 4^{2+} and the corresponding distances of the π-stacking interaction.

Table S1. Crystallographic data for complex 4^{2+}.

Empirical formula	C25 H30 B2 F8 N6 O5 Ru	
Formula weight	769.24	
Temperature	100(2)K	
Wavelength	0.71073 Å	
Crystal system	Monoclinic	
Space group	P2(1)/n	
Unit cell dimensions	a = 12.7198(12) Å	a = 90.00 °.
	b = 13.6489(16) Å	b = 108.488(5) °.
	c = 18.6702(19) Å	g = 90.00 °.
Volume	3074.1(6) Å^3	
Z	4	
Density (calculated)	1.662 Mg/m^3	
Absorption coefficient	0.605 mm^{-1}	
F(000)	1552	
Crystal size	0.40 x 0.05 x 0.01 mm^3	
Theta range for data collection	1.88 to 32.93 °.	
Index ranges	-19 <=h<=17 ,-20 <=k<=20 ,-28 <=l<=28	
Reflections collected	38867	
Independent reflections	11294 [R(int) = 0.0542]	
Completeness to theta =32.93 °	0.979 %	
Absorption correction	Empirical	
Max. and min. transmission	0.9940 and 0.7938	
Refinement method	Full-matrix least-squares on F^2	

250

Data / restraints / parameters	11294 / 34 / 487
Goodness-of-fit on F^2	1.039
Final R indices [I>2sigma(I)]	R1 = 0.0614 , wR2 = 0.1634
R indices (all data)	R1 = 0.0920 , wR2 = 0.1900
Largest diff. peak and hole	2.991 and -2.684 e.Å^{-3}

Figure S9 Plot of absorbance ($\lambda = 292$ nm) *vs.* time during during CPE of $\mathbf{4^{2+}}$ in an aqueous solution at pH = 8 (phosphate buffer). $E_{app} = 0.65$ V *vs.* SSCE.

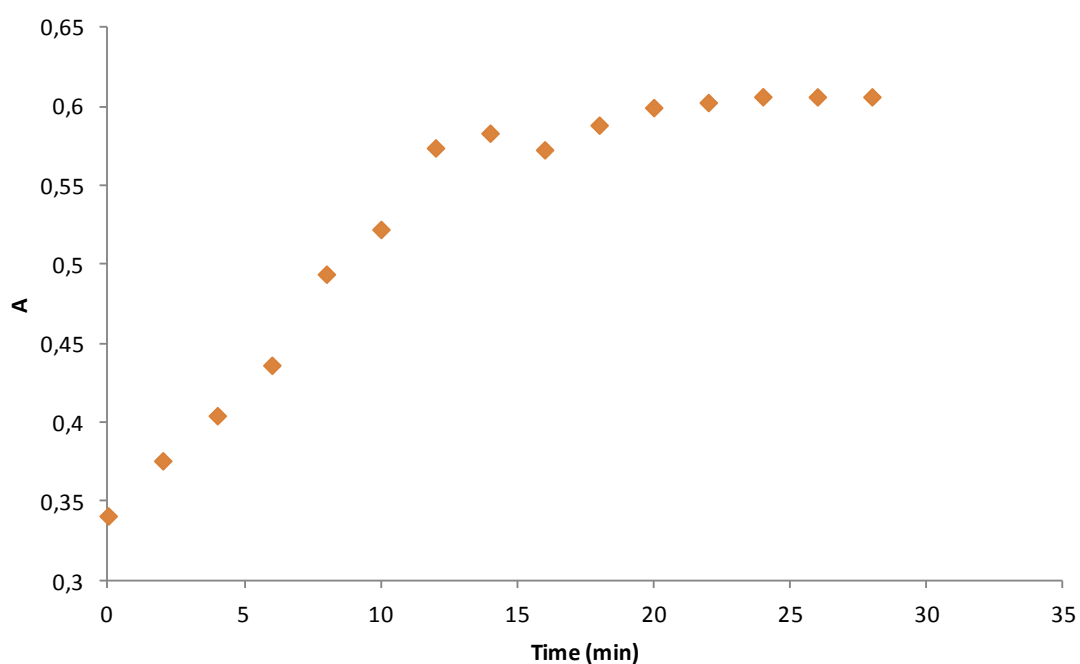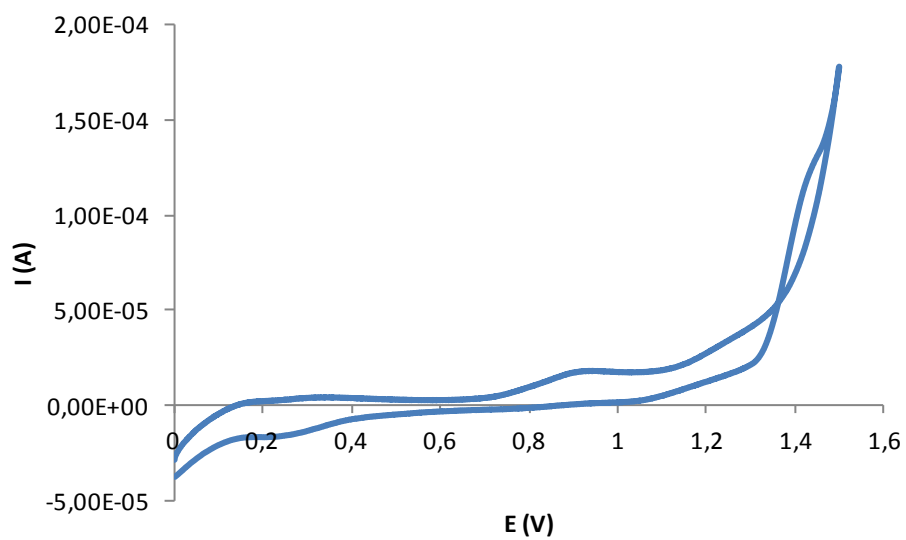VI

Figure S10. Cyclic voltammetry of **4²⁺** after CPE at pH = 8 (phosphate buffer in water). FTO used as working electrode and potential measured *vs.* Ag/AgCl.

CHAPTER VII

Conclusions and Future Work

Taking into account the initial objectives proposed for this thesis and the final experimental data obtained some conclusions, remarks and future work are reported in this chapter.

I

> A new family of Ru dinuclear complexes ($\mathbf{5^{4+}}$ and $\mathbf{7^{4+}}$) containing the positively charged trpyPyr ligand 4'-(-*p*-(Pyridin-1-ylmethyl)phenyl)-2,2':6',2''-terpyridine (**L3(PF$_6$)**) have been synthesized and fully characterized, both in the solid state and in solution.

> The anchoring of the new catalysts onto TiO_2, SiO_2 and Nafion® has been achieved and the new hybrid materials prepared have been characterized by means of electrochemical and spectroscopic techniques.

> The catalytic performance of the homogeneous bis-aqua derivate resulted in similar results than those reported for the related Hbpp catalyst. No CO_2 evolution was observed together with oxygen formation. However, Silica-$\mathbf{8^{5+}}$ has shown a high CO_2:O_2 ratio when chemically activated with Ce/IV), thus revealing the oxidative degradation of the catalyst. This degradation is probably due to the activation of the methylene in alpha to the pyridylic residue when the positive charge is dislocated interacting with the SiO^- residues.

> Catalyst leaching from FTO-TiO_2-$\mathbf{5^{4+}}$ was observed when the electrochemical activation of the hybrid material was performed to trigger the system for water oxidation. This fact reveals the weak character of the interaction between the positively charged pyridines and the TiO_2 electrode.

> Despite the electrocatalytic activation of Nafion-$\mathbf{5^{4+}}$ has been observed by DPV, its performance as chemically-driven WOC using Ce(IV) is poor, only yielding stoichiometric amounts of O_2. On the other hand, the lack of catalytic activity of Nafion-$\mathbf{7^{4+}}$ has been attributed to the blocking of its active sites by coordination of sulfonate groups of the polymeric support to the Ru metal ions.

> Silica and Nafion® have demonstrated to be the best solid surfaces in terms of the stability of the catalyst-support interaction, meanwhile TiO_2 has shown a much weaker anchoring. The work herein presented is a clear example of how new efforts have to be spent looking for new hybrids systems which have to be

VII

highly stable under strong oxidative conditions meanwhile maintaining or increasing the catalytic activity of the WOCs attached on them.

II

➢ A new Ruthenium bis-facial dinuclear complex, $\mathbf{2^{2+}}$, containing the hexadentate pyrazolate-bridging ligand Hbimp and bpy as auxiliary ligands has been synthesized.

➢ DFT calculations have been mandatory in order to elucidate the *trans* character of the new complex.

➢ $\mathbf{2^{2+}}$ has been fully characterized in solution by means of spectrometric, spectroscopic and electrochemical techniques.

➢ The new compound has been tested with regard to its capacity to oxidize water. The *in situ* generated bis-aqua complex $\mathbf{3^{3+}}$ resulted in low efficiencies and selectivities when performing as WOC, which was attributed to the intramolecular catalyst-catalyst oxidative degradation of the surrounding ligands in the harsh and highly oxidative reaction conditions.

➢ $\mathbf{3^{3+}}$ has shown to be an excellent catalyst for the epoxidation of a wide range of alkenes. From the scope of substrates analyzed, the following conclusions can be pointed out:

    o *cis* alkenes were epoxided faster and in higher yields than their corresponding *trans* counterparts, thus reveling the important effect of the steric hindrance around the catalytically active sites in the final catalytic output.

    o Substrates containing electron-donor groups yielded better results than those bearing electron-withdrawers, which points out the high electrophilic character of the $Ru^{IV}=O$ active site.

    o The catalytic systems described here are stereospecific in nature, in the sense that no *cis*/*trans* isomerization takes place for the c*is*-alkenes.

- o Either a concerted oxygen atom transfer from the Ru^{IV}=O active site to the alkene double bond or a radical path were the C-C rotation of the generated radical is much slower than the ring closing that generates the final epoxide can be plausible mechanisms for this transformation.

➢ Future prospects will be focused on the better understanding of the mechanism that is directing the stereoselectivity observed in the epoxidation reaction, as well as in the expansion of the substrate scope.

III

➢ The intermediate **5** has been prepared by means of cross-coupling reactions between a di-halo phthalazine and acetylene derivatives. However, neither good yields nor acceptable reproducibility have been obtained. The two new ligands, **3a** and **3b**, have been obtained in low yields and fully characterized in solution and in the solid state.

➢ **3a** has been employed for the preparation of the dinuclear Cl-bridged Ru complex **9^{3+}** that has been structurally (X-ray), spectroscopically and electrochemically characterized. Comparison of **9^{3+}** solid state structure with the one of the related and previously reported [Ru$^{II}_2$(μ-Cl)(bpp)(trpy)$_2$]$^{2+}$ complex pointed out relevant differences about the disposition and constrains of the metal centers.

➢ All the attempts of preparing the bridging tetradentate N/C-donor ligands **2a** and **2b** failed, However, two new bidentate N/C-donor ligands, **7$^+$** and **8$^+$**, were prepared and structurally characterized. These new ligands were the result of the always favored alkylation of a N atom of the the central phthalazine scaffold with regards to the peripheral nitrogen atoms of the triazole rings.

VII

➢ Future prospects should be focused on the optimization of the cross-coupling process to obtain **5** in higher yields and reproducibility. On the other hand, the selective alkylation of **3a** and **3b** should be attempted under acidic media,

preventing in this manner the non-desired nucleophilic attack of the phthalazine nitrogen atoms.

IV

> We have prepared and thoroughly characterized a novel family of complexes of formula $[Ru^{II}(PY4Im)(X)]^{n+}$ (X = Cl, n = 1or X = H_2O, n = 2), which represent the first class of ruthenium complexes containing a pentadentate ligand bearing an NHC scaffold on its axial position

> Both $Ru^{III}(OH)$ and $Ru^{IV}(O)$ high oxidation state species have been electrochemically generated and spectroscopically characterized.

> The strong σ-donor character of the carbene ligand is clearly manifested in **4²⁺** by both, the important reduction of its redox potentials and the clear increase of its pKa values when comparing this data with that of the paradigmatic Ru-N_5 complex $[Ru(trpy)(bpy)(H_2O)]^{2+}$.

> The use of a pentadentate moiety likewise PY4Im provides interesting hydrogen bonding interactions between the H in alpha to the nitrogen atoms in the equatorial pyridines and the hydroxo group of the Ru^{III}-OH species, thus stabilizing them towards its oxidation to $Ru^{IV}(O)$.

> The catalytic activity of $[Ru^{II}(PY4Im)(H_2O)]^{2+}$ as water oxidation catalyst has been tested by using both chemical (CeIV) and electrochemical (CPE) sacrificial oxidants. Degradation of the initial catalyst, potentially due to intermolecular catalyst-catalyst oxidative degradation processes, has been observed with both methodologies.

> Promising preliminary results has been achieved when employing **4²⁺** as catalyst for the epoxidation of alkenes.